



**TAILORING THE GRAIN SIZE OF METHYLAMMONIUM LEAD
IODIDE PEROVSKITE FILM WITH FUNCTIONALIZED RGO FOR
ENHANCED MORPHOLOGICAL AND OPTICAL PROPERTIES**

**Utilizing functionalized rGO to tailor the grain size of MAPbI₃ perovskite for
properties enhancement.**

Submitted in accordance with the requirement of the Universiti Teknikal
Malaysia Melaka (UTeM) for the Bachelor Degree of Manufacturing Engineering
(Hons.)

UNIVERSITI TEKNIKAL MALAYSIA MELAKA

by

NUR SABRINA SAHIRA BINTI SYED OMAR

FACULTY OF MANUFACTURING ENGINEERING

2021

DECLARATION

I hereby, declared this report entitled “Tailoring the grain size of methylammonium lead iodide perovskite film with functionalized rGO for enhanced morphological and optical properties” is the result of my own research except as cited in references.

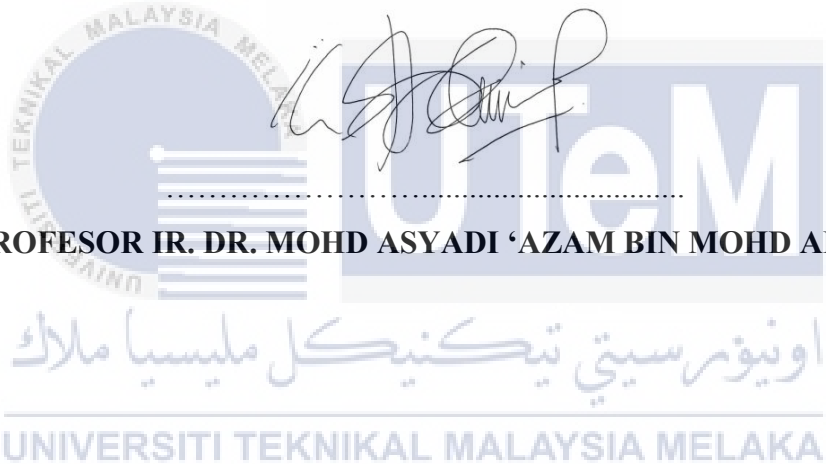

Signature 
Author's Name : NUR SABRINA SAHIRA BINTI SYED OMAR
Date : 29th AUGUST 2021



UNIVERSITI TEKNIKAL MALAYSIA MELAKA

APPROVAL

This report is submitted as partial fulfilment of the subject BMFU4912 Bachelor Degree Project 2 to the Faculty of Manufacturing Engineering of Universiti Teknikal Malaysia Melaka to meet the criteria completion of Degree of Manufacturing Engineering (Hons) Supervisor as follows:



(PROFESOR IR. DR. MOHD ASYADI 'AZAM BIN MOHD ABID)

اونيورسيتي تيكنيكل مليسيا ملاك
UNIVERSITI TEKNIKAL MALAYSIA MELAKA

ABSTRAK

Sel Surya Perovskite (PSC) adalah salah satu jenis sel suria yang paling terkenal. Bahan perovskite banyak digunakan kerana sifat elektrik dan optiknya yang unggul. Bahan perovskite berfungsi sebagai lapisan penyerap dalam sel suria perovskite, menyerap tenaga foton dan menghasilkan pasangan lubang elektron. Dengan kecekapan penukaran tenaga yang tinggi, ciri fotolistrik yang luar biasa, dan spektrum penyerapan kecekapan yang kuat, metilamonium plumbum iodida adalah salah satu jenis bintang yang menjadikan PSC bersinar. Kerana kualiti yang luar biasa ini, ia adalah bentuk sel suria yang paling stabil. Walau bagaimanapun, PSC terus mengalami beberapa kekurangan yang mengganggu reputasinya. Pertama, terdapat kekurangan dalam aplikasi kestabilan jangka panjang kerana terdedah kepada persekitaran terbuka dengan perubahan cuaca yang mengakibatkan reaksi antara kationnya dengan air dan oksigen. Akibatnya, ciri optik dan morfologi gagal. Kedua, morfologi perovskite yang buruk menyebabkan perangkap yang merosot dalam ciri-ciri pentingnya, seperti pergerakan dan penyerapan cas. Kerosotan ini menyebabkan morfologi rosak, yang akhirnya mempengaruhi kecekapan penukaran kuasa peranti berdasarkan bahan perovskite. Kajian ini bertujuan untuk meningkatkan sifat morfologi dan optik bahan perovskite dengan memasukkan *sulfonated graphene oxide (s-rGO)* sebagai dopan. Oksida graphene yang dikurangkan adalah sintesis melalui kaedah Hummer yang diubah suai, difasilitasi oleh agen pengurangan persekitaran, dan selanjutnya di sulfonasi sebelum dimasukkan ke dalam larutan perovskite dalam keadaan sekitar. S-rGO mengandungi kumpulan fungsi asid sulfanilik yang mencukupi, penting untuk membentuk ikatan dengan kation perovskite untuk menyelaraskan filem nipis perovskite dan mengelakkan pengagregatan. Oleh itu, ia meningkatkan ukuran butiran filem nipis perovskite dan mengurangkan ketumpatan perangkap cas di batas butiran. Dalam kajian ini, pembentukan s-rGO dopan kedalam perovskite disahkan melalui Spektroskopi Raman secara ulsan kajian. Selain itu, Spektrofotometer Ultraviolet-Visible (UV-Vis) digunakan untuk mengkaji analisis sifat optic juga melalui kaedah secara ulsan kajian. Sementara itu, peningkatan morfologi perovskite dianalisis dengan menggunakan Mikroskopi Elektron Imbasan (SEM). Menggabungkan s-rGO sebagai dopan diharapkan dapat meningkatkan morfologi perovskite tanpa mempengaruhi sifat optiknya sebagai bahan aktif dalam sel suria perovskite.

ABSTRACT

Perovskite Solar Cells (PSC) are one of the most well-known types of solar cells. Perovskite materials are widely used due to their superior electrical and optical properties. Perovskite material functions as an absorber layer in perovskite solar cells, absorbing photon energy and generating electron-hole pairs. With high energy conversion efficiency, outstanding photoelectric feature, and intense efficiency absorption spectrum, methylammonium lead iodide is one of the star-growing types that make the PSC shine. Because of these exceptional qualities, it is the most stable form of the solar cell. However, PSC continue to suffer from several flaws that jeopardize its excellent reputation. First, there are flaws in the long-term stability application since it is exposed to an open environment with weather fluctuations resulting in the reaction between its cation to water and oxygen. As a result, the optical and morphological characteristics are flawed. Second, poor perovskite morphology causes traps that degrade in their essential features, such as charge mobility and absorption. This degradation has led to its poor morphology, which eventually affects the device's power conversion efficiency based on this perovskite material. This study aims to enhance the morphological and optical properties of the perovskite material by incorporating sulfonated reduced graphene oxide (s-rGO) as a dopant. The reduced graphene oxide is synthesis through modified Hummer's method, facilitated by an environmentally reducing agent, and further sulfonated before incorporated into the perovskite solution in ambient condition. S-rGO contains sufficient sulfonic acid functional groups, essential to forming a bonding with perovskite cation to align the perovskite thin film and avoid agglomeration. Thus, it increases the perovskite thin-film grain size and reduces the charge trap density in the grain boundaries. In this study, the perovskite doped s-rGO formation confirmed via Raman spectroscopy via critical review. Besides, the Ultraviolet-Visible Spectrophotometer used to study the optical properties analysis also by critical review. Meanwhile, the improvement of the perovskite morphology analyzed using Scanning Electron Microscopy. Incorporating s-rGO as a dopant improve the perovskite morphology without affecting its optical properties as active material in perovskite solar cells. Furthermore, reduced graphene oxide hydrophobic properties help enhance the perovskite stability in the ambient atmosphere.

DEDICATION

To my supportive supervisor and co-supervisor thank you so much for the endless support and guidance,

To my beloved father, Syed Omar Bin Syed Mansoor thank you for the moral support,

To my appreciated mother, Rosenani Binti Hussain thank you for keep giving me moral support, funding, collaboration, encouragement and understanding.

To my dearest friends that you for being there for one another,

Thank you very much for everything.

I love you all.



ACKNOWLEDGEMENT

In the name of Allah SWT, The most humble, gracious, with the highest praise of Allah that I succeed without difficulty in completing this final year of project 2.

First and foremost, I would like to thank my supervisor, Profesor Ir. Dr. Mohd Asyadi 'Azam Bin Mohd Abid, for his assistance, support, and availability throughout my final year project journey. My dearest superior, Miss Nur Ezyanie Binti Safie, whose assistance and support was also critical to this work's development. I want to thank you for all of your expertise and kindness.

There are not enough words for my mother and father to thank you for everything you do for me each day and the support you offer me in every choice I make. Without you, it would not have been possible, and I hope you are proud of me. Thank you for all the assistance and support in every stage of my life for my family.

Thank you to my precious Mok for always being here after all these years and for keep growing with me. Thank you for making it so wonderful and part of my journey. In my heart, you always have a place.

Thank you for all the beautiful memories, support, assistance, and love from my dearest housemates and best buddy. You know who you are. Who were constantly with me and made these four years the finest of my life thus far. It would have been impossible to get here without all of you, and I couldn't have asked for a more gracious group of people.

My gratitude to Encik Azhar for assisting me with sample characterization and make it possible. To all lab assistants who provide me with complete instruction throughout the process of finishing my lab work. Even though you were just a portion of this journey, you added to its beauty. I shall never forget your contribution, advice, and teaching to all outstanding FKP, UTeM lectures.

TABLE OF CONTENTS

BORANG PENGESAHAN STATUS LAPORAN PROJEK SARJANA MUDA	i
DECLARATION	ii
APPROVAL	iii
ABSTRAK	iv
ABSTRACT	v
DEDICATION	vi
ACKNOWLEDGEMENT	vii
TABLE OF CONTENTS	viii
LIST OF FIGURES	xii
LIST OF TABLES	xv
LIST OF ABBREVIATIONS	xvi
CHAPTER 1 : INTRODUCTION	
1.0 Research Background	1
1.2 Problem Statement	5
1.3 Objectives	6
1.4 Scope of the Research	6
1.5 Rational of the Research	7
1.6 Thesis Organization	7
CHAPTER 2 : LITERATURE REVIEW	
2.0 Introduction	8
2.1 Perovskite Solar Cell	8

2.1.1	Perovskite Solar Cell Device Architecture	11
2.1.2	Perovskite Active Layer	13
2.1.3	ETL (Electron Transport Layer)	13
2.1.4	Hole Transport Layer (HTL)	13
2.2	Working Principle of Perovskite Solar Cell	14
2.3	Limitation of Perovskite Solar Cell	14
2.3.1	Problem in the Morphological Properties of Perovskite Solar Cell	15
2.3.2	Problem in the Optical Properties of Perovskite Solar Cell	16
2.4	Perovskite Materials in Solar Cell	16
2.4.1	Methylammonium Lead Iodide (MAPbI ₃) Based Perovskite Solar Cell	18
2.4.2	Graphene-Based Perovskite Solar Cell	18
2.4.3	Graphene, Graphene Layer, GO, and rGO	19
2.4.4	Synthesis Methods for Graphite Oxide	20
2.4.5	Reduced Graphene Oxide (rGO)	21
2.4.6	Functionalized Reduced Graphene Oxide	22
2.4.7	Previous Study Results	23
2.5	Characterization Method	28
2.5.1	Scanning Electron Microscopy	28
2.5.1.1	Working Principle of SEM	29
2.5.2	Raman Spectroscopy	30
2.5.2.1	Working Principle of Raman Spectroscopy	31
2.5.3	Ultraviolet Visible Spectroscopy	32
2.5.3.1	Working Principle of Ultraviolet Visible Spectroscopy	32
2.6	Material Preparation Method	34
2.6.1	Chemical	34
2.6.2	Preparation of MAPbI ₃	34
2.6.3	Preparation of Reduced Graphene Oxide	36

2.6.4 Preparation of Functionalized rGO (S-rGO)	38
---	----

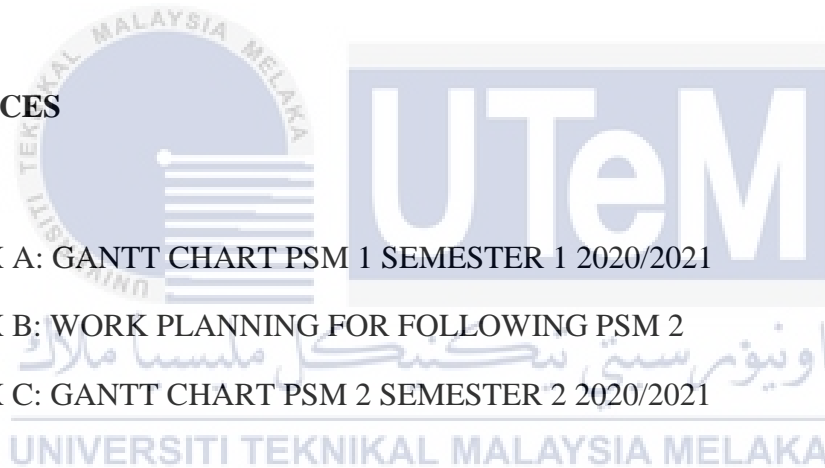
CHAPTER 3 : METHODOLOGY

3.0 Introduction	39
3.1 Flow Chart of Research Methodology	40
3.2 List of Chemicals	41
3.3 Preparation of Materials	46
3.3.1 Methylammonium Lead Iodide	46
3.3.2 Synthesis of Reduced Graphene Oxide	52
3.3.3 Functionalized Reduced Graphene Oxide	57
3.3.4 Preparation of Thin Film	60
3.4 Characterization Method	63
3.4.1 Scanning Electron Microscopy	63
3.4.2 UV-Visible Spectroscopy	63
3.4.3 Raman Spectroscopy	63
3.5 Execution of Critical Review: UV-Vis and Raman	64
3.6 Critical Review of Raman	65
3.7 Critical Review of UV-Vis	69
3.8 Summary of Chapter 3	74
3.9 Expected Result	74

CHAPTER 4 : RESULTS AND DISCUSSION

4.1 Structural properties	75
4.2 Morphological properties based on experimental findings.	77
4.2.1 SEM Morphological Experimental Results	78
4.2.2 Sulfonated reduced graphene oxide (S-rGO) influences grain size	83
4.2.3 Reduced graphene oxide (rGO) influences grain size	84

4.2.4 Pre heating process overcome humidity effect on Perovskite grain size	84
4.3 Optical properties	86
CHAPTER 5 : CONCLUSION	
5.1 Conclusion	87
5.2 Recommendation for Future Work	89
5.3 Sustainable Design and Development	90
5.4 Complexity	90
5.5 Long Life Learning	91
5.6 Achievement	91
REFERENCES	92
APPENDIX A: GANTT CHART PSM 1 SEMESTER 1 2020/2021	108
APPENDIX B: WORK PLANNING FOR FOLLOWING PSM 2	109
APPENDIX C: GANTT CHART PSM 2 SEMESTER 2 2020/2021	110



LIST OF FIGURES

Figure 1.1 Classification of Photovoltaic Solar Cells	2
Figure 1.2: Factors of degradation of PSC thin film (Wang et al., 2019)	4
Figure 2.1: Power Efficiency of Solar Cells from 1975 to 2020 (The NREL Website)	10
Figure 2.2: A) Mesoscopic and, B) Planar heterojunction structure (Zhou et al., 2018)..	11
Figure 2.3: The defects presence at surface and grain boundaries of the perovskite film...	15
Figure 2.4: (a) Intrinsic characteristics and defects in perovskite compared ideal lattice...	16
Figure 2.5: ABX_3 perovskite structure (Brittman et al., 2015).....	17
Figure 2.6 Graphene to reduced graphene oxide (Bianco et al., 2013)	20
Figure 2.7 Top-down and Bottom-up flow of Graphite to rGO (Stankovich et al., 2007)..	21
Figure 2.8: SEM image grain of (a) control and (b) s-GO	23
Figure 2.9: SEM image grain of functionalized rGO + Perovskite	24
Figure 2.10: UV-Vis absorbance spectra.....	24
Figure 2.11: UV-Vis absorption spectra of functionalized rGO	25
Figure 2.12 Raman spectra of GO and SGO and I_D/I_G ratio (Guo et al., 2017)	27
Figure 2.13 Raman spectra of GO and rGO and I_D/I_G ratio (Palma et al., 2016).....	27
Figure 2.14: Scanning Electron Microscopy	28
Figure 2.15 SEM working illustration (SEM - EVOCD, 2017).....	29
Figure 2.16: Raman Spectroscopy	30
Figure 2.17 Raman Spectroscopy working illustration (Yohk co.ltd. 2020).....	31
Figure 2.18: Ultraviolet Visible Spectroscopy	32
Figure 2.19: Working principle of ultraviolet visible spectroscopy (Rocha et al., 2018)..	33
Figure 2.20: The procedures to prepare MAPI films using the two-step routes.	35
Figure 3.2 Weight of PbI_2	46
Figure 3.3 Pipetting the DMSO	47
Figure 3.4 Pipetting the DMF	47
Figure 3.5 Stirring procees	48
Figure 3.6 PbI_2 final mixture solution	48
Figure 3.7 2 mL of IPA	49
Figure 3.8 Mixture of IPA, MAI and 20 % of S-rGO	50

Figure 3.9	Stirring process of S-rGO 0%, 20% and 40%	50
Figure 3.10	Summary of synthesis process of Methylammonium Lead Iodide	51
Figure 3.11	1g of graphite flakes in 50ml of sulfuric acid stirring in an ice-water bath.....	52
Figure 3.12	Magnetic stirrer	52
Figure 3.13	Stirring process of the mixture	53
Figure 3.14	Sonication in the ultra-sonicate with water bath	53
Figure 3.15	Quench of the GO and distilled water	54
Figure 3.16	Process of altering the pH level at ~6	54
Figure 3.17	Reduction process of GO	55
Figure 3.18	Filtration, pH level alteration and final rGO powder	55
Figure 3.19	Summary flow synthesis process of Reduced Graphene Oxide.....	56
Figure 3.20	Functionalize rGO initial process.....	57
Figure 3.21	Ice bath and measured sulfanilic acid, HCl, and distilled water.	57
Figure 3.22	Drying in the vacuum oven	58
Figure 3.23	Final S-rGO powder	58
Figure 3.24	Summary flow synthesis process of Sulfonated Reduced Graphene Oxide	59
Figure 3.25	Substrate preparation and washing.....	60
Figure 3.26	Working table during preparation	60
Figure 3.27	Yellow form from PbI ₂ deposition	61
Figure 3.28	Final look of Perovskite thin film	61
Figure 3.29	Summary fabrication Perovskite doped S-rGO thin film at room temt	62
Figure 3.30	Flow chart of critical review study	64
Figure 3.31	Raman spectra of GO and SGO and ID/IG ratio (Guo et al., 2017)	66
Figure 3.32	Raman spectra of GO and rGO and ID/IG ratio (Suragtkhuu et al., 2020).....	67
Figure 3.33	Raman spectra of GO and rGO and ID/IG ratio (Palma et al., 2016)	69
Figure 3.34	UV-Vis and SEM result of difference grain size (Balis et al., 2018).....	71
Figure 3.35	UV-Vis spectra between sGO and GO (Hu, X et al., 2021)	72
Figure 3.36	Absorbance (UV-Vis) with different grain size (Mamun 2019).....	73
Figure 4.1	Sample A (0% S-rGO) grain size at 10.00K mag, 1 μ m.....	78
Figure 4.2	Sample A (0% S-rGO) grain size at 20.00K, 200nm mag, 1 μ m.....	78
Figure 4.3	Particle size of Sample A (0% S-rGO) grain size (nm) with average 384nm....	79
Figure 4.4	Sample B (20% S-rGO) grain size at 10.00K mag, 1 μ m.....	80
Figure 4.5	Sample B (20% S-rGO) grain size at 20.00K mag, 200nm	80
Figure 4.6	Particle size of Sample B (20% S-rGO) grain size (nm) with average 638nm..	81

Figure 4.7 Sample C (40% S-rGO) grain size at 10.00K mag, 1 μ m..... 82
Figure 4.8 Sample C (40% S-rGO) grain size at 20.00K mag, 200nm 82



LIST OF TABLES

Table 3.1: Table of the list chemical used in the material preparation of MAPbI ₃	41
Table 3.2: Table of the list chemical used in the material preparation of rGO.	43
Table 3.3: Table of the list chemical used in the material preparation of S-rGO.....	45



LIST OF ABBREVIATIONS

CdTe	- Cadmium telluride
CIGS	- copper indium gallium diselenide
CH ₃ NH ₃ PbI ₃	- Methylammonium Lead Iodide
CH ₃ NH ₃ PbBr ₃	- Methylammonium Lead Bromide
PSCs	- Perovskite Solar Cells
ITO	- indium tin oxide
MAPbI ₃	- Methylammonium Lead Iodide
rGO	- Reduced Graphene Oxide
GO	- Graphene Oxide
s-rGO	-Sulfonated reduced graphene oxide
CaTiO ₃	- Calcium Titanium Oxide
ETM/ ETL	- Electron Transport Material / Layer
HTL	- Hole Transport Layer
TCO	- Transparent Conducting Oxide
FTO	- Fluorine-doped Tin Oxide
LHP	- Lead Halide Perovskites
VB	- Valence Band
SEM	- Scanning Electron Microscopy
UV-Vis	- Ultraviolet Visible Spectrometer
AA	- Ascorbic Acid
LUMO	- Lowest Unoccupied Molecular Orbital
CB	- Conduction Band

CHAPTER 1

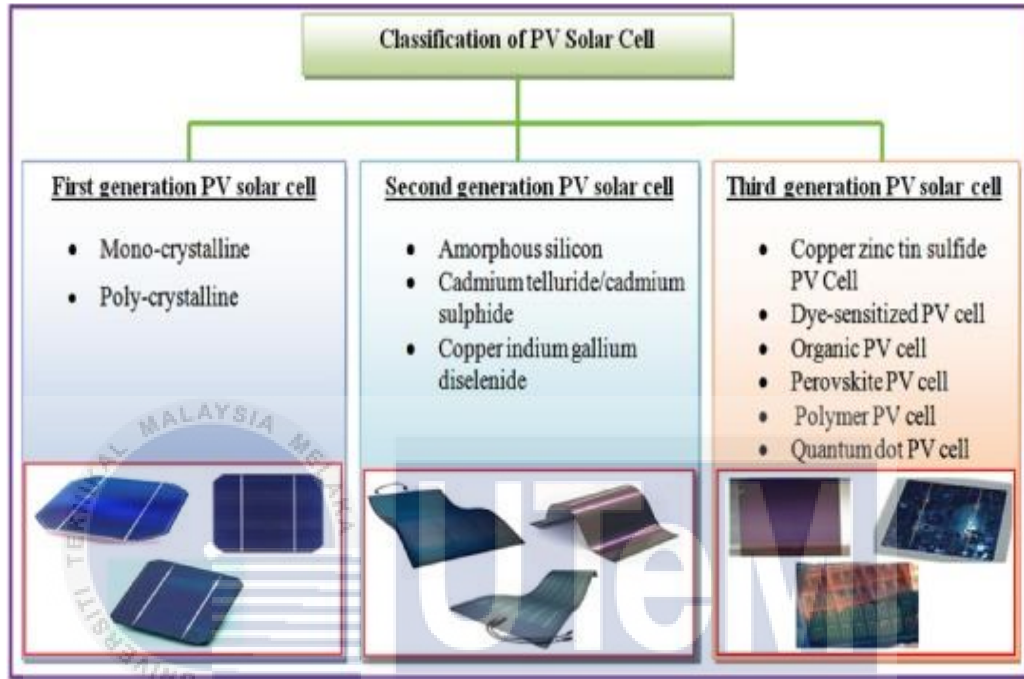
INTRODUCTION

1.0 Research Background

In electrical energy, solar energy is generated by the interplay of collected sunlight and heat, which is subsequently transformed back into the light. Solar energy is considered to be one of the most sustainable and environmentally friendly sources of electricity. Malaysia is known for having a pleasant environment, which is why many people visit the nation. Because we have warm, bright days nearly every day of the year, it is beneficial for us to use solar panels. We have an adequate quantity of solar energy on hand. Because of its geographic position in the tropical area, Malaysia reaps the benefits of solar energy generation. Miss Yeo Bee Yin, Minister of Energy, Research, Technology, Environment, and Climate Change, said that if solar panels were installed on all of Peninsular Malaysia's home roofs, the country could generate 1.4 times the amount of energy it does now. Wow, what a fantastic chance we have here. The usage of solar cells helps us save money on energy bills, helps to protect our mother planet, and, last but not least, ensures that we will never run out of available sunshine. Also, Malaysia has a natural tropical environment with typical sunlight received for about 12 hours each day, or around half of our daily routine.

Solar cells in a bundle are becoming more popular. There have been three generations of solar cells developed up to this point as shown in figure 1.1 below. The first generation of solar cells, which is the first kind of solar cell found by an expert, is made of crystalline silicon and is the most advanced type of solar cell. Monocrystalline silicon, polycrystalline silicon, thick-film silicon, and amorphous silicon are all examples of the earliest kinds of solar cells. Polycrystalline silicon is another example. Solar panels constructed of non-silicon materials are the next generation of solar cells, followed by the second generation of

solar cells. Two examples of second-generation solar cell technologies are cadmium telluride (CdTe) and copper, indium, gallium diselenide (CIGS). Meanwhile, dye-sensitized solar cells, sustainable solar cells, and perovskite solar cells are the most commonly used or most recent solar cells. The improvements made to solar cells are intended to result in a more cost-effective and stable version of solar cells in the future.



اونيو، تي تي فيكٽيولٽايك سولر سيلس
 Figure 1.1 Classification of Photovoltaic Solar Cells

UNIVERSITI TEKNIKAL MALAYSIA MELAKA

In this research, I'm concentrating on the kinds of Perovskite materials that are being used in solar cells. It is a substance with the crystal structure form ABX_3 that is used to make perovskite materials. The crystal structure of this kind of crystal structure is the same as that of calcium titanium oxide. The letters 'A' and 'B' represent cations, and X represents an anion that forms a bond with both. Two components in the Perovskite itself contribute to the enhancement of the characteristics of PSC. The ammonium lead iodide ($CH_3NH_3PbI_3$) and the methylammonium lead bromide ($CH_3NH_3PbBr_3$) are the two components that have been discussed before (Kojima et al. 2009). Out of these two components, methylammonium lead iodide ($MAPbI_3$) is emerging as the brightest star in the solar cell community, thanks to the tremendous improvement in the quality of perovskite solar cells, which has resulted in significant improvements in energy conversion efficiency, with recent devices achieving more than 31 % conversion efficiency (Sha el 2015). The following properties of the $MAPbI_3$

Perovskite result in a well-defined architectural structure. According to Safie and colleagues (2020), the photoelectric characteristics of methylammonium lead iodide are superior, with a smaller binding force of the excitation energy and strong coefficients of absorption spectrum (up to 10^4 cm^{-1}); this characteristic contributes to improving the stability of solar cells, which was the primary goal of this research. Furthermore, when MAPbI_3 is present, the Perovskite's light-absorbing component can gather the sun's rays more efficiently than when it is not there. Another advantage is that due to its high dielectric constant, electrons and holes can be transported and collected efficiently; this feature will improve the absorption ability of solar cells (Zhou et al. 2018).

The benefits of MAPbI_3 PSCs are many and continue to grow in popularity; nevertheless, PSCs still face several constraints that reduce the quality and long-term viability of the technology. The major shortcoming of MAPbI_3 PSC is their inability to maintain long-term stability of operation. Because of environmental variables such as heavy rainy seasons, intense sunlight radiation, and oxygen, MAPbI_3 PSC quickly deteriorate and lose their stability as shown in figure 1.2. In addition, MAPbI_3 PSC are also susceptible to degradation and degradation (Agregi et al., 2016). The optical and morphological characteristics of MAPbI_3 PSC will be degraded as a result of the constraints that they encounter. In terms of optical characteristics, the deterioration will result in the conversion to a broad bandgap, the formation of a surface trap, current leakage, and a reduction in the capacity to absorb sunlight. From a structural standpoint, deterioration of the MAPbI_3 PSC will result in ion movement at grain boundaries, grain size reduction, decreased short-term stability, and a reduction in light-harvesting efficiency.

If we consider the current situation, one of the most effective methods to enhance the stability of the photovoltaic device is to use functionalized graphene oxide as an addition to assisting in the elimination of the restriction. In addition, due to the hydrophobic nature of graphene and its derivatives (Suragtkhuu et al., 2020), graphene may serve as an interfacial layer in the MAPbI_3 PSCs structure acting as an additional shield to protect the perovskite thin film from moisture absorption. Eventually, this graphene with hydrophobic characteristics that offer extra protection will assist in overcoming the deterioration possibilities caused by the reasons listed above, such as when it constantly rains for an extended period during the rainy season. In addition, graphene has been extensively utilized as transparent electrodes in photovoltaic systems PSCs because it has greater transparency

in the visible area than traditional indium tin oxide (ITO) transparent electrodes in the visible region. Moreover, it has been shown to have very high carrier mobilities (Zhang et al., 2016).

Furthermore, it benefits from being bipolar, meaning that it may be used as both a photoelectrode and a counter electrode (Koefoed L. et al., 2017). Apart from that, according to Kim et al. (2018), graphene exhibits exceptional mechanical flexibility and bending endurance, making it a suitable substitute for flexible transparent electrodes in the fabrication of flexible photovoltaic systems. On the other hand, the literature has only a small number of research that focused on enhancing the shape and optical characteristics of perovskite films by adding functionalized rGO to increase the efficiency and stability of solar cells.

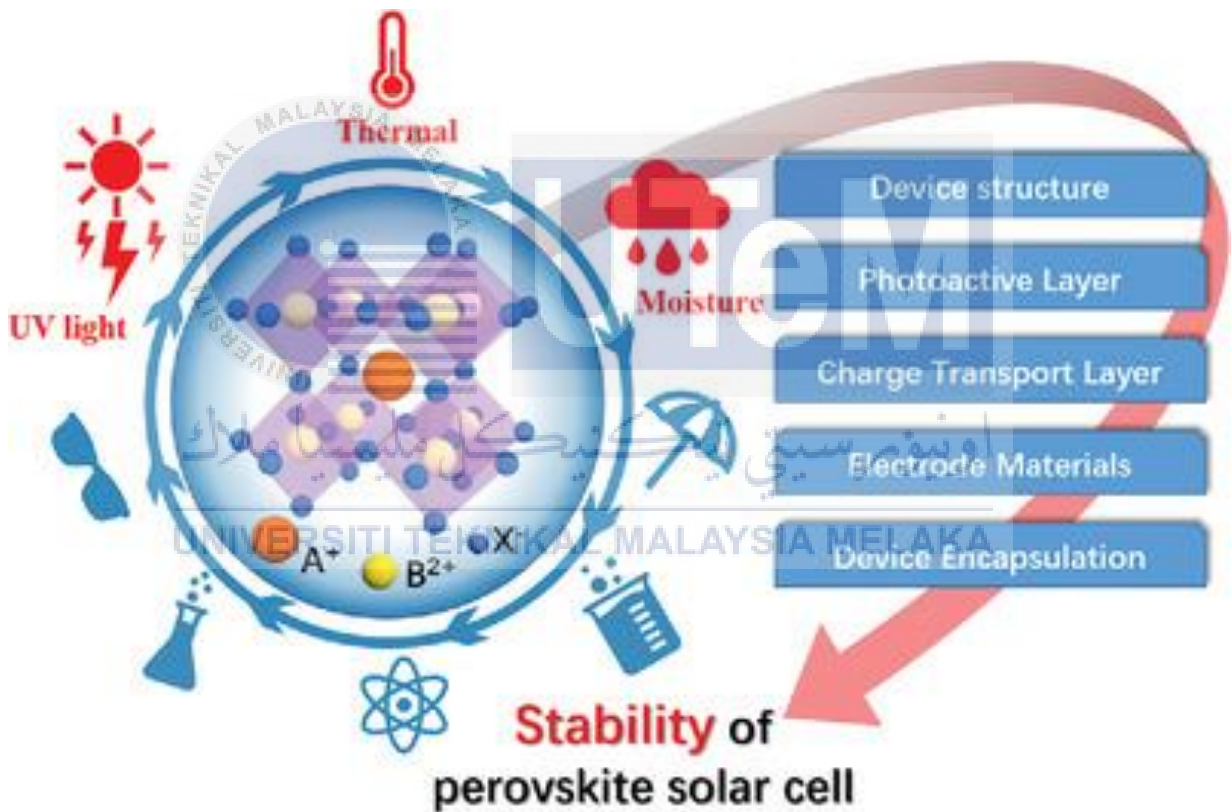


Figure 1.2: Factors of degradation of PSC thin film (Wang et al., 2019)

1.2 Problem Statement

Methylammonium lead iodide PSC are well known for their excellent electrical and optical properties in the applications of solar cells. MAPbI₃ Perovskite material acts as an active layer that plays a role as the absorbing film in PSC. Poses characteristics of high coefficient of light absorption help the whole visible solar spectrum by ultra-thin films of solar cells around 500 nm (Yin et al. 2014). These features that belong to the MAPbI₃ Perovskite make it possible to manufacture low-cost at high volume, high-efficiency, small, lightweight, and compact solar panels.

However, the aspect of short-term and long-term stability is the main challenge for MAPbI₃ PSCs. The main weakness of the PCS is the long-term stability of operations as it is exposed to the high heat and humidity uncovered area for the long term. The factors that lead to the deterioration and stability of the solar cells because of environmental variables such as heavily raining seasons, extreme sunlight radiation, and oxygen. These factors lead to the swift destruction of MAPbI₃ PSC, which do not last long (Agresti et al., 2016). The limitations faced by the MAPbI₃ PSC will cause a defect in optical and morphological properties.

The degradation will cause the conversion to a wide bandgap, surface trap, and current leakage and drop in the sunlight absorption ability from the optical properties view. This problem will decrease the stability of the MAPbI₃ PSC. Meanwhile, from the morphological aspect, the degradation of the MAPbI₃ PSC will cause ion migration at grain boundaries, grain size to be minor, short-term stability, and decrease in light-harvesting. These factors lead to the deterioration of the perovskite critical characteristics and strength.

Thus, to tackle the problems mentioned above, this project's main objective is to study the effect of functionalized reduced graphene oxide (rGO) in MAPbI₃ Perovskite thin-film. The assumed return is the enlargement of the grain size and tunable bandgap to intensify its morphological and optical properties from incorporating the MAPbI₃ Perovskite and functionalized rGO in the thin film. Thus, to see the differences in MAPbI₃, the crystal structure grain size and the optical absorbance ability will be examined. Furthermore, the future analysis and effect of functionalized rGO with MAPbI₃ Perovskite thin-film on the thin film structure using Raman spectroscopy that show the D and G band properties. Meanwhile, for the thin film's morphological and light absorption spectrum, scanning

electron microscopy (SEM) and Ultraviolet-Visible spectroscopy (UV-Vis) was used in study the optical morphological properties.

1.3 Objectives

1. To characterize the Sulfonated reduced graphene oxide (S-rGO) in MAPbI₃ Perovskite thin film prepared by the Sulfonation process.
2. To analyze the morphology of S-rGO incorporated with MAPbI₃ Perovskite films by using Scanning Electron Microscopy.
3. To investigate the structural and optical properties of S-rGO incorporated with MAPbI₃ Perovskite thin film with different surface morphology by using Raman Spectroscopy and Ultraviolet visible Spectrometer based on critical review.

1.4 Scope of the Research

1) To achieve objective 1:

The first process is the preparation of MAPbI₃ Perovskite thin film by using two-step spin coating methods. The process begins with the isopropanol combination of methylammonium iodide (MAI) and lead iodide (PbI₂). Second, Synthesis of rGO from graphite via the top-down method. Lastly, surface functionalization through the treatment of sulfanilic acid to the pristine rGO– Sulfonation process.

2) To achieve objective 2:

Preparation of different ratios of S-rGO incorporated with MAPbI₃ Perovskite thin-film S-rGO: MAPbI₃ Perovskite with 0% S-rGO (100% of MAI₃), 20% S-rGO and 40% S-rGO. Follow by the analyzation of the morphological structure of samples by using Scanning Electron Microscopy. Here, the grain size was the main priority - enlargement of the grain size.

3) To achieve objective 3:

Investigate the optical properties of S-rGO incorporated with MAPbI₃ Perovskite thin film by using Ultraviolet-visible Spectroscopy. The focus is on absorbance performance- increase in light absorption ability. Also, to confirm the structural properties of S-rGO incorporated with MAPbI₃ Perovskite thin film by using Raman. The main agenda is to check the structure. The quality was than examined from the G band and D band analyses. Both UV-Vis and Raman was performed by Critical Review.

1.5 Rational of the Research

The rationale of research as follows:

1. To analyze the incorporation behavior of graphene-based materials for altering and changing components, including the existence of perovskite composition, morphology and optical properties.
2. Acquiring expertise behind technical analysis by improving the efficiency of perovskite solar cells. Create improved material for use in perovskite solar cells by researching the causes of destruction.

1.6 Thesis Organization

This study is organized as follows: Chapter 1 starts with a research background, problem statement, research objective, and research scope, all of which represent the studies reasoning and research methods and assist in more easily defining the rGO perovskite solar cell's heredity (MAPbI₃). In Chapter 2, the overview of the literature on perovskite solar cells (MAPbI₃) and functionalized rGO. Chapter 3 Methodology discusses the characteristics and steps involved in manufacturing a MAPbI₃ perovskite film utilizing S-rGO. Following Chapter 4, the gathered data will be reviewed and evaluated, and some results from the Critical Review method. Finally, Chapter 5 will end with a conclusion, a proposal, a discussion of sustainable design and development, and the project's long-term learning.

CHAPTER 2

LITERATURE REVIEW

2.0 Introduction

This chapter discusses an overview of previous research related to this study. It introduces perovskite solar cells, including the device structure in subtopic 2.1, the working principle in subtopic 2.2, and limitations encountered by the device in subtopic 2.3. The material that is used in this study will be discussed in the following subtopic. In subtopic 2.4, the perovskite material will be further explained in terms of its chemical structure and properties, wherein this study, Methylammonium Lead Iodide (MAPbI₃), is the studied material. Next, the subtopic will discuss functionalized Reduced Graphene Oxide (S-rGO) and its capability as a promising material to be integrated with perovskite material to enhance morphology and optical properties. Lastly, subtopic 2.5 will discuss the characterization technique used.

2.1 Perovskite Solar Cell

Most countries in the world are already turning to renewable energy sources to meet their energy needs and reduce the impact of emissions (Gielen et al., 2019). Energy demand increases with the growth of the world's population, and the proportion of renewable energy sources is expected to grow globally. Solar energy has attracted great interest in renewable energy, primarily because of its abundant availability. The working principle of solar cells is to absorb light or photochemical reaction and convert it into electrical energy. Solar cells can be divided into three generations, among which silicon wafer-based devices are called

first-generation solar cells. So far, silicon wafers have achieved the highest efficiency in other equipment and therefore occupy a dominant position in the solar industry. However, due to the high price of silicon, the researchers introduced the second generation, which is based on inorganic thin-film technologies, including cadmium telluride (CdTe) and copper indium gallium selenide (CIGS). Devices based on thin-film technology have been further developed to the third generation, where people pay attention to high-efficiency, low-cost materials, and convenient manufacturing processes. Organic solar cells, dye-sensitized solar cells, quantum dot photovoltaic cells, and perovskite solar cells belong to this solar cell generation.

In perovskite solar cells, after ultraviolet rays are irradiated to the device, the active layer plays a vital role in electron supply. Also, perovskite materials can be used as the light absorption layer and the charge transport layer. The many advantages of perovskite materials include a significant extinction coefficient, high charge mobility, long carrier life, long-distance diffusion, excellent photoelectric performance, and lower production costs, paving the way for perovskite-type solar cells, device efficiency. The remarkable improvement over the second generation is shown in Figure 2.1. Furthermore, in less than a decade of perovskite solar cells, the photoelectric power conversion efficiency has shown a significant improvement. The power conversion efficiency was 3.8% in 2009 (Yang et al., 2017) and increased to 25.2% in 2020 (Feria et al., 2020), reaching the efficiency level of crystalline silicon thin films. This fantastic progress makes perovskite solar cells the best choice for the next generation of solar cells to replace traditional silicon solar cells.

Best Research-Cell Efficiencies

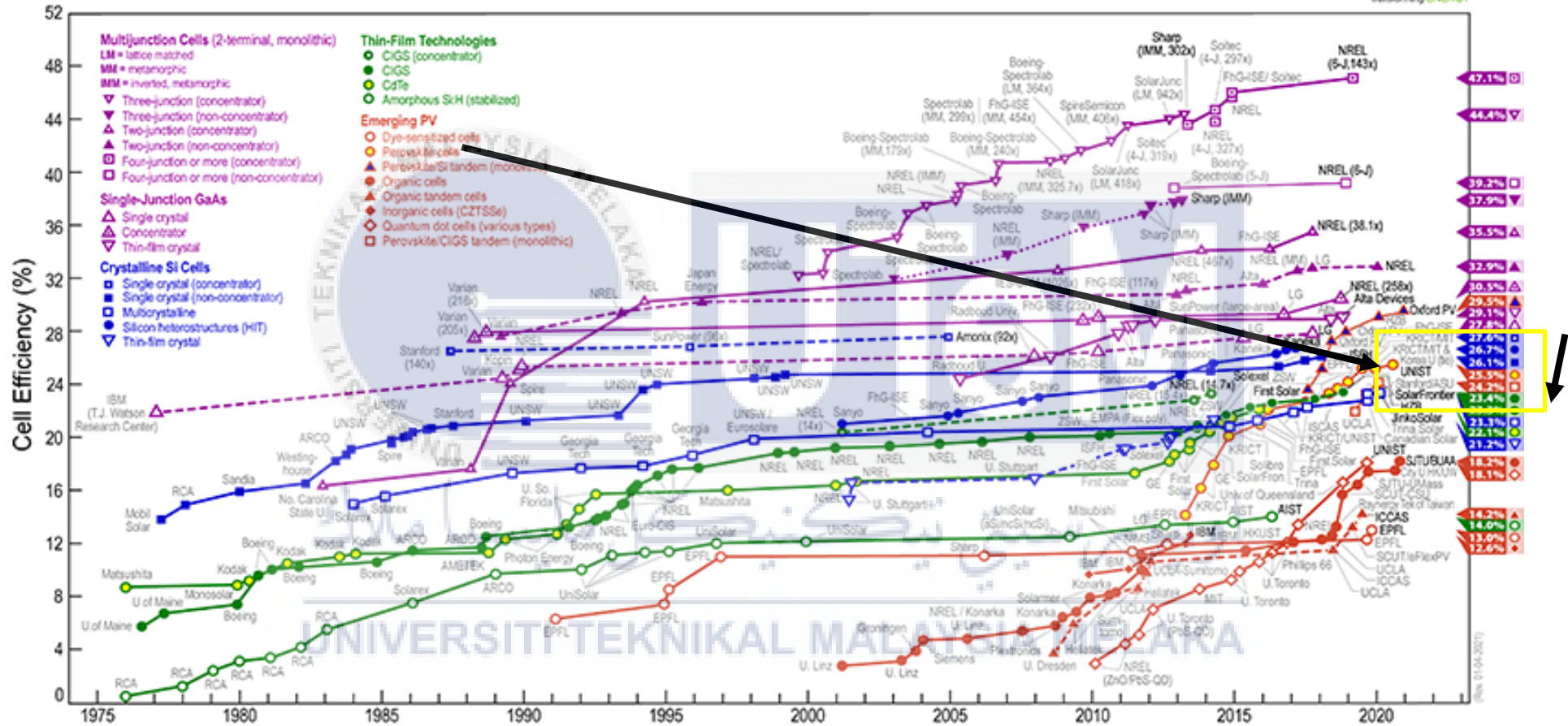


Figure 2.1: Power Efficiency of Solar Cells from 1975 to 2020 (The National Renewable Energy Laboratory Website)

2.1.1 Perovskite Solar Cell Device Architecture

One of the most important considerations for determining the overall efficiency is the perovskite solar cell system design. Perovskite solar cells can typically split perovskite solar cells into two architectures, direct (n-i-p) and inverted (p-i-n) configurations, based on which material transport charges are present on the outer portion the cell met by incident light. Furthermore, in two structures, mesoscopic and planar structures, these two architectures can occur. As seen in Figure 2.2 (A), the mesoscopic architecture consists of a mesoporous layer. As for the planar, it consists of all planar layers shown in figure 2.2. (B). In direct n-i-p architecture, the solar cell is illuminated through the electron-transport layer (ETL) side, while in the p-i-n structure, it is illustrated through the hole-transport layer (HTL) surface shown in Figure 2.2.

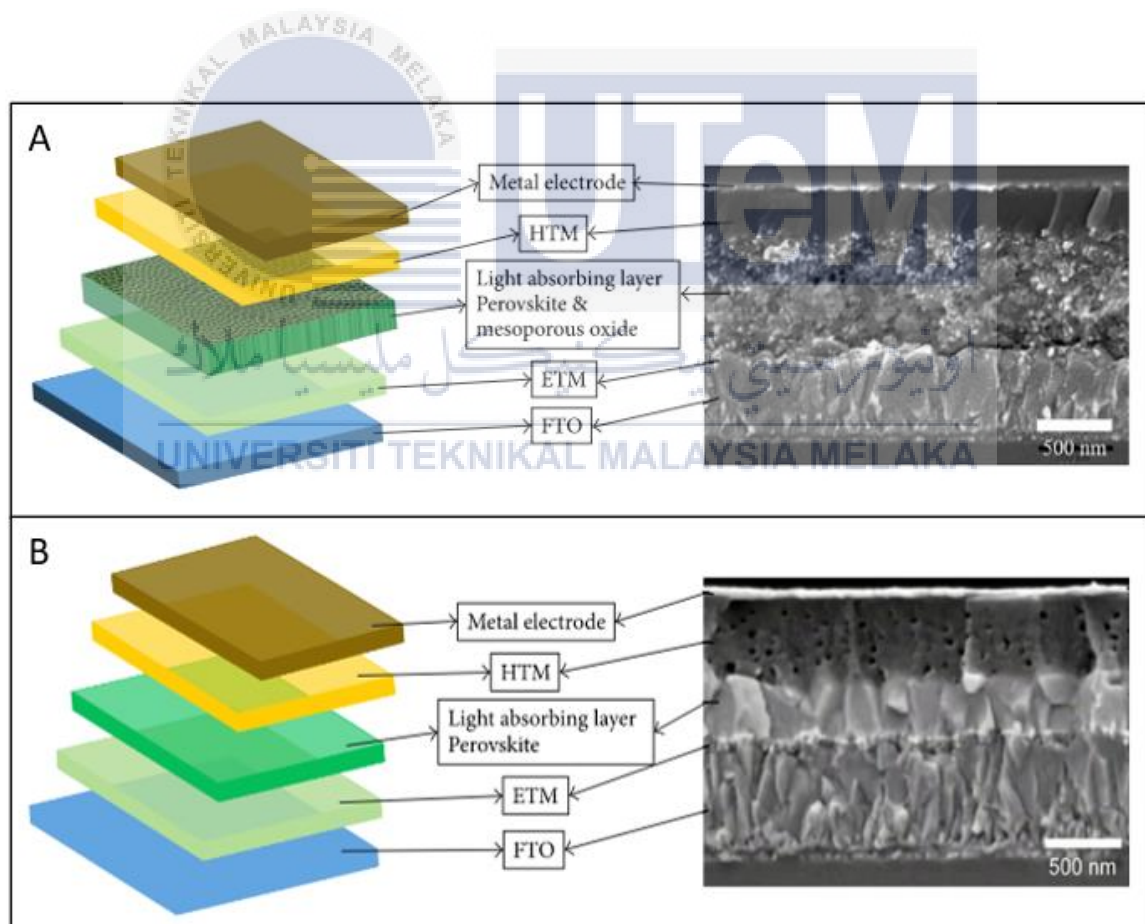


Figure 2.2: A) Mesoscopic and, B) Planar heterojunction structure (Zhou et al., 2018).

The original system structure of studying perovskite solar cells is a direct n-i-p mesoscopic structure. For the natural (n-i-p) architecture, the electron transport material (ETM) is fabricated on top of a transparent conductive oxide (TCO) such as fluorine-doped tin oxide (FTO) or indium tin oxide (ITO). Then a perovskite layer is fabricated, Hole Transport Material (HTM) and top contact electrode. The advantage of the mesoscopic structure is the device performance of PCS efficiency, which has higher performance compared with other architectures (Hussain et al., 2018). For example, the best mesoscopic n-i-p system to date shows a PCE of 21.6% (Saliba et al., 2016), while planar n-i-p cells have the highest recording efficiency at 20.7% (Anaraki et al., 2016).

While mesoporous PSC is recorded to be more efficient than planar, a thinner mesoporous layer is required, which is less than 300 nm (Im et al., 2011). Besides, mesoscopic metal oxide also requires high thermal treatment, resulting in system output destruction and narrowing the roll-to-roll industrial manufacturing process towards versatile device implementation (Safie et al., 2019). These limitations lead to the introduction of planar layers, especially in the inverted (p-i-n) configuration. In this architecture, HTM is deposited onto the TCO while ETM is layered onto the perovskite material before implementing the top contact electrode. Unlike the mesoporous structure, the planar system could produce the planar in a low-temperature process (Shi, 2018).

UNIVERSITI TEKNIKAL MALAYSIA MELAKA

2.1.2 Perovskite Active Layer

When it comes to light harvesting, the active layer of Perovskite is critical since it is responsible for generating the movements of the charges as well as the movement of an electron to the same contact. Active layer main purpose is to collect light while also stimulating the growth of electrons.

2.1.3 ETL (Electron Transport Layer)

Another selective layer of charge that performs essential roles for electron retrieval from the CB of materials of the perovskite ETL. The necessary parameters in the ETL layer are:

1. For a significant electron-accepting feature, high electron mobility.
2. The corresponding energy band should be located marginally lower than that of perovskite materials for the conduction band (CB) or the lowest unoccupied molecular orbital. Ensure effectively injected inside the ETL/perovskite interface.
3. Hydrophobicity and chemical stability improve moisture tolerance and prevent unwanted chemical reactions in the system architecture with other components.

UNIVERSITI TEKNIKAL MALAYSIA MELAKA

2.1.4 Hole Transport Layer (HTL)

HTL plays a role as a whole accumulation in the perovskite/HTL interface. Several criteria need to fulfill for excellent device performance, such as:

1. High hole mobility and low affinity of electrons are useful for electron blocking to inhibit recombination of charges.
2. Compatible energy band fitting where perovskites should be similar to the location of the valence band (VB) or the maximum occupied molecular orbital for efficient hole mobility.
3. Good thermal performance and resistance to humidity to prevent the deterioration of devices.
4. Low expenditure, matched with industrial development.

2.2 Working Principle of Perovskite Solar Cell

The working mechanism of the perovskite solar cell (PSC) begins with the absorption of photons on the outer surface of the perovskite solar cell. When absorbed in sunlight, the absorption produces free electrons (electron-hole pairs). Due to the changes in the binding energy of excitons in the perovskite compound, these excitons can form carriers (free electrons and holes) to generate current or fuse into excitons. As a result, the carrier has a long diffusion distance and long life. Consequently, it leads to a lower possibility of carrier recombination in MAPbI_3 and other perovskite materials and higher carrier mobility. As a result, Perovskite solar cells have excellent performance, longer diffusion time, and carrier lifetime.

In addition, energy orientation also plays an essential role in the perovskite structure. The electron transport layer (ETL) conduction band (CB) should be located near the perovskite material. Exposure of photons in the perovskite material will generate excited electrons. Then, transport materials (ETM) and hole transport materials (HTM) capture these free electrons and holes, respectively. Finally, electrons are transmitted throughout the external circuit and generate photocurrent (Zhou et al., 2018).

2.3 Limitation of Perovskite Solar Cell

The degradation of perovskite solar cells is caused by a variety of reasons, including environmental conditions such as humidity, oxygen, heat, light, and applied electrical bias. Not only that, the temperature and inert conditions of solar cells may cause thermal degradation. The reason affects the instability of the perovskite and reduces its morphology and optical properties.

2.3.1 Problem in the Morphological Properties of Perovskite Solar Cell

In order to maintain the excellent efficiency and stability of the perovskite solar cell (PSC), a high light absorption coefficient (10^5 cm^{-1}) is required to absorb more light in the film, a long carrier lifetime is required to increase the diffusion length of the carrier, and the recombination loss is reduced, and the transport of the load in the perovskite to the collection electrode is very balanced (Miller et al., 2014).

The existence of non-radiative recombination centers caused by defects found on the surface of the perovskite or its grain boundaries will also affect the stability of the system because they will cause various basic properties of the perovskite sheet, such as the circuit voltage limit V_{oc} (Liu (2019 and Stranks et al., 2014). The hole and electron transport layer also play a vital role in the efficiency and stability of the system. The weak energy alignment at these interfaces and the number of surface traps. The chemical reaction causes the degradation of the absorber and the surrounding layer. The thermal loss of their bandgap energy is the main limitation experienced by PSC. The perovskite band defines its optical and electronic properties, such as long carrier lifetime, strong visible light absorption, and complete mobility of holes and electrons (Vasilopoulou et al., 2020). As shown in figure 2.3 is the defects presence at the surface and grain boundaries of the perovskite film (Vasilopoulou et al, 2020) such as uncoordinated ions, vacancies, antisite, cluster of Pb and ion migration at the grain boundaries.

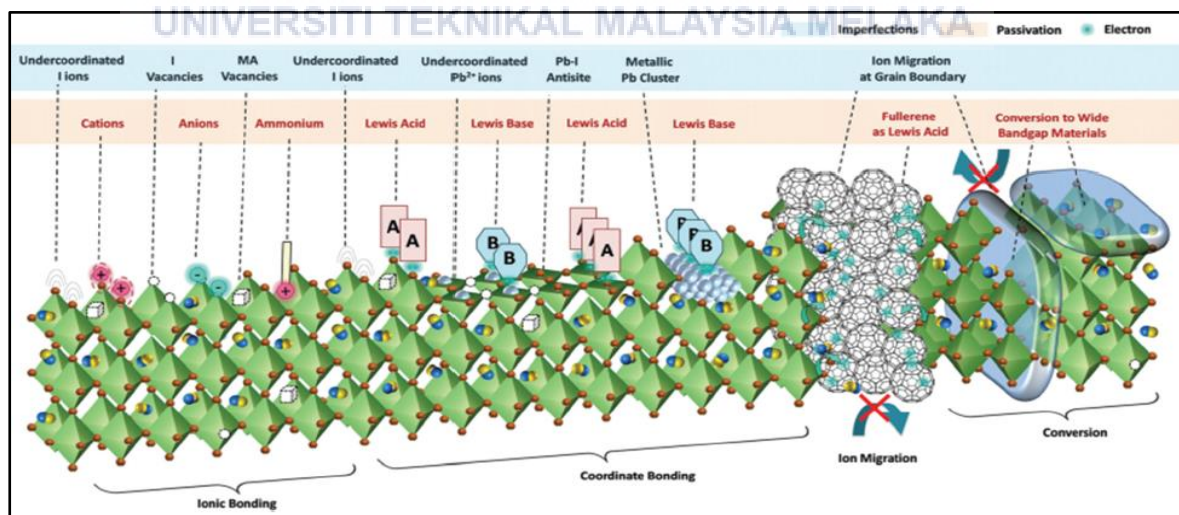


Figure 2.3: The defects presence at the surface and grain boundaries of the perovskite film

(Vasilopoulou et al, 2020).

2.3.2 Problem in the Optical Properties of Perovskite Solar Cell

In order to maintain the excellent efficiency and stability of the perovskite solar cell (PSC), a high light absorption coefficient (10^5 cm^{-1}) is required to absorb more light in the film, a longer carrier lifetime is required to increase the diffusion length of the carrier, and reduce compound loss, and the transport balance between the load in the perovskite and the collecting electrode is good (Miller et al, 2014). In figure 2.4 shown the common problem faced by optical properties of PSC such as vacancy, interstitial, anti-site, substitutional, trap states, line defect and grain boundary defect. Figure 2.4 shown the defect lattice position based on certain defects.

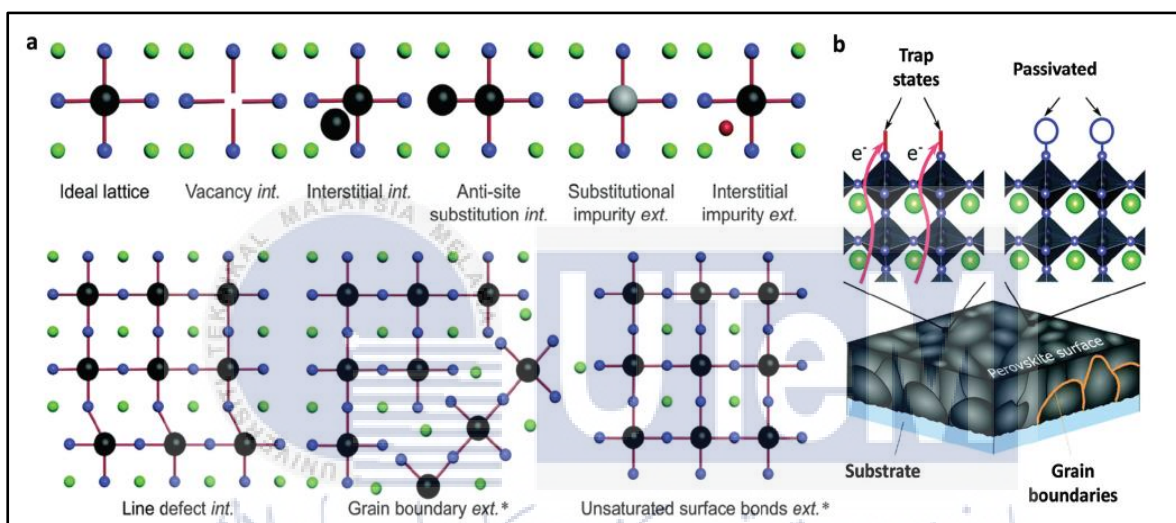


Figure 2.4: (a) Intrinsic characteristics and defects in lead halide perovskite compared ideal lattice.

The figure (b) shows the surface trap and its passivation by introducing other atoms of the molecule represented by the blue circle, which binds to the incorrectly bound orbital, resulting in the trap state. The green, black and blue spheres represent the A, B and X elements, while the gray and red represent different impurities (Vasilopoulou et al., 2020).

2.4 Perovskite Materials in Solar Cell

Perovskite, named after Lev Perovskit, is a mineral with the same crystal structure as perovskite oxide (CaTiO_3), originally discovered in the Ural Mountains (Park et al., 2015). The composition of the perovskite crystal is the general structure ABX_3 shown in Figure 2.5, where A represents a monovalent cation, such as methylammonium (MA), formate (FA), cesium (Cs) and rubidium (Rb). Specific metal cations, such as lead (Pb^{2+}) and tin (Sn^{2+}), and X is a halide anion (I⁻, Br⁻). The variable cubic lattice nested octahedral layered structure of

perovskite materials as shown in Figure 2.5 has tunable optical, thermal and electromagnetic properties, which has led to the application of perovskite materials in solar cells attention.

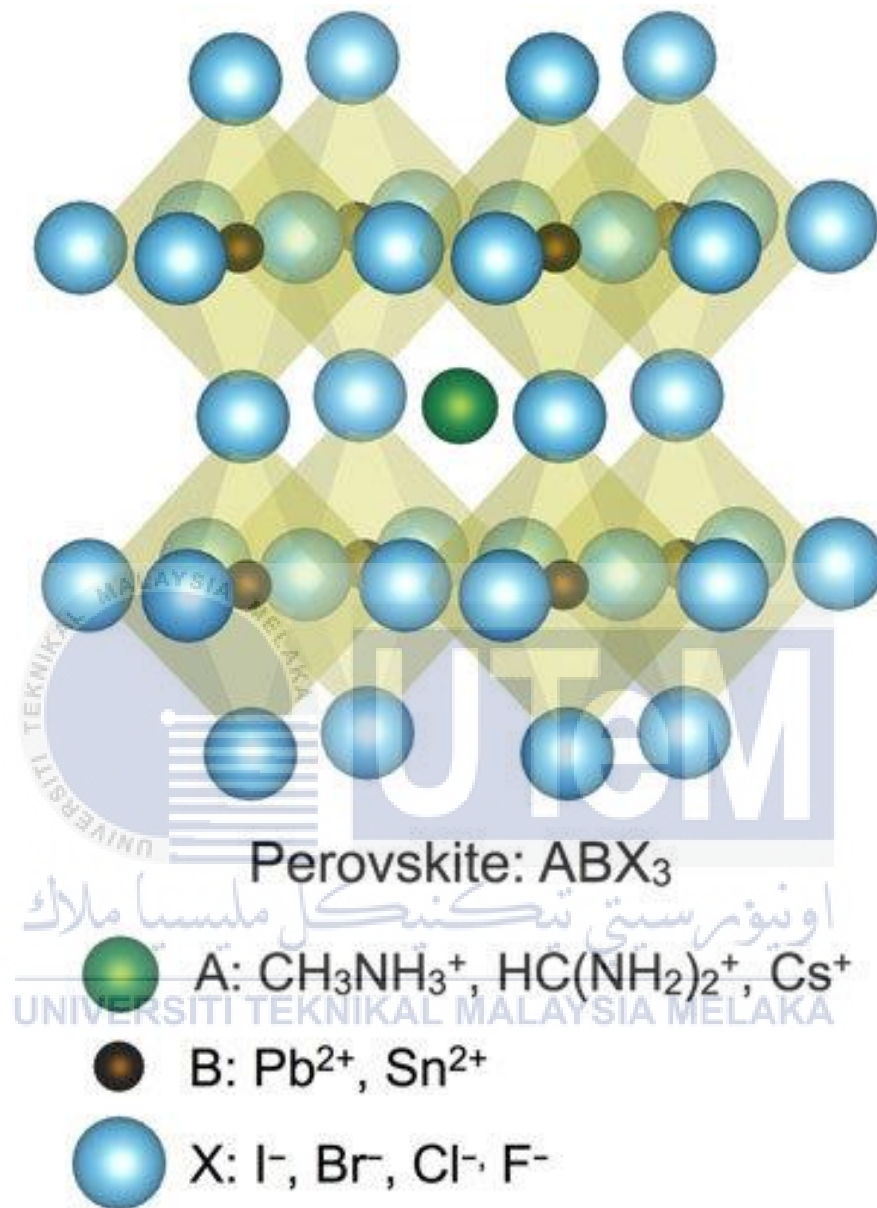


Figure 2.5: ABX_3 perovskite structure (Brittman et al., 2015)

2.4.1 Methylammonium Lead Iodide (MAPbI₃) Based Perovskite Solar Cell

For its various merits, methylammonium lead iodide (MAPbI₃) is one of the most well-known materials utilized by solar cell specialists to produce solar cells. Performance conversion efficiency (PCE) of MAPbI₃ demonstrated is about 20%, with an average efficiency of almost 17 % and minimal hysteresis effects, according to theoretical calculations (Johansson et al. 2020). Furthermore, MAPbI₃ has good photoelectric capabilities, a low exciton binding force, and a high light absorption coefficient, among other characteristics (up to 10⁴ cm⁻¹). The benefits mentioned above contribute to the improvement of the performance of the perovskite active layer in terms of light absorption, which allows it to absorb solar radiation than previously possible more efficiently. Furthermore, the presence of MAPbI₃ in the perovskite active layer contributes to preserving a high dielectric constant, which allows for efficient transit and collection of electrons and holes (Zhou et al., 2018). However, it is also reported to have a tunable bandgap (1.5-1.4eV), high absorption coefficients up to (10⁴-10⁵cm⁻¹), with an increased range of power coefficient efficiency between 14 % and 20 %, low excitation binding energy with a value less than 50meV, tremendous advantages with long-term stability, easy crystallization at low temperature, and simple fabrication as some of its most essential characteristics, among others (Kim, 2019; Leitens and Wang, 2017). According to the study conducted by Zhoe and colleagues in 2014, they discovered that MAPbI₃ is one of the most promising light-absorption materials, as shown by the experiments' results. Light absorption coefficient levels are increased in MAPbI₃, and the bandgap is optimized, as well as the long-range excitation diffusion length is shown in this material.

2.4.2 Graphene-Based Perovskite Solar Cell

Graphene-based materials are the ideal additives for improving the quality of PSCs because of their unique properties. When exposed to halides, graphene materials are passive. These materials are also water-resistant to ion movement, tolerant of a wide range of temperatures, and consistently stable (thus the term "hydrophobic moisture barrier") (Habisreutinger et al., 2016 and Chen et al., 2017). In addition, the increasing industrial-scale production of low-cost and readily accessible carbon-based materials has contributed to the further development of PSCs as commercial products. Santos et al. (2017) found that

graphene-based materials are very flexible and show distinct energy band and electrical characteristic groupings, which may be tuned. They have been implemented in nearly all of the PSC layers currently available or as interface modifications (Hadadian et al., 2020).

2.4.3 Graphene, Graphene Layer, GO, and rGO

Graphene a one-atom-thick sheet of hexagonally organized as shown in figure 2.6 (a), sp^2 -bonded carbon atoms that is not incorporated into a carbon substance but is suspended or attached to a foreign substrate. Graphene's lateral dimensions range from a few nanometers to the macroscale. Notably, additional members of the graphene family of two-dimensional materials cannot simply be termed "graphene." Still, they must be given a distinct multi-word designation that differentiates them from the isolated monolayer (Bianco et al., 2013).

Graphene-layer s shown in figure 2.6 (b), a hexagonally organized, one-atom-thick sheet of sp^2 -filled carbon atoms occurring inside a structure of carbon material, whether or not a graphic structure has an order of 3D (turbostratic or rotationally faulted). "Graph layer" is a conceptual structural unit that describes the structure and texture of 3D carbon materials with primary sp^2 hybridized bonding for several years (Bianco et al., 2013).

Graphene oxide (GO) based on figure 2.6 (c) is a chemically modified graphene produced with a substantial change of the basal plane via oxidation and exfoliation. Graphene oxide is a high oxygen monolayer material defined by atomic C/O ratios of less than 3.0 and closer to 2.0 (Bianco et al., 2013).

Reduced graphene oxide (rGO) shown in figure 2.6 (d) is the photothermal or the micro-bacterial/ bacterial oxide used to reduce its oxidation content by chemical, thermal, microwave, photochemical and photothermal techniques (Bianco et al., 2013).

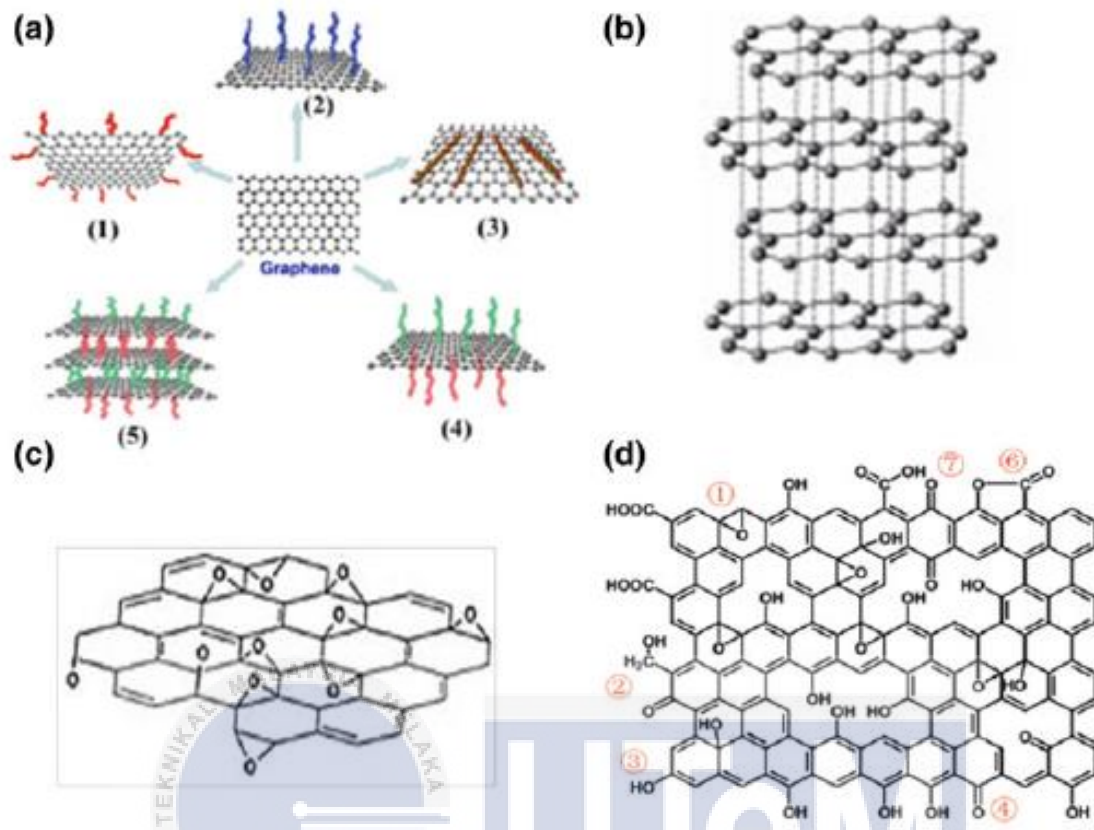


Figure 2.6 Graphene to reduced graphene oxide (Bianco et al., 2013)

2.4.4 Synthesis Methods for Graphite Oxide

Both the "top-down" and the "bottom-up" approaches have been used in synthesizing GO. Initially devised by Hummers and colleagues in 1958, Fujiwara and colleagues (Hirata et al., 2004) later refined the top-down methodology and became recognized as the improved Hummers' method. As shown in figure 2.7, significant portion of this technique includes the exfoliation of bulk graphite to produce graphite oxide. In specifically, the Hummers technique involves the oxidation of graphite using oxidants such as strong sulfuric acid, nitric acid, and potassium permanganate, which results in the formation of GO. The graphite oxide (GO) generated by this oxidative treatment of graphite maintains the multiple-layered structure of graphene (i.e., the material is still in the graphite oxide state). Still, it is much lighter in color than graphite owing to the loss of electronic conjugation caused by oxidation (Stankovich et al., 2007).

Even though many alternative techniques for the synthesis of graphite oxide have been discovered, Hummers' method (and modified Hummers' method) continues to be a significant topic of interest since it is a simple way to generate large amounts of graphite oxide for industrial purposes (Kafle et al., 2019).

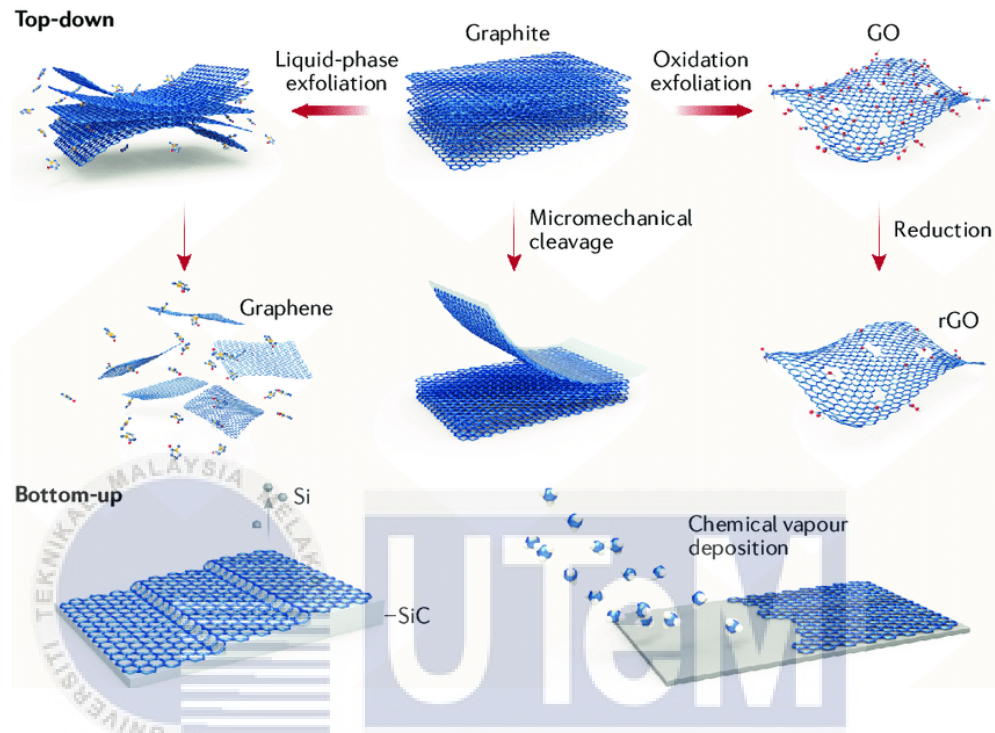


Figure 2.7 Top-down and Bottom-up flow of Graphite to rGO (Stankovich et al., 2007)

2.4.5 Reduced Graphene Oxide (rGO)

MAPbI₃ increases the size of the perovskite grains, resulting in a more uniform and smooth film with enhanced crystallinity and increased crystallinity. The addition of extra rGO perovskite solar cells to a PSC increases the power conversion performance of the associated PSC by about 20% compared to the reference units.

The presence of rGO within the ETL increases conductivity while simultaneously increasing electron transport and charge mobility. This results in the growth of large perovskite crystals with increased crystallinity, which acts as a passive or Perovskite trap state, as demonstrated in this study. Additionally, the presence of rGO in the CH₃NH₃PbI₃ layer causes the size of the perovskite grains to become even more prominent, facilitating

the formation of smooth and uniform films (Balis et al., 2019). The presence of rGO in the architecture of Perovskite solar cells also helps to improve stability, as demonstrated by research conducted by Balis and colleagues in 2019. RGO helps Perovskite maintain its power conversion efficiency (PCE) of 40% for 50 days even when stored in a humid environment with low light. Apart from that, the inclusion of rGO in the design enhances the transit and injection of photo citation electrons while also imparting the hydrophobicity feature to the material (Tarekegne et al., 2019).

2.4.6 Functionalized Reduced Graphene Oxide

In material science, functionalization refers to introducing new functions, features, capabilities, or qualities to a substance by altering the surface chemistry of the importance. Based on our work, we suggest that moderated rGO linking-up with the functionalized group be used to perovskite film as an effective interfacial layer with the goal of passivating the traps. The functionalized reduced graphene oxide is the mechanism of interlayer materials, and it works by integrating the passivation effects of different functionalized organic groups with the hole transfer properties of functionalized reduced graphene oxides. Thus, it is a valuable technique for minimizing energy loss, increasing V_{oc} , and ultimately improving the performance of all-solid-state PSCs (Li et al., 2017). Furthermore, the functionalized rGO also benefits from increasing the efficiency of interfacial electron injection in the electron transport layer (ETL) (Yin et al., 2014). Not only that, but according to the results of prior research conducted by Z. Yin and colleagues published their findings in 2014, they discovered that when functionalized rGO is present in Perovskite solar cells, the structure's stability is enhanced, and that functionalized rGO aids in improving the hydrophobicity of rGO.

2.4.7 Previous Study Results

Based on the journal paper reading, incorporation functionalized GO with methylammonium lead iodide Perovskite thin-film helps in the enlargement of grain size shown in figure 2.8. Figure 2.8 shows the interaction between the sulfonic groups of s-GO with the lead atom of perovskite does make the thin-film better. The perovskite film with s-GO. The result indicates better crystallinity and orientation compared to the one without s-GO (Hu et al, 2020). From this result, it showed that functionalized of graphene based materials helps in increasing the size of methylammonium lead iodide perovskite solar cells.

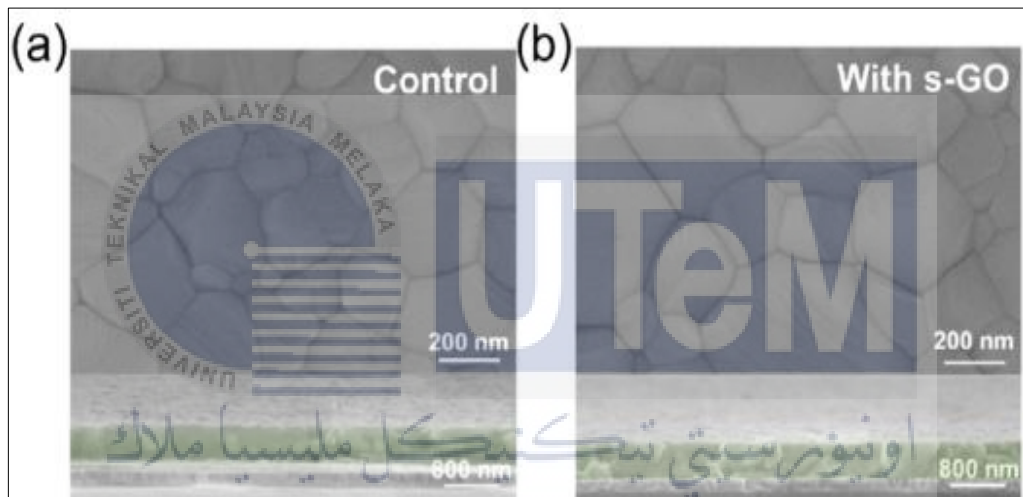


Figure 2.8: SEM image grain of (a) control and (b) s-GO

(Hu et al, 2020).

Moreover, figure 2.9, shows the MAPbI_3 Perovskite thin-film was perfectly modified with functionalized rGO. In this case, experts used polymers based on functionalized materials. The materials used are Perovskite + rGO-g- P_3HT . From the diagram shown in figure 2.9 it shows the enhancement shown in the grain size in is $\text{CH}_3\text{NH}_3\text{PbI}_3$ Perovskite + rGO-g- P_3HT compared to the $\text{CH}_3\text{NH}_3\text{PbI}_3$ + Perovskites (Yousif et al, 2019).

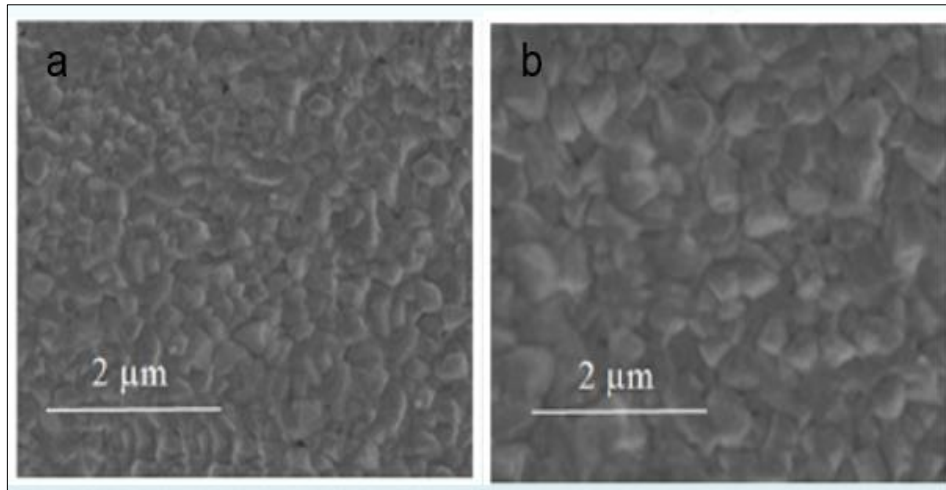


Figure 2.9: SEM image grain of functionalized rGO + Perovskite

(a) $\text{CH}_3\text{NH}_3\text{PbI}_3$ + Perovskites and (b) $\text{CH}_3\text{NH}_3\text{PbI}_3$ + rGO-g-P₃HT (Yousif et al, 2019).

Moving to figure 2.10 shows the graph of Ultraviolet-Visible (UV-Vis) absorption spectra results in the range from 400 to 800 nm in wavelength. One with control (MAPbI_3 Perovskite) and functionalized graphene oxide (MAPbI_3 Perovskite + s-GO). Results obtained showed stronger diffraction intensity in the MAPbI_3 Perovskite + s-GO compared to the MAPbI_3 Perovskite. Further, verifies higher crystallinity and larger grain size of the perovskite films with MAPbI_3 Perovskite + s-GO. The result corresponds to the stronger absorption in the UV-vis spectra by s-GO (Hu et al, 2019).

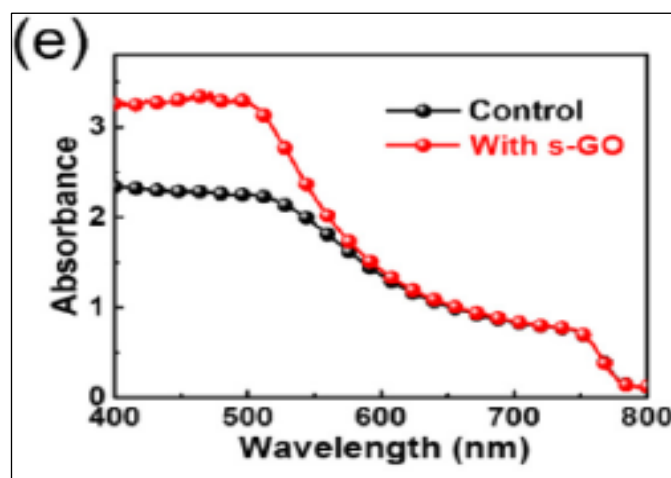


Figure 2.10: UV-Vis absorbance spectra

MAPbI_3 Perovskite and MAPbI_3 Perovskite + s-GO (Hu et al, 2020).

Additionally, figure 2.11 shows UV-Vis absorption spectra by functionalized rGO doped into the materials. From this result, it can be concluded that materials incorporated with functionalized graphene based materials show the highest absorbance ability compared to the one that do not have functionalized graphene based materials. $\text{CH}_3\text{NH}_3\text{PbI}_3 + \text{rGO-g-P}_3\text{HT}$ and $\text{CH}_3\text{NH}_3\text{PbI}_3 + \text{CNT-g-P}_3\text{HT}$ are the toppers among other five types of mixture. Both of these material mixtures possess the largest absorbance light intensity level. Conclusion, the functionalized graphene based materials helps in enlargement of the MAPbI_3 perovskite grain size and increase in the optical absorbance ability.

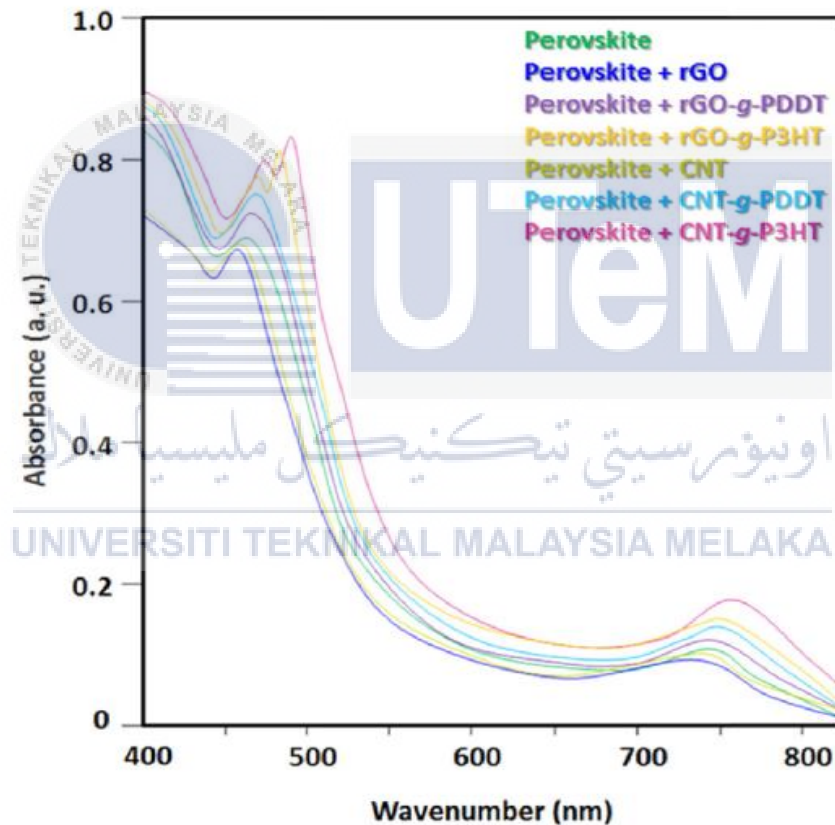


Figure 2.11: UV-Vis absorption spectra of functionalized rGO

$\text{CH}_3\text{NH}_3\text{PbI}_3 + \text{rGO-g-P}_3\text{HT}$ and $\text{CH}_3\text{NH}_3\text{PbI}_3 + \text{CNT-g-P}_3\text{HT}$ with largest absorbance (Yousif et al, 2019).

Next, the structural properties of PSC with doped of S-rGO. Using an experiment from Guo et al., 2017, authors experimented on the Perovskite solar cells' efficiency is increased via the synergetic impact of sulfated graphene oxide (sGO) hole transporting layer. Authors implement sulfated graphene oxide (sGO) as an HTL in place of the more often utilized graphene oxide (GO) to see the difference in the efficiency of Perovskite solar cells. Study on structural characteristics of the S-GO in this research analyzing by the Raman Spectroscopy findings from the conducted experiment. The following section will discuss the interpretation of the G and D bands.

From the reading, the authors characterize the structural features using a Raman spectrometer (Renishaw) equipped with a 514 nm laser. The Raman spectroscopy of the GO and sGO powders was used to describe them further, as seen in the figure below. In particular, it exhibits two significant peak regions, including a strong G peak, which also addresses a G band indicating 1590 cm^{-1} , and a D peak, also common as a D band showing 1350 cm^{-1} . The intensity of the sp^2 G band is linked to the vibration of bonded carbon sp^2 atoms. This analysis supported by Palma et al, .2016, as shown in figure 2.13 the G peak is related to the in-plane vibration of sp^2 hybridized carbon atoms located near 1580 cm^{-1} . Meanwhile, the intensity of the D band is related to the distortion in the sp^2 carbon atoms. The D band located near 1350 cm^{-1} results from vacancies or dislocations in the graphene layer and at the edge of this layer. This band is also related to the presence of defects in the material. From the figure below 2.12, the relative intensity ratio I_D 700 a.u and I_G 686 a.u resulting (I_D/I_G) for GO is 1.02, while the intensity ratio sGO, I_D 2000a.u and I_G 1941a.u resulting the (I_D/I_G) for sGO is 1.03.

In particular, the D band's relative intensity ratio (I_D/I_G) to the G band indicates the size of the in-plane sp^2 domains and the degree of structural disorder in the carbon atoms and molecules. The intensity of both the D and G bands is substantially enhanced once the sulfonation process is completed. While the only slightly greater power of I_D/I_G ratio is found for sGO powder, this suggests that oxygen groups in the basal plane of the second phase have decreased and that there are more isolated C domains in sGO powder compared to the first phase of the phase diagram. Proven that, D peak for both Raman shifts higher compared to the G peak. Results show more elevated in the D peak after the sulfonation process is carried out and lower in the G peak. In conclusion, they result in the low plane vibration of sp^2 hybridized carbon atoms and an increase in the presence of defects in the material.

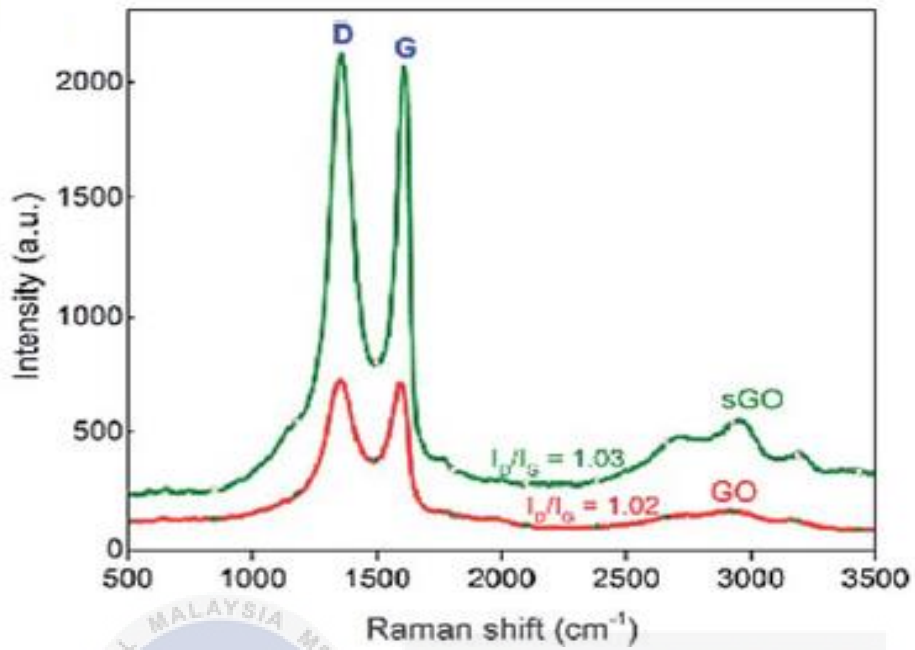


Figure 2.12 Raman spectra of GO and sGO and I_D/I_G ratio of both spectra (Guo et al., 2017)

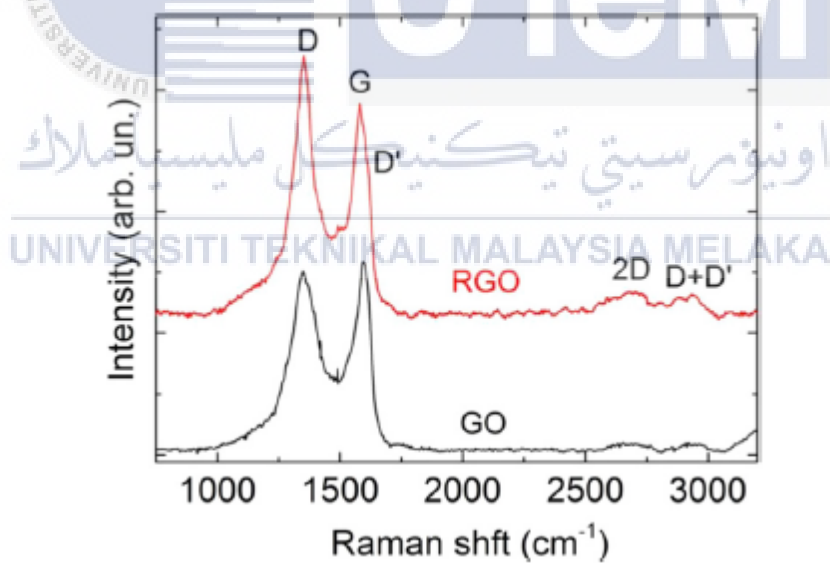


Figure 2.13 Raman spectra of GO and rGO and I_D/I_G ratio of both spectra (Palma et al., 2016)

2.5 Characterization Method

2.5.1 Scanning Electron Microscopy

In material science, scanning electron microscopy (SEM) is widely used to examine grain orientation, shape, and size (morphology), surface conditions (topography), the compound and element makeup of the material (composition), and the arrangement of atoms (crystallography). This method is more powerful than optical microscopy for seeing the surface structure of materials since the SEM's depth focus is more significant (Meyer et al., 2016). SEM's fundamental operating concept began with accelerating a high-energy electron via lenses and apertures to produce a fine electron beam. The electron beam is then focused on the material, and the emitted electrons are analyzed to get an image. SEM methods need the use of an electron, a magnetic lens, focus electrons, electron detectors, chambers, a cathode ray tube, and a computer system for image analysis (Singh et al., 2016). SEM can produce an image of particles as small as 1nm, a detailed picture of the material's surface conditions. SEM is classified as a superior characterization method based on its characteristics, even though the material's internal structure cannot be analyzed when the technique is used. SEM is used to study the morphological changes in a material after physical or chemical changes. SEM is another method that may magnify pictures up to 300,000 times and provide high-resolution images when appropriately used (Akhtar et al., 2018).



Figure 2.14: Scanning Electron Microscopy

2.5.1.1 Working Principle of SEM

To acquire visuals of a sample, an electron microscope scans the surface of a sample with a focused stream of electrons. SEM stands for scanning electron microscopy. For example, when electrons contact atoms on a sample's surface, they generate a variety of signals that include information about the surface topography and composition of the sample. Therefore, instead of using glass lenses to focus, defocus, magnify, or collimate the electron beam, magnetic lenses are used to achieve the desired results. The surface of materials is mainly examined using scanning electron microscopy (SEM). The observed samples are usually 1x1x1 cm in size and may be made out of any material except glass. If the material is not electrically conductive, thin gold or carbon coating is applied to prevent electron charging and image degradation from occurring as shown in figure 2.13.

The electrons emitted by the electron cannon initiate the functioning of the SEM. First, an accelerator with a voltage ranging from 1 to 30 kV accelerates the electrons, which are subsequently demagnified by a pair of condenser lenses. Following that, a sequence of scanning coils is used to compel the electron beam to scan over a specimen area, while magnetic lenses are used to focus the laser beam on the sample itself. Last but not least, a detector will pick up on the signal produced by the electron-sample interaction. The specimen may be seen when viewed in secondary or backscattered mode.

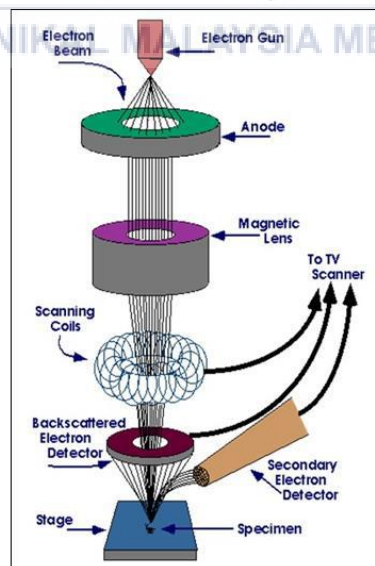


Figure 2.15 Scanning Electron Microscope working illustration (Scanning Electron Microscopes - EVOCD (2017, April 12).

2.5.2 Raman Spectroscopy

As a non-destructive chemical analysis technique, Raman spectroscopy gives comprehensive information on the chemical composition, phase, crystallinity, and molecular interaction of a sample. It is based on the interaction of light with chemical bonds in the matter to function. Raman investigated the variations in the polarizability of molecular bonds as a function of time. When the light comes into touch with a molecule, the electron cloud inside it will distort. According to this definition, the deformation represents a change in the polarization rate. Because of the unique energy conversion of the chemical bond, in which the polarizability conversion takes place, the Raman active modes are generated as a result. Polarizability varies, for example, when a molecule has bonds between homonuclear atoms such as carbon-carbon, sulfur-sulfur, and nitrogen-nitrogen, as well as bonds between photons and other molecules. Spin-coated absorber-grade perovskite films based on methylammonium (MA) lead iodide (MAPbI_3) will be investigated for Raman use in perovskite-type methylammonium solar cells, as well as for the application of Raman in other solar cell types. It is possible to acquire 532 different excitation wavelengths using Raman spectroscopy. Last but not least, Raman spectroscopy can be used to determine the necessary characteristics of photovoltaic materials, such as film thickness, crystal structure, defect density, and composition, as well as to use as a compact and fast quality management and process monitoring tool (Pistor et al., 2016).



Figure 2.16: Raman Spectroscopy

2.5.2.1 Working Principle of Raman Spectroscopy

The Raman spectroscopy method is a complement to the infrared approach and is, in theory, similar to the latter way. It does, however, make use of a laser (monochromatic light) as well as scattered light as a source of illumination. When lighting a sample, it is common to practice utilizing a laser beam. A lens gathers light from the illuminated region and transmits it to the camera via a filter. It is possible to filter out elastic Rayleigh scatterings since the wavelength of the reflected beam and incident beam is identical. The remaining light may then be distributed onto a detector. The dispersed light is produced by two types of scattering: Rayleigh scattering and Raman scattering. Rayleigh scattering, in which the elastic scattering occurs at the same frequency as the incoming beam and has a high intensity, while Raman scattering, which is inelastic and occurs at frequencies higher or lower than the incident beam, has a lesser intensity at higher or lower frequencies.

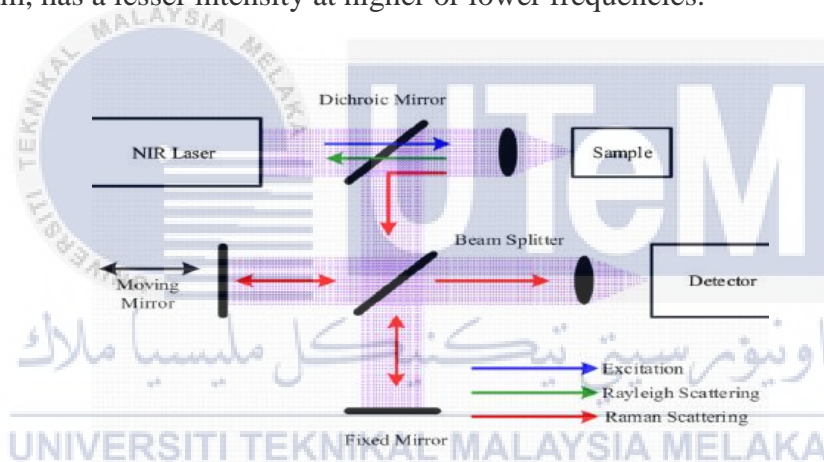


Figure 2.17 Raman Spectroscopy working illustration (Yohk co.ltd. (2020, October 15))

Raman spectroscopy is widely utilized in chemistry because the vibrational information it provides is unique to the chemical bonds and symmetry of molecules. Examples include the characterization of materials, the measurement of temperature, and the determination of crystallographic orientation using spontaneous Raman spectroscopy in solid-state physics.

2.5.3 Ultraviolet Visible Spectroscopy

Ultraviolet-visible light refers to the visible components of the absorbed ultraviolet spectrum and the electromagnetic spectrum. As the molecule absorbs photons (usually starting from a single ground state) it becomes an excited state molecule. According to the selection law of quantum mechanics, the molecule will be in a single excited state. UV-Vis spectrophotometry is a tool for measuring the absorbance in the ultraviolet and visible regions of the electromagnetic spectrum. When incident light reaches the sample, it may be absorbed, reflected or emitted. UV-VIS is a cheap and easy-to-use technology. For street samples involving complex mixtures, it requires fewer applications.



Figure 2.18: Ultraviolet Visible Spectroscopy

2.5.3.1 Working Principle of Ultraviolet Visible Spectroscopy

UV spectroscopy is a kind of absorption spectroscopy in which light in the ultraviolet range (200-400 nm) is absorbed by a molecule, resulting in the excitation of electrons from the ground state to a higher energy state. UV spectroscopy is used to study the structure of molecules. Spectroscopy, in its most basic definition, is the study of the interaction of light with matter. As light is absorbed by matter, the energy content of the atoms or molecules increases as a consequence of the absorption of light. Tungsten filament lamps and Hydrogen-Deuterium lamps are the most commonly used and most appropriate light sources since they span the whole ultraviolet range of the visible spectrum. Tungsten filament lights produce a high concentration of red radiations; more precisely, they emit

radiations at a wavelength of 375 nm, while the intensity of Hydrogen-Deuterium lamps is below this wavelength.

This occurs in the excitation of electrons from their ground state and into a higher energy state when a material absorbs UV radiation. UV-light-absorbing molecules with π -electrons or nonbonding electrons (n -electrons) may be excited to higher anti-bonding molecular orbitals by absorbing energy in the form of ultraviolet light. The longer the wavelength of light absorbed, the more readily the electrons stimulated. There are four different kinds of transitions ($\pi \rightarrow \pi^*$, $n \rightarrow \pi^*$, $\pi \rightarrow \pi^*$, and $n \rightarrow \pi^*$), and they are arranged in the following order: $\pi \rightarrow \pi^* > n \rightarrow \pi^* > \pi \rightarrow \pi^* > n \rightarrow \pi^*$. The absorption of UV light by a chemical compound will result in the formation of a unique spectrum, which is used to identify the chemical component referred by Rocha et al., 2018.

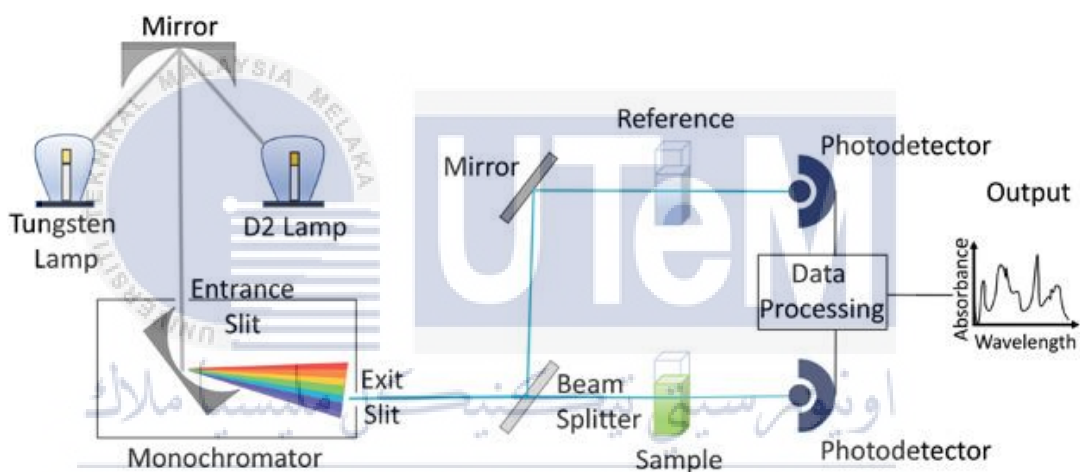


Figure 2.19: Working principle of ultraviolet visible spectroscopy (Rocha et al., 2018).

2.6 Material Preparation Method

2.6.1 Chemical

Chemical is a substance used in the process or reaction involving modifications or alterations of atoms or molecules. Generally, chemistry has been classified into five main subcategories. There are organic, analytical, physical, inorganic and biochemistry. Chemical reactions happen when chemical bonds within atoms are created or destroyed. The component that is linked in the chemical reaction process is called reactants, and the substances that formed after the reaction are defined as the products.

2.6.2 Preparation of MAPbI₃

Previous studies shown that the preparation methods for MAPbI₃ films can be distinguished into three different synthesis routes. There is a one steps spin-coating method followed by two-step spin coating methods.

One Spin Coating Method:

The first method for producing deposited MAPbI₃ films is based on a one-step spin-coating procedure. This technique is often used in the production of high-efficiency solar cells. The following is a breakdown of the preparation process. Following that, the sample was deposited using a one-step spin coating process at a speed of 4000 rpm, followed by a drying process. Following that, a 0.4M solution was produced by dissolving equimolar quantities of PbI₂ and MAI in -butyrolactone and mixing them together. Alternate between toluene anti-solvent treatment and annealing the sample for 10 minutes at a temperature of 110 degrees celsius. Additionally, the spin coating method was the same as that utilised for the MAPbI₃ sample growth in order to produce MA_xFA_{1-x}PbI₃ films with distinct MA/FA molar ratios (G. Gordillo et al., 2020).

Two-steps Coating Method with Layer of PbI_2 is deposited by Conventional Evaporation

The contemporary two-step technique for producing methylammonium lead iodide is the second approach available today. The conventional evaporation technique is used to operate the technology on the PbI_2 film, which is then annealed in the air using the typical evaporation method at a temperature of 200°C for 40 minutes after being exposed to the heat. The program was then switched to the immersion phase for 30 minutes in a 0.031 M MAI solution dissolved in butanol, and the results were recorded. The $MAPbI_3$ film was then annealed in air at 100°C for a total of 30 minutes (G. Gordillo et al., 2020).

Two-steps Coating with Second Layer of MAI (methylammonium iodide) is deposited by Dipping and CSS (close spaced sublimation) Method

The third technique, which was developed using the same two-step procedure, was utilised to produce methylammonium lead iodide. However, there are two measures that must be taken into consideration this time. Next the deposition of the PbI_2 layer using a standard evaporation technique, the CSS procedure is carried out in the following phase. A heating ramp that maintains a steady heating rate is used to heat the evaporation source until a final temperature of 290°C is achieved within 20 minutes is used to conduct the CSS deposition process of the MAI film. Afterwards, it is annealed in air at a temperature of 110°C for 15 minutes at room temperature. Figure 2.18 depicts a schematic representation of the method that was utilized to produce MAPI membranes in accordance with the two-step approach previously described by G. Gordillo et al (2020).

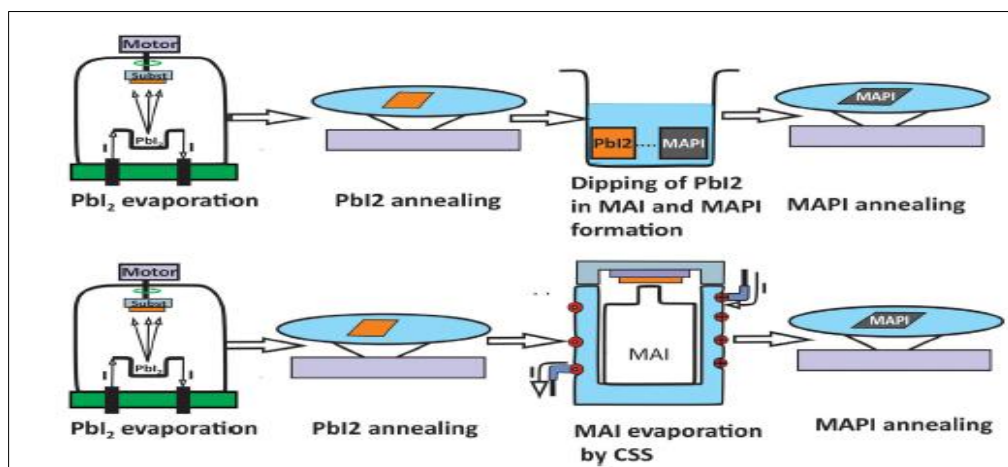


Figure 2.20: The procedures to prepare MAPI films using the two-step routes.

Yang et al., 2018 used the technique to synthesis MAPbI₃ using the DMF as solvent. DMF was used to dissolve 553.2 mg PbI₂ (1.2 mmol) and 190.8 mg MAI (1.2 mmol) (0.70 mL). As a result of this stirring, the solution remained at ambient temperature overnight. The concentration of hydrochloride was then altered by adding different amounts of HCl/DMF. An additional 1.0 mL of DMF solvent was added to the final solution to make it 1.0 mL total.

2.6.3 Preparation of Reduced Graphene Oxide

Reduction of graphene oxide may be split into two stages, which many authors have argued. It is possible to accomplish this reduction by using ascorbic acid or sulfuric acid as the reducing agent. Ascorbic acid is used as a reducing agent to decrease graphene oxide, which is then reduced further. GO powder is dispersed in purified water in the first stage of preparation, which involves dissolving 400 mg in 400 ml (0.1 mg•ml⁻¹) of pure water. In the next step, 4g of ascorbic acid (AA) was added to the solution and agitated with a magnetic stirrer for 30 minutes at a temperature of 60 °C. After 40 minutes, the decreased liquid was centrifuged at 4000r/s for 10 minutes to remove the supernatant, which was then discarded. The surplus is then calculated as 30% of the total weight. During 30 minutes of stirring at 60°C, % of H₂O₂ was bound to the black paste, allowing it to be used to oxidise the remaining ascorbic acid. A black material was produced after mixing by centrifugation at 4000 r/s for 30 minutes, followed by three washes with ethanol and clean water, followed by dehydration at 120°C for 24 hours. The process of producing reduced graphene oxide (rGO) is divided into three stages: oxidation or intercalation, exfoliation, and reduction (in that order).

The process of oxidation or intercalation starts with a reaction between graphite powder and the powerful oxidant potassium permanganate, which results in the formation of GTO. The combined H₂SO₄/H₃PO₄ (9:1) (v/v) solution was then allowed to settle for 12 hours in a water bath at 50°C. H₂SO₄ is the most well-known intercalation agent that is frequently used. To carry out the exfoliation process in order to shape a single layer of graphene oxide, scatter the oxidised form of graphite in distilled water until it is completely dissolved (GO). Following that, the solution was heated in a water bath to 60°C in order to produce a black paste. 12 hours in a magnetic stirrer using a magnetic stirrer. After many

rounds of filtering and centrifugation, a black paste was produced, which was then dried at 60°C for 24 hours.

It was necessary to complete the reduction process in order to manufacture the graphene oxide that had been reduced (rGO). In this procedure, the GO acquired through exfoliation is distributed throughout the solution. As a reduction agent, ascorbic acid was first added and then heated at 60 °C for 30 minutes to activate it. Following that, the decreased material is removed via the use of filtering and centrifugation. The black paste was then rinsed three times with ethanol and filtered water, and the process was repeated. Last but not least, the product was gathered and dried in an oven at 120 °C for 24 hours.

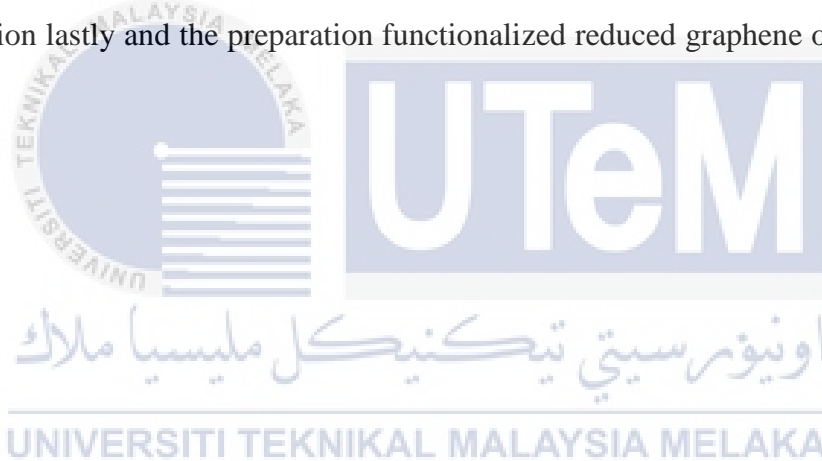
While this was going on, 1 g of graphite flakes (99 %, Alfa Aesar) were introduced to 50 mL of concentrated sulfuric acid (98 %, Merck), which was then stirred in an ice water bath, and the graphene oxide was reduced by sulfuric acid. Continue by adding 3 g of potassium permanganate (>99 %, Sigma Aldrich) at a rate of 1 g per minute while maintaining a temperature below 10°C. After that, the mixture was mixed at ambient temperature for 25 minutes before being sonicated in an ultrasonic bath (SO-TEC, MUY-4) for 5 minutes to complete the procedure. In the next steps, the stirring and ultrasonic treatment were repeated 12 times, and the reaction was quenched by adding 200 mL of distilled water to the mixture.

After that, the process continue with the ultrasonic therapy for an additional 2 hours. After lowering the pH to 6 by adding 1M sodium hydroxide (>98 %, Sigma Aldrich) solution, the suspension was further sonicated for 1 hour to remove any remaining contaminants. After that, 10 g of L-ascorbic acid (99 %, Sigma Aldrich) added and dissolve it in 100 mL of distilled water before moving on to the next stage. Meanwhile, at room temperature, exfoliated graphite oxide was progressively added to the solution to make it more stable. The reduction was carried out at 95 C for one hour. In order to achieve neutral pH, the black precipitates were filtered through cellulose filter paper and then washed with a 1M hydrochloric acid solution (37 % concentration, Merck) followed by distilled water to remove any remaining acid. After that, the filtrate was freeze-dried to produce the final product (D. Morales-Acosta et al, 2019).

2.6.4 Preparation of Functionalized rGO (S-rGO)

According to Eda et al (2020) preparation of the functionalized rGO starts by the rGO was dispersed in 150 mL of filtered water to achieve the desired dispersion. Then put the mixture in a water bath for a few minutes. The diazonium salt solution (sulfanilic acid, 1 N HCl, and 10 mL of purified water) had been previously produced and progressively added to the rGO-pure water combination in the water bath at 0 °C. Next, followed by stirring the mixture overnight at room temperature, filtration, washing with distilled water (3 × 20 mL), and drying in a vacuum oven set at 80 °C.

The study above used as guidance in the experiment that executed in the chapter 3. Preparation of MAPbI₃ carried out by two-step coating layer followed by MAI, preparation of reduced graphene oxide that will start using raw graphite flakes and undergo oxidation and exfoliation lastly and the preparation functionalized reduced graphene oxide by Eda et al, 2020.



CHAPTER 3

METHODOLOGY

3.0 Introduction

This chapter discusses the method for this specific study topic throughout this chapter. Every stage of the research procedure is covered in detail in this chapter, which will begin with a list of the chemicals used in this study and work its way through them. This chapter focused on three significant subjects. The MAPbI₃ manufacturing method, reduced graphene oxide (rGO), and functionalized graphene oxide sulfonation (S-rGO). This chapter described a method for producing functionalized reduction graphene oxide. Perovskite thin films were created utilizing various S-rGO composition ratios, beginning with 0%, 20%, and 40% methylammonium lead iodide (MAPbI₃) solutions. Raman spectroscopy is used to analyze S-rGO to determine whether or not the sulfonation process has been finished, and the vibration of sp² carbon vibration is maximum. Following that, the scanning electron microscopy (SEM) approach for assessing the morphological and optical properties of the perovskite was integrated with S-rGO utilizing an ultraviolet-visible spectrophotometer (UV-Vis) reported.

3.1 Flow Chart of Research Methodology

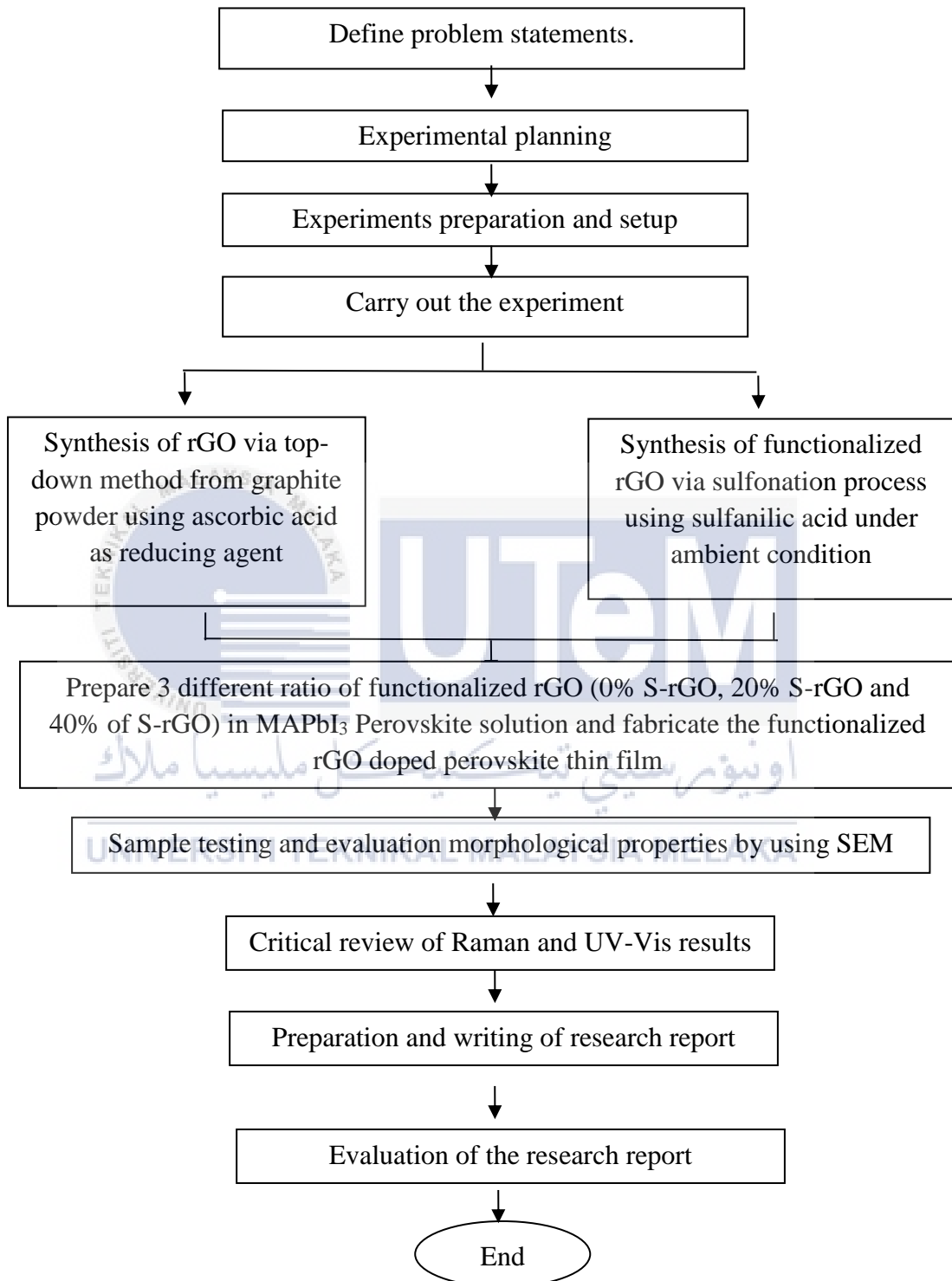


Figure 3.1: Flow Chart of Research Method

3.2 List of Chemicals

According to the table below, the chemical will be used to produce the materials MAPbI₃, reduced graphene oxide, and sulfonated reduced graphene oxide in a particular amount, refer source from National Library of Medicine, National Center for Biotechnology Information

Table 3.1: Table of the list chemical used in the material preparation of MAPbI₃.

<p>50 mg Methylammonium iodide (MAI)</p> 	<p>The organic halide CH₃NH₃I stands for methylammonium iodide. It's an ammonium salt with methylamine and iodide. Methylammonium iodide is used in perovskite crystalline solar cells.</p>
<p>46 mg Lead iodide (PbI₂)</p> 	<p>Lead iodide uses to make high-efficiency solar cells.</p>
<p>0.8 ml Dimethylformamide (DMF)</p> 	<p>Dimethylformamide (CH₃)₂NC(O)H is a chemical substance. It is a colourless liquid that is miscible with water and most organics. In this process, DMF act as the dispenser for the PbI₂.</p>

0.2 ml Dimethyl sulfoxide (DMSO)





DMSO is an organosulfur compound ($(\text{CH}_3)_2\text{SO}$). In this process, DMSO act as the dispenser for the PbI_2 .

2 ml Isopropyl alcohol (IPA)



IPA contributes to PbI_2 dispersibility, making it the ideal candidate for generating a smooth surface and a low crystalline (small crystal-sized) PbI_2 layer.

Table 3.2: Table of the list chemical used in the material preparation of rGO.

<p>1 g Graphite flakes</p> 	<p>Graphite is a natural crystalline carbon substance. It is found in metamorphic and igneous rocks. Extremes abound in graphite. It is exceedingly soft, cleaves easily, and has a low specific gravity. It is, nevertheless, heat resistant and virtually inert when in contact with other materials.</p>
<p>50 ml Sulphuric acid</p> 	<p>Sulfuric acid is a mineral acid having the chemical formula H_2SO_4. Unscented and colorless viscous liquid that dissolves in water. Sulfuric acid is also used to dehydrate or oxidize. Hummer's technique uses sulphuric acid and potassium permanganate to make rGO.</p>
<p>3 g Potassium Permanganate</p> 	<p>Potassium permanganate ($KMnO_4$) is an inorganic compound made up of K^+ and MnO_4^-. It's a pink or purple crystalline salt that dissolves in water. Potassium permanganate is a powerful oxidizing agent utilized in chemistry and biology.</p>








<p>400 ml Distilled water</p> 	<p>Distilled water is water that has been heated into vapor and then condensed into liquid. Impurities in the initial water that do not boil stay in the original container. Distilled water is cleansed water.</p>
<p>10 g Ascorbic acid</p> 	<p>L-ascorbic acid is a white to pale yellow crystalline powder with a pleasant acidic flavor. Almost completely devoid of odor. Ascorbic acid is a naturally occurring water-soluble vitamin that is both environmentally friendly and harmless. It is also a green reductant and a natural reducing agent that has a moderate reducing capacity and is nontoxic.</p>
<p>1 M Hydrochloric acid</p> 	<p>Pickling processes utilize hydrochloric acid to remove rust and other impurities from carbon. It is a water-based solution. HCl is a very caustic, powerful acid that appears clear/colorless or light yellow in liquid form. HCl has a strong odor and is very corrosive in its concentrated liquid state.</p>

Table 3.3: Table of the list chemical used in the material preparation of S-rGO.

<p>75 mg rGO</p> 	<p>In contrast to reduced graphite oxide, which is produced by graphite oxidation and allows for larger basal graphite plane spacing and function, graphite oxide is the material formed by graphite oxidation.</p>
<p>150 ml Distilled water</p> 	<p>Distilled water is vaporised water that is subsequently condensed. Impurities in the initial water do not boil off. Distilled water is purified.</p>
<p>46 ml Sulfanic acid</p> 	<p>H₂SO₄, a colorless, odorless, highly corrosive, greasy liquid. It's also called vitriol oil. A good electrophile requires sulfuric acid. Sorbic acid protonates Nitric acid to produce Nitrium (water molecule is lost). Benzene may assault the nitronium ion.</p>
<p>1 M Hydrochloric acid</p> 	<p>Pickling uses hydrochloric acid to clean carbon of rust and other impurities. Water-based solution HCl is a strong caustic acid that is clear/colorless or pale yellow in colour. HCl has a pungent odour and is caustic when concentrated.</p>

3.3 Preparation of Materials

Synthesis process needs to be carried out for methylammonium lead iodide (MAPbI_3), reduced graphene oxide (rGO) and functionalized reduced graphene oxide.

3.3.1 Methylammonium Lead Iodide

In order to fabricate thin layers later on, the preparation of MAPbI_3 can be divided into two solutions. The preparation of the MAI solutions comes first, followed by the preparation of the PbI_2 solutions.

The PbI_2 solutions begin by weighing 0.416g of PbI_2 on an automated scale as shown in figure 3.2. Next, the PbI_2 was mixed with 0.2 mL of DMSO and 0.8 mL of DMF in a small container for stirring as shown in figure 3.3 and figure 3.4. Pipette used to measure the volume of DMF and DMSO for precise. A pipette is a scientific equipment that is used to measure out or transfer small amounts of liquid in millilitres (mL) or microliters (μL) volumes. The container was then placed on the magnetic stir plate and easily stirred at 500 rpm with an aid magnetic stirrer measuring 4mm x 10mm in size as shown in figure 3.5. The stirring operation lasted 3 hours at a temperature of 60 °C. Final solution of PbI_2 shown in figure 3.6.



Figure 3.2 Weight of PbI_2



Figure 3.3 Pipetting the DMSO

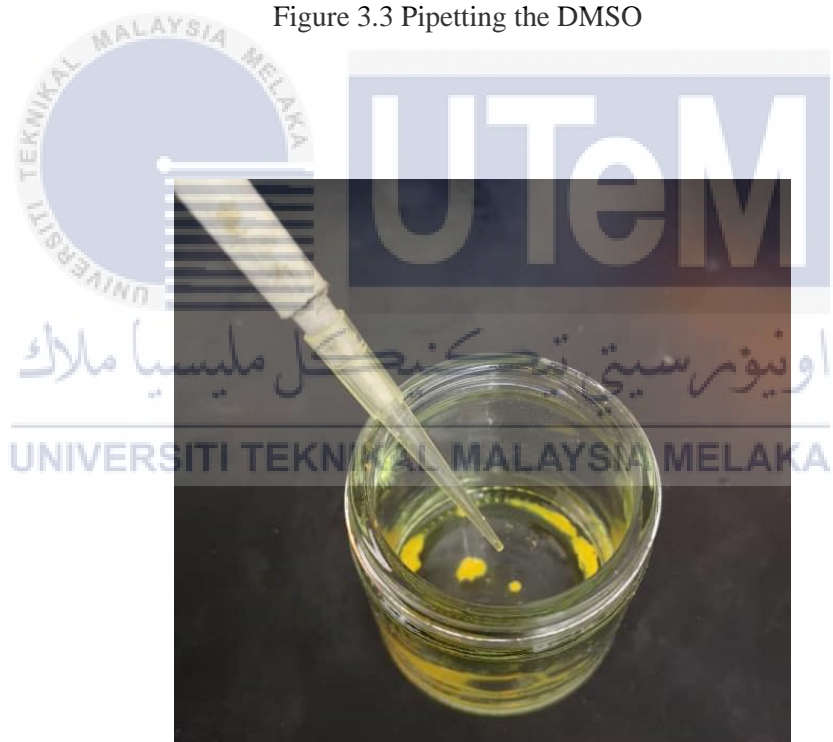


Figure 3.4 Pipetting the DMF



Figure 3.5 Stirring process



Figure 3.6 PbI_2 final mixture solution

Moving to the MAI solution, 50g of MAI is mix with 2 mL of the IPA. IPA was measure using the measuring cylinder as shown in figure 3.7. There are 100% MAI mixture with no addition of S-rGO and another two mixture with the present of S-rGO starting from 20% as shown in figure 3.8 and 40% of S-rGO. Each mixture was then stir at the 800 rpm using magnetic stirrer with 60 °C as shown in figure 3.9.

MAI	S-rGO	IPA
100% = 0.05g	0 g	2 mL
80% = 0.04g	20% = 0.01g	2 mL
60% = 0.03g	40 % = 0.02g	2 mL



Figure 3.7 2 mL of IPA

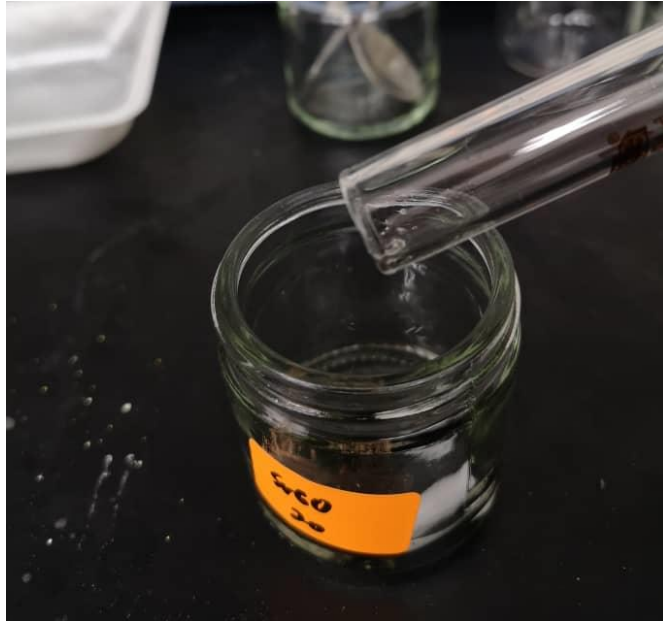


Figure 3.8 Mixture of IPA, MAI and 20 % of S-rGO



Figure 3.9 Stirring process of S-rGO 0%, 20% and 40%

The MAI (with and without S-rGO) and PbI_2 mixture then employed process of in the thin film process fabrication step two approach. Figure 3.10 shown summary of synthesis process of methylammonium lead iodide from start to the end.

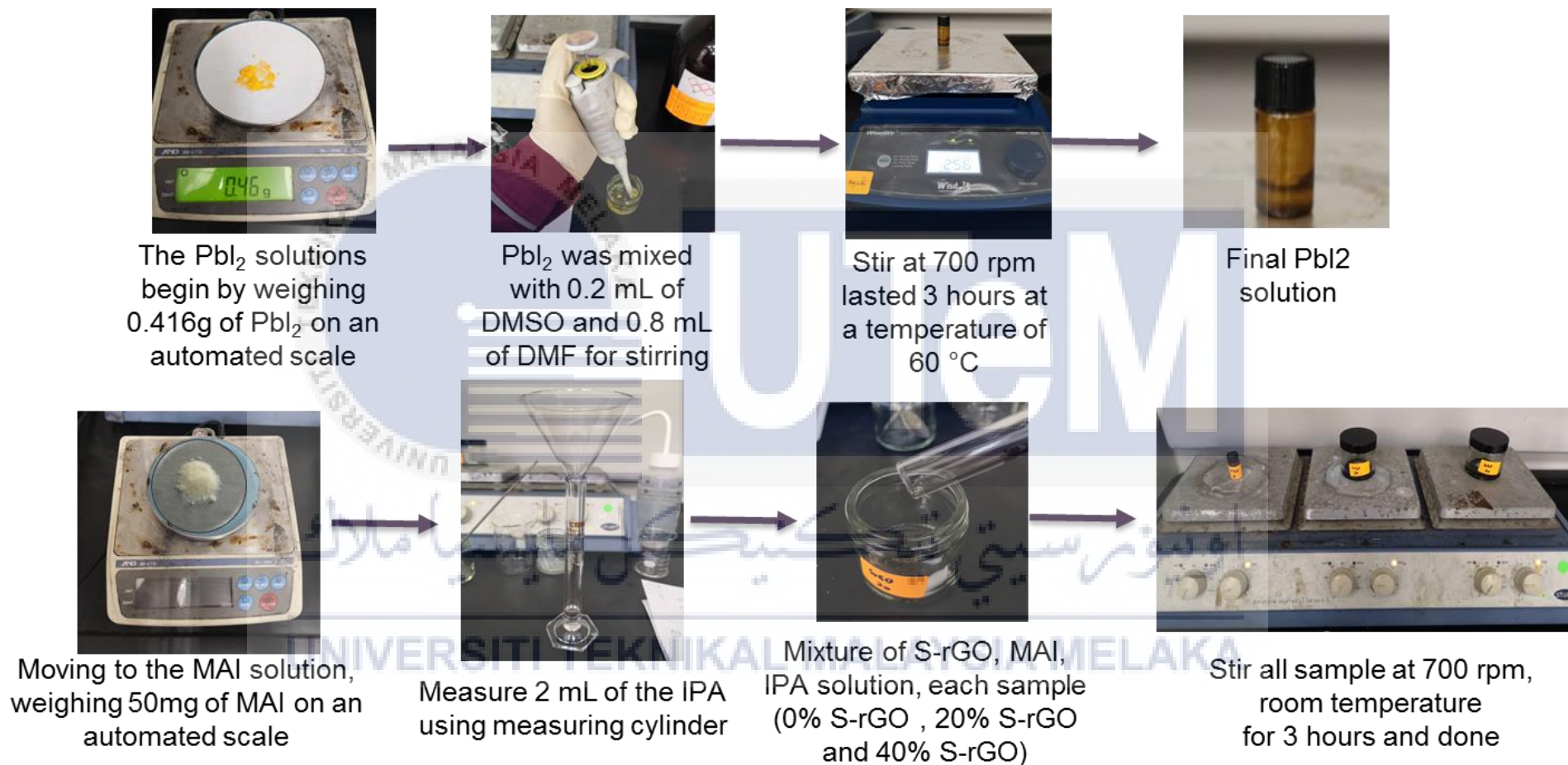


Figure 3.10 Summary of synthesis process of Methylammonium Lead Iodide

3.3.2 Synthesis of Reduced Graphene Oxide

To begin reducing graphene oxide powder, dissolve 1 gram of graphite flakes in 50 milliliters of sulfuric acid, constantly stirring in an ice-water bath as shown in figure 3.11. Throughout the process, the mixture is stirred using the magnetic stirrer plate and magnetic stirrer as shown in figure 3.12. Plastic covers the bar magnet, and the plate contains a rotating magnet. The micromotor drives the magnet, which produces a spinning magnetic field and stirs the stirring bar in the jar, allowing the solution to undergo a complete mixing reaction. The stirring speed is adjustable, and the device is often used to mix solvents with varying viscosities. Next, 3 g of potassium permanganate will be added in by maintaining the temperature under 10 °C.

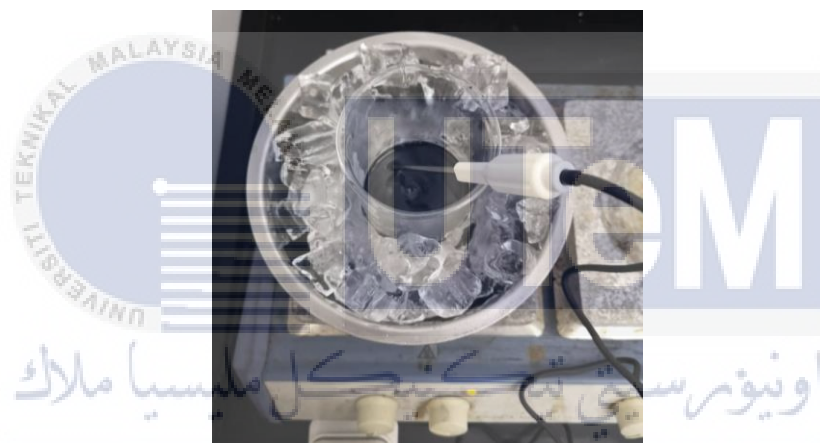


Figure 3.11 1g of graphite flakes in 50ml of sulfuric acid stirring in an ice-water bath



Figure 3.12 Magnetic stirrer

The mixture then stirred at room temperature for 25 min as shown in figure 3.13 followed by 5 min sonication in an ultrasonic bath as shown in figure 3.14. Sonication uses

sound waves to agitate particles in a solution. It converts an electrical signal into a physical vibration to break substances apart. These disruptions can mix solutions, accelerate the dissolution of a solid into a liquid. Ultra-sonication frequency is reported to be 20–40 kHz. Sonication is performed to achieve multiple purposes including agglomeration of nanoparticles, size reduction, and dispersion in the base fluid. Later repeating the stirring-sonication process for 12 times.



Figure 3.13 Stirring process of the mixture

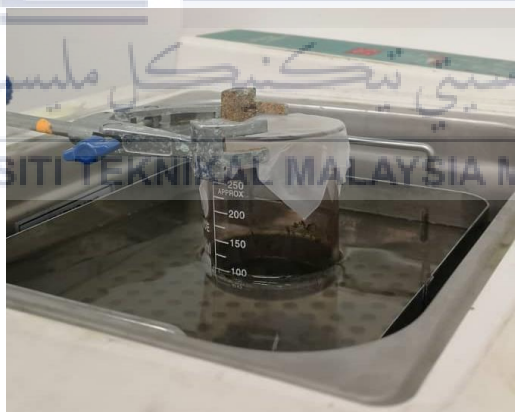


Figure 3.14 Sonication in the ultra-sonicate with water bath

The reaction then quenched by the addition of 200 mL distilled water. Quench is a term that refers to the process of extinguishing, eliminating, or reducing a physical attribute, such as heat. The solution is wrapped in parafilm to avoid contamination and maintain its purity as shown in figure 3.15. Parafilm is both flexible and self-sealing, it is very convenient to use. Additionally, the parafilm is permeable to gaseous substances such as oxygen, carbon dioxide, and water vapor.



Figure 3.15 Quench of the GO and distilled water

Another 2-hour ultrasonic treatment was carried out. After altering the pH at ~ 6 by adding 1M of sodium hydroxide solution as shown in figure 3.16. The pH altering using the pH paper the suspension further sonicated for another 1 hour.



Figure 3.16 Process of altering the pH level at ~ 6

Moving to the next steps, 10 g of L-ascorbic acid will be added and let it dissolve in 100 mL of distilled water. Meanwhile, exfoliated graphite oxide slowly added to the suspension at room temperature. The reduction was performed at $95\text{ }^{\circ}\text{C}$ for 1 hour as shown in figure 3.17.

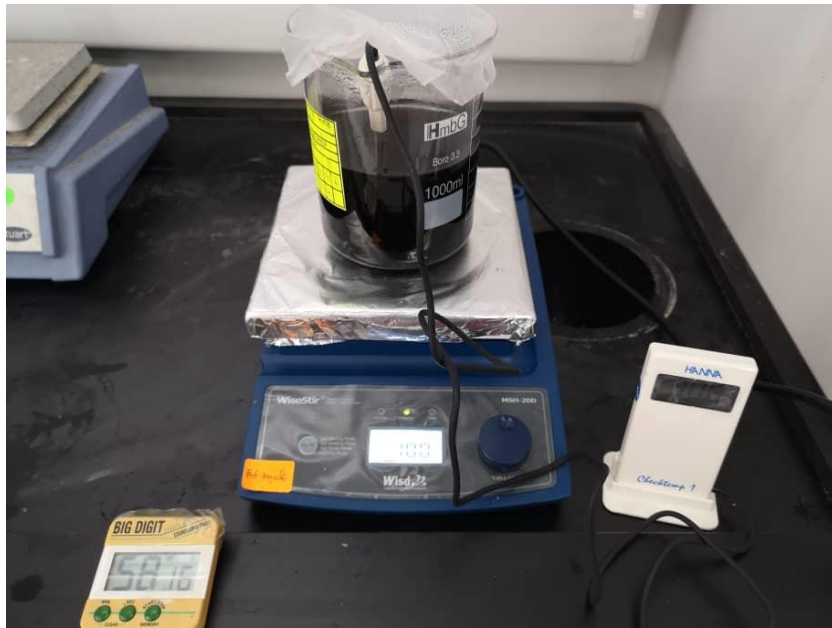


Figure 3.17 Reduction process of GO

The resultant black precipitates are filtered by cellulose filter paper and further washed with a 1M hydrochloric acid solution and distilled water to neutral pH. Finally, the filtrate was freeze-dried to obtain the rGO as shown in the figure 3.18. Figure 3.19 present the summary of synthesis process of rGO from beginning to the end.

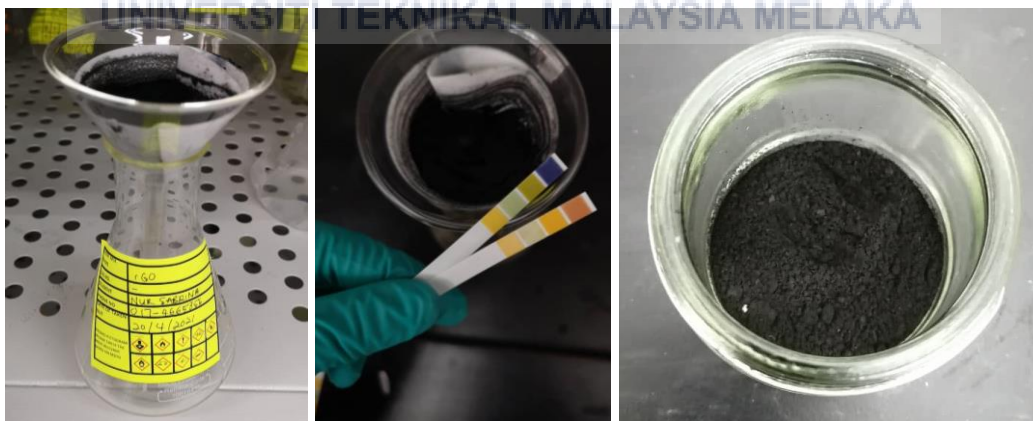


Figure 3.18 Filtration, pH level alteration and final rGO powder

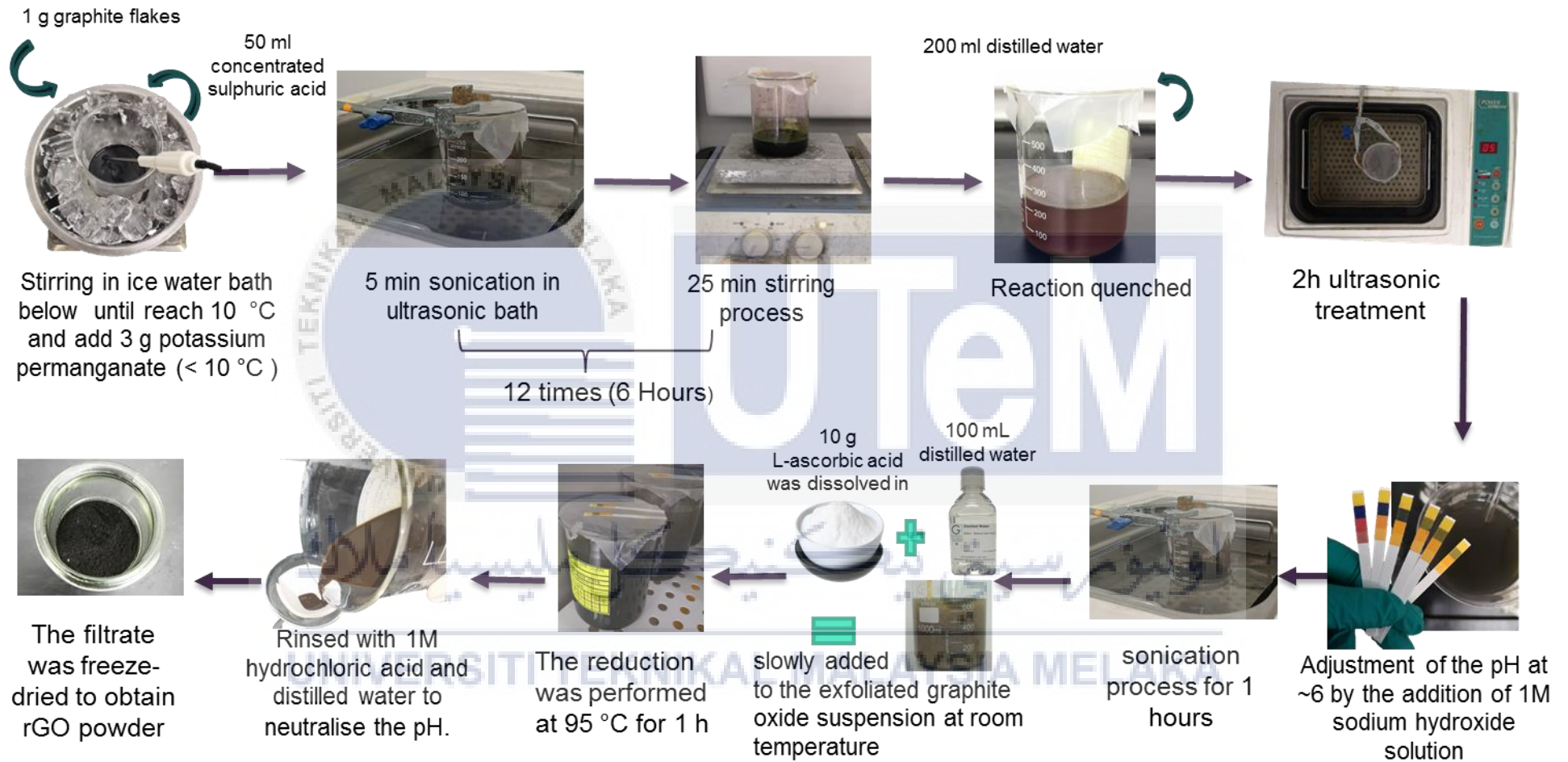


Figure 3.19 Summary flow synthesis process of Reduced Graphene Oxide

3.3.3 Functionalized Reduced Graphene Oxide

Functionalized reduced graphene oxide was performed for this experiment as a guide. The functionalized rGO was prepared by dispersing the rGO in 150 mL of filtered water using an ultrasonic bath as shown in figure 3.20.



Figure 3.20 Functionalize rGO initial process

The mixture was then put in a water bath to cool as shown in figure 3.21. In the water bath at 0 °c, the diazonium salt solution (sulfanilic acid, 1 N HCl, and 10 mL distilled water) was gradually applied to the rGO-pure water mixture.



Figure 3.21 Ice bath and measured sulfanilic acid, HCl, and distilled water.

After the 4 hour reaction, the sulfonated reduced graphene oxide was centrifuged and washed with deionized water several times and dried at 60 °C under vacuum as shown in figure 3.21. The resulting material dried to obtain rGO-SO₃H as shown in figure 3.23. Figure 3.24 shown the summary of synthesis process of S-rGO from beginning until end product of S-rGO powder.



اونيور سیتی تیکنیکل مالایا ملاک
Figure 3.22 Drying in the vacuum oven

UNIVERSITI TEKNIKAL MALAYSIA MELAKA



Figure 3.23 Final S-rGO powder

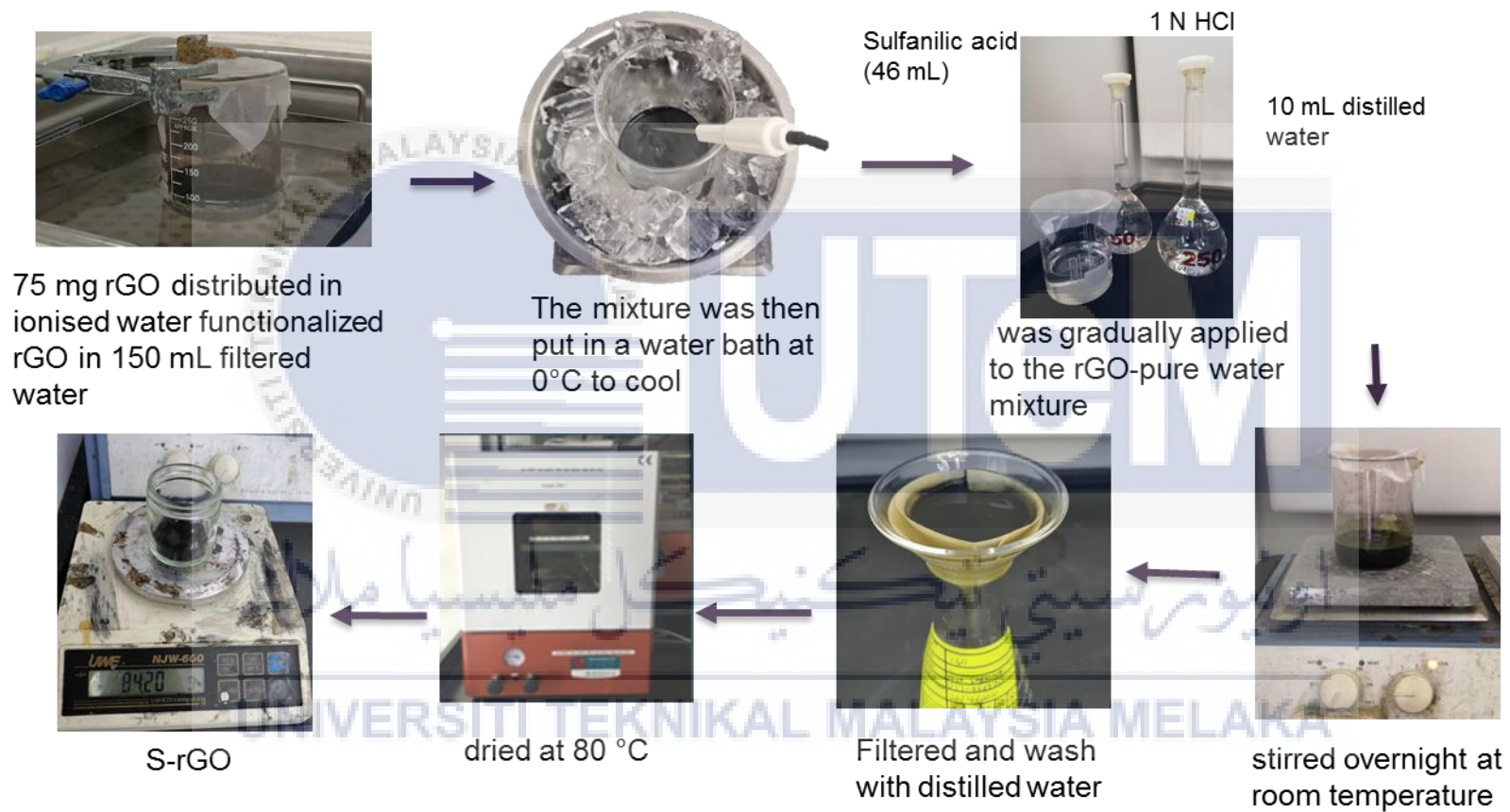


Figure 3.24 Summary flow synthesis process of Sulfonated Reduced Graphene Oxide

3.3.4 Preparation of Thin Film

To begin the process of producing the thin film, first steps is clean the glass plate that will serve as our substrate. The glass substrate was washed with three different solutions for 15 minutes each to ensure no contaminants remained as shown in figure 3.25. Start with detergent, then ethanol, and finally distilled water. The washing process used sonication wash for 15 minutes. The substrate was cleaned and then dried at room temperature.

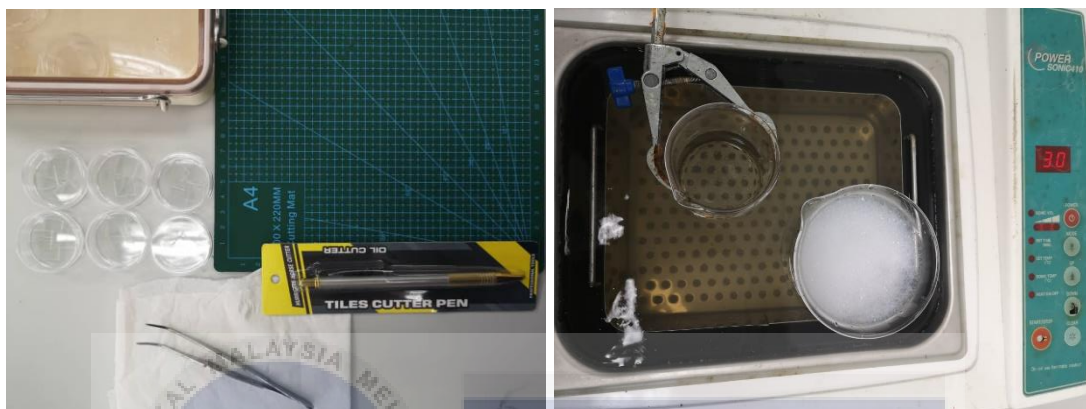


Figure 3.25 Substrate preparation and washing

First steps is anneal the substrate on the hotplate for 10 minutes at 70 °C to begin the deposition process. After that, install the preheated substrate on the spin coating machine and double-check that it is securely attached. The working table shown in the figure 3.26.



Figure 3.26 Working table during preparation

Use a pipette to deposit PbI_2 on the substrate for 40 seconds at 4000rpm (preheat the PbI_2 for 20 minutes at 80 °C before starting the deposition process). The substrate was then annealed

for 10 minutes at 70°C. The substrate should have a light yellow layer on it at this point as shown in figure 3.27.



Figure 3.27 Yellow form from PbI₂ deposition

Then, at the same speed and rpm as PbI₂, deposit MAI. After that, at 4000rpm for 5s, deposition of Chlorobenzene (CB) as an anti-solvent. Addition of anti-solvent in order to act as sealant that helps in slower or decrease the possibilities of degradation of the perovskite. After the deposition and spin coating processes are completed, the substrate should be annealed at 120°C for 20 minutes, revealing a thin black film as shown in figure 3.28. The summary of the synthesis flow shown in the figure 3.29.



Figure 3.28 Final look of Perovskite thin film

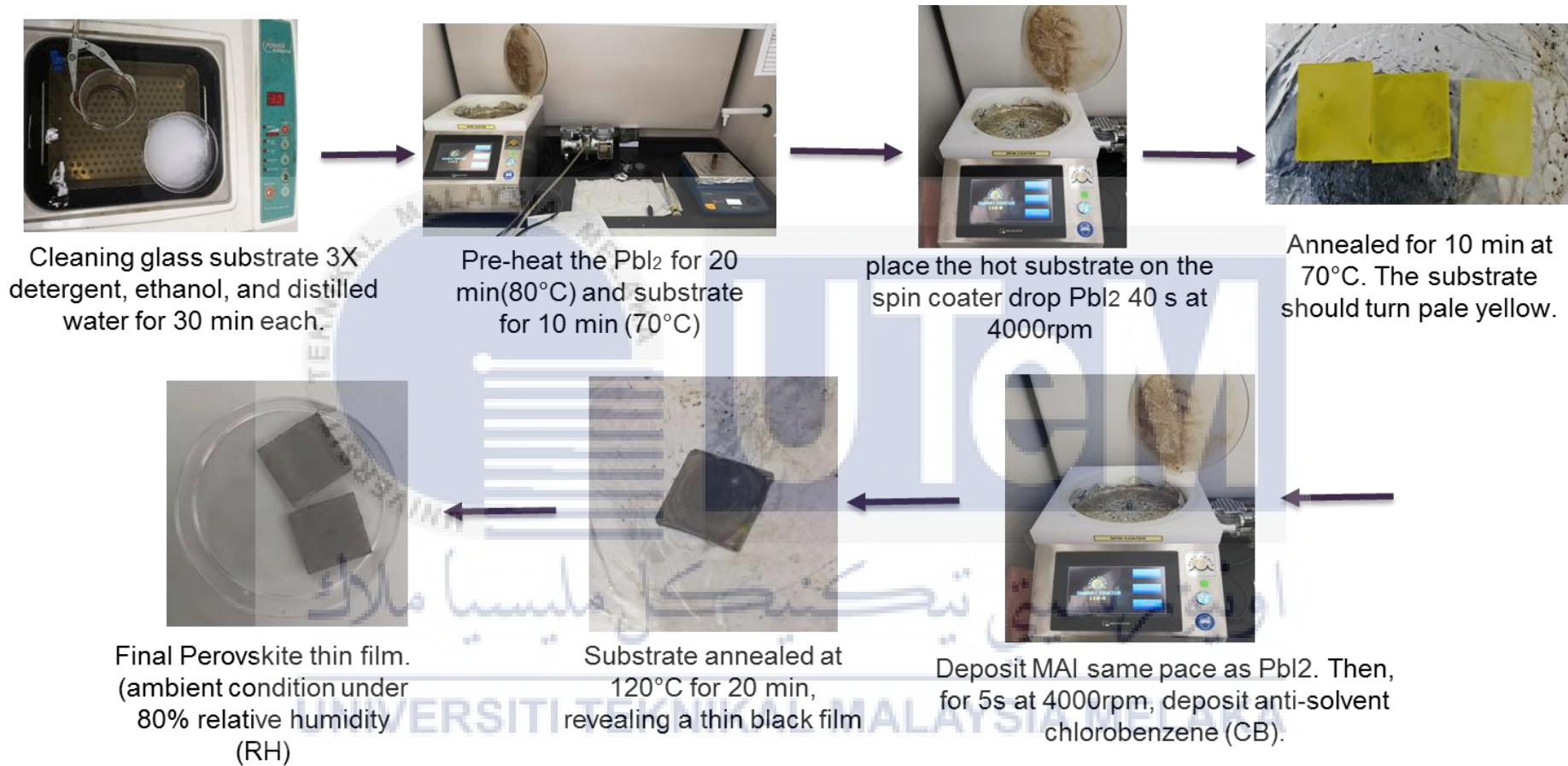


Figure 3.29 Summary flow fabrication Perovskite doped S-rGO thin film at ambient temperatur

3.4 Characterization Method

Engineering applications require various materials, which need to be characterized to understand their properties. Material characterization is the method of analysis and confirmation on the physical, biological, mechanical and microstructural properties of materials. In this project, the characterization method applied is Scanning Electron Microscopy (SEM), UV-Vis spectrophotometer (UV-Vis) and Raman Spectroscopy.

3.4.1 Scanning Electron Microscopy

The Scanning Electron Microscopy, Zeiss EVO 50 XVP, located at the FKP, UTeM main campus. SEM was used to examine the morphology changes especially the changes in the grain size of the Perovskite thin film after integrating with functionalized rGO and with bare rGO. The electron accelerating voltage that will be used is 20kV. The image surface of the film will be a focus on 10 000 and 20 000 magnification. There are 3 samples tested which is 0% of S-rGO, 20% of S-rGO and 40% of S-rGO. All the sample in the size of 1x1 cm².

3.4.2 UV-Visible Spectroscopy

UV-visible absorption spectroscopic (UV-Vis) was used to study the level of absorption spectra and transmittance of the samples. UV-Vis used to indicate the optical properties of photovoltaic cells that show the ability of the Perovskite thin film to absorb the sunlight. The various phenomena involved reflectance, transmittance and absorbance. This characterization was performed by critical review method.

3.4.3 Raman Spectroscopy

Raman Spectroscopy was used to monitor structural changes during the reduction and functionalized rGO processes. To validate the formation of rGO and S-rGO based on the D and G peak result will be studied. The G band is due to in-plane vibrations of bound carbon atoms, while the D band is due to out-plane vibrations caused by the presence of structural defects with the laser excitation 532nm green Nd:YAG. . This characterization was performed by critical review method.

3.5 Execution of Critical Review: UV-Vis and Raman

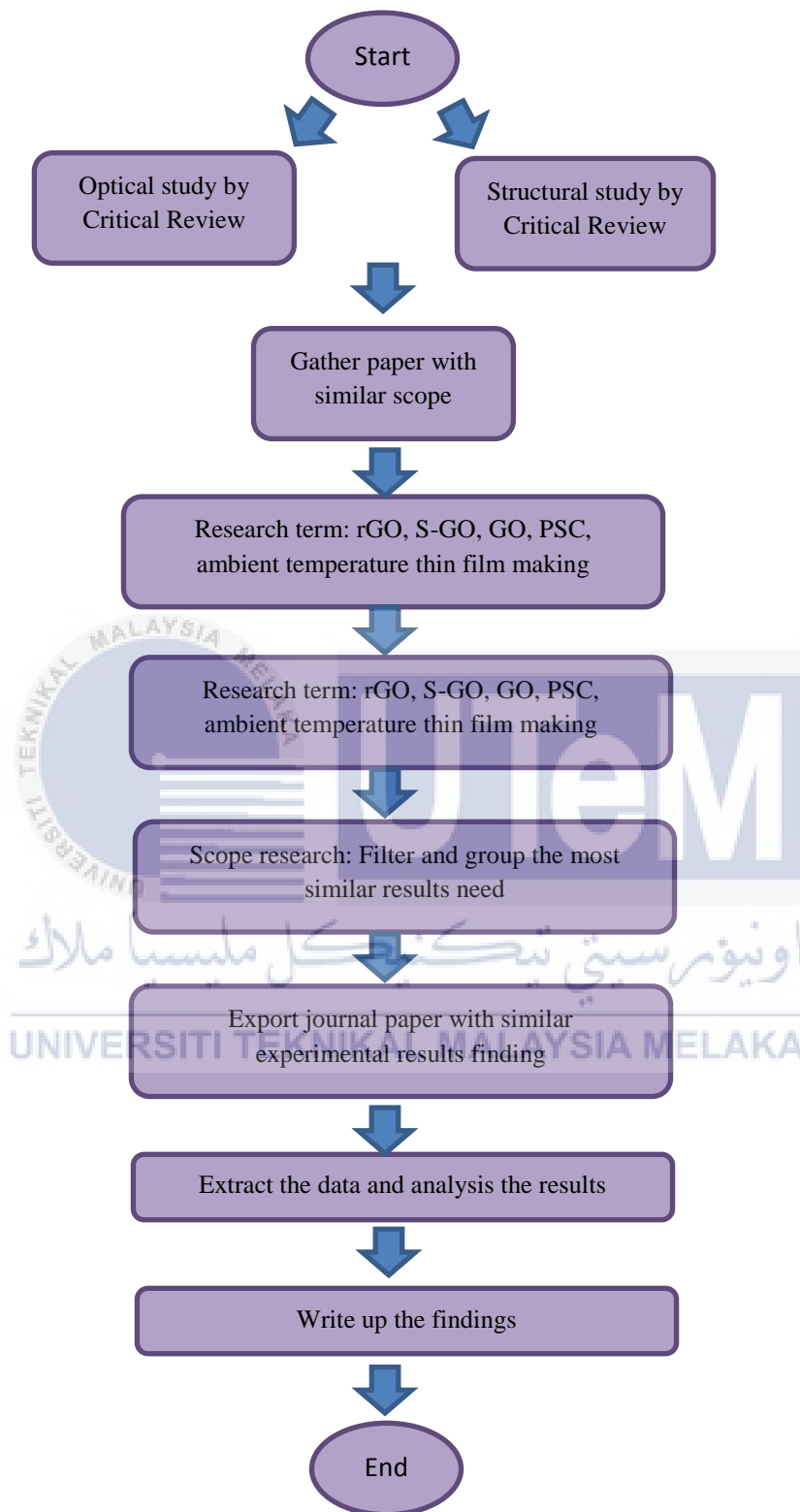


Figure 3.30 Flow chart of critical review study

The flow chart above illustrates the process of conducting a critical review of structural and optical properties using Raman and UV-Vis. Several papers collate data based on research terms such as rGO, GO, S-GO, and PSC. The papers gathered will then be filtered according to the research term to reduce the number of papers to focus on and facilitate data extraction and writing the findings.

3.6 Critical Review of Raman

1. Structural properties between S-GO and GO (influence of sulfonation process)

Using an experiment from Guo et al., (2017), authors experimented on the Perovskite solar cells' efficiency is increased via the synergetic impact of sulfated graphene oxide (sGO) hole transporting layer. Authors implement sulfated graphene oxide (sGO) as an HTL in place of the more often utilized graphene oxide (GO) to see the difference in the efficiency of Perovskite solar cells. Investigate on the structural characteristics of the S-GO in this research by analyzing the Raman Spectroscopy findings from the conducted experiment. The following section discussed on the interpretation of the G and D bands.

From the reading, the authors characterize the structural features using a Raman spectrometer (Renishaw) equipped with a 514 nm laser. The Raman spectroscopy of the GO and sGO powders was used to describe them further, as seen in the figure below. In particular, it exhibits two significant peak regions, including a strong G peak, which also addresses a G band indicating 1590 cm^{-1} , and a D peak, also common as a D band showing 1350 cm^{-1} . The intensity of the sp^2 G band is linked to the vibration of bonded carbon sp^2 atoms. The G peak is related to the in-plane vibration of sp^2 hybridized carbon atoms located near 1580 cm^{-1} . The D band located near 1350 cm^{-1} results from vacancies. Meanwhile, the intensity of the D band is related to the distortion in the sp^2 carbon atoms or dislocations in the graphene layer and at the edge of this layer. This band is also related to the presence of defects in the material. From the figure 3.31 below, the relative intensity ratio $I_D 700\text{ a.u}$ and $I_G 686\text{ a.u}$ resulting (I_D/I_G) for GO is 1.02, while the intensity ratio sGO, $I_D 2000\text{a.u}$ and $I_G 1941\text{a.u}$ resulting the (I_D/I_G) for sGO is 1.03.

In particular, the D band's relative intensity ratio (I_D/I_G) to the G band indicates the size of the in-plane sp^2 domains and the degree of structural disorder in the carbon atoms and molecules. The intensity of both the D and G bands is substantially enhanced once the sulfonation process is completed. While the only slightly greater power of I_D/I_G ratio is found

for sGO powder, this suggests that oxygen groups in the basal plane of the second phase have decreased and that there are more isolated C domains in sGO powder compared to the first phase of the phase diagram. Proven that, D peak for both Raman shifts higher compared to the G peak. Results show more elevated in the D peak after the sulfonation process is carried out and lower in the G peak. In conclusion, they result in the low plane vibration of sp² hybridized carbon atoms and an increase in the presence of defects in the material.

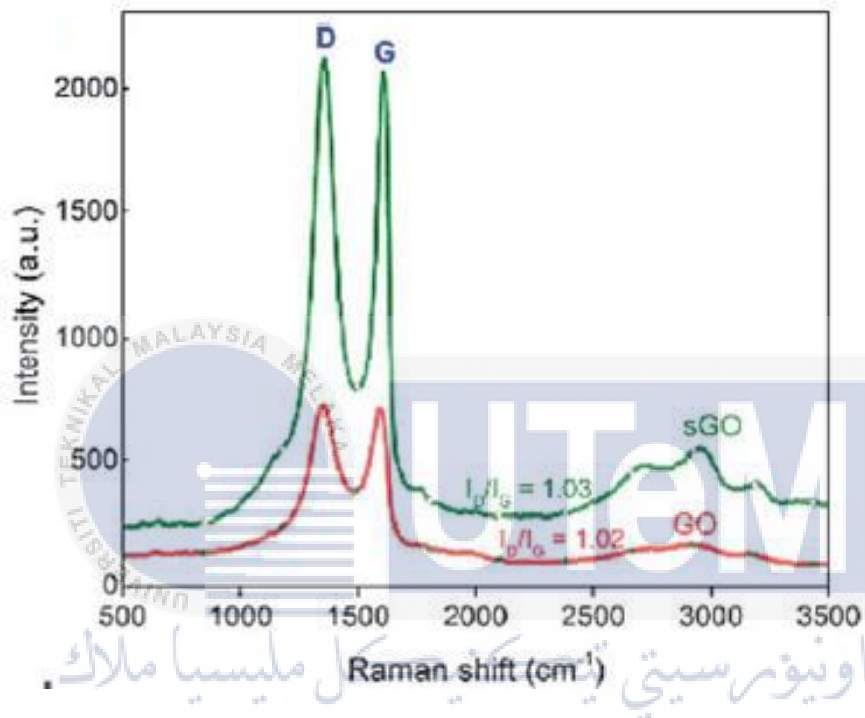


Figure 3.31 Raman spectra of GO and SGO and I_D/I_G ratio of both spectra (Guo et al., 2017)

2. Structural properties between rGO and GO (influence of reduction process)

Suragtkhuu and colleagues published another intriguing paper in 2020 about improving the efficiency and durability of perovskite solar cells by utilizing reduced graphene oxide produced from earth-abundant natural graphite. The experiment to determine the structural characteristics of rGO for usage in Perovskite Solar Cells to boost its stability over the commonly utilized GO material. The structural characteristics of rGO and GO were determined using Raman spectroscopy with a 532 nm excitation laser. The structural features of the rGO used in this study by evaluating the Raman Spectroscopy data from the experiment.

The authors find Raman signals for GO and rGO at the same peak at 1352cm^{-1} presenting D and 1606cm^{-1} presenting G bands, respectively as shown in figure 3.32. D band attributed to the disorder supported by Ferrari et al., 2007 basal plane defects in the structure arising from defects in the sp^2 carbon in and graphitic peak. The G band causes waking from the in-plane vibrational E_{2g} mode of the sp^2 carbon. The E_{2g} mode and associated with in-plane stretching of the C–C bond in graphitic materials common to all sp^2 carbon systems. This band is associated with bond stretching of sp^2 carbon atoms in rings and stretching in chains Ferrari et al., (2007).

Moving into the I_D/I_G ratio it is well established that the D to G band (I_D/I_G) intensity ratio is used to determine the level of defects. The lowest value of I_D/I_G ratio for graphite is associated with a small number of structural defects according to the Tuinstra-Koenig relation and vice versa. The I_D/I_G for the GO and rGO were 0.96 and 1.04. A slight increase in the I_D/I_G observed upon reduction of GO is well accepted due to the defects introduced to the sp^2 carbon during the reduction. The reduction process generates chemicals, such as hydrazine radicals, and attacks the oxygen functional groups before the reduction process is completed, damaging the graphitized structure, resulting in a slight increase in the I_D/I_G ratio.

From this experiment, the I_D/I_G ratio of rGO higher compared to GO. After the reduction process, the D band high due to the defects introduced to the sp^2 carbon during the reduction process on the graphene oxide. In conclusion, they result in the low plane vibration of sp^2 hybridized carbon atoms and an increase in the presence of defects in the material.

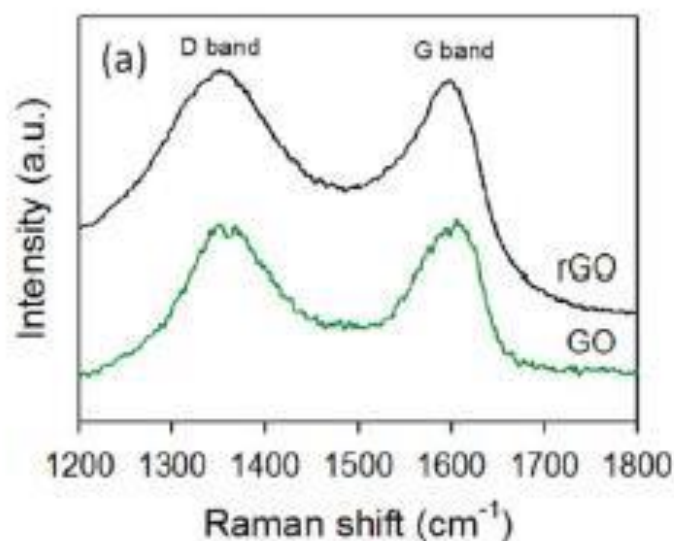


Figure 3.32 Raman spectra of GO and rGO and I_D/I_G ratio of both spectra (Suragtkhuu et al., 2020)

3. Structural properties between rGO and GO (influence of reduction process)

Palma and colleagues (2016) conducted another experiment rGO as an Efficient and Stable Hole Transporting Material in Perovskite Solar Cells. The experiment was designed to characterize the structural properties of rGO for use in PSC to evaluate the material's efficiency and stability as a hole transport layer material. Raman spectroscopy with a 532 nm excitation laser was used to investigate the structural properties of rGO and GO. The structural characteristics of the rGO utilized in this reading by analyzing the Raman Spectroscopy data from the experiment. The following section will discuss the interpretation of the G and D bands in GO and rGO.

The authors observe Raman signals for GO and rGO at the same peak at 1356 cm^{-1} (D band) and 1591 cm^{-1} (G band) as shown in figure 3.33. The D peak is related to the breathing modes of s rings and needs a defect for double resonance activation (Ferrari et al., 2000). The G band causes the sp^2 carbon to awaken from its in-plane vibrational E_{2g} state. In graphitic materials, the E_{2g} mode is linked with in-plane stretching of the C–C bond common to all sp^2 carbon systems. This band is connected with the stretching of bonds between sp^2 carbon atoms in rings and chains (Ferrari et al., 2007). Moving on to the I_D/I_G ratio, the intensity ratio of the D to G bands (I_D/I_G) is utilized to assess the degree of faults. According to the Tuinstra-Koenig relationship, graphite's lowest I_D/I_G ratio is linked with a limited number of structural flaws and vice versa rGO ($I_D/I_G=1.18$) to GO ($I_D/I_G=0.95$). There is an increase in the I_D/I_G ratio when GO is reduced to rGO.

The rise in I_D/I_G seen during GO reduction is widely recognized as a result of defects incorporated into the sp^2 carbon during the reduction. Because I_G is approximately constant as a function of disorder and is linked to the relative mobility of sp^2 carbons (Ferrari et al., 2013) and an increase in I_D is directly related to the existence of sp^2 rings, an increase in the I_D/I_G ratio may be interpreted as the restoration of sp^2 rings. The reduction process produces molecules such as hydrazine radicals, which attack the oxygen functional groups before the reduction is complete, resulting in damage to the graphitized structure and a slight rise in the I_D/I_G ratio.

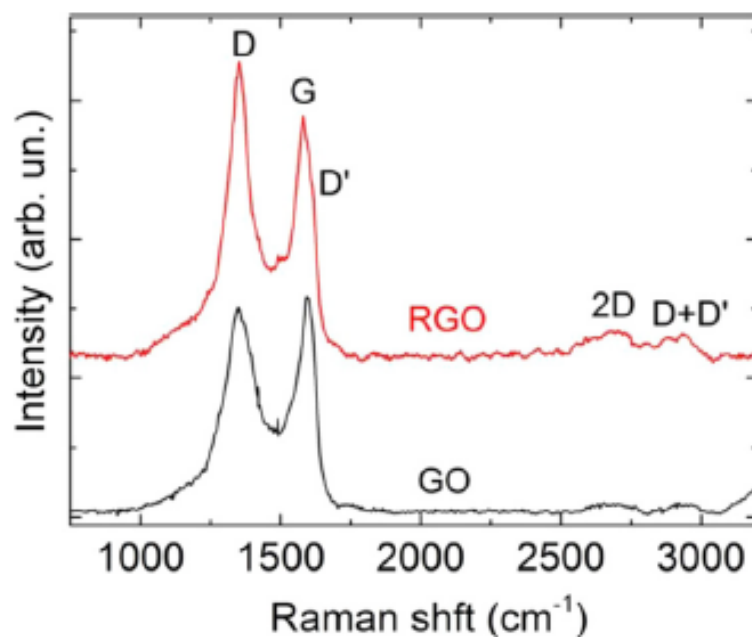


Figure 3.33 Raman spectra of GO and rGO and I_D/I_G ratio of both spectra (Palma et al., .2016)

3.7 Critical Review of UV-Vis

1. Influence of rGO in the MAPbI₃ in the optical properties

According to the research of Balis et al., 2020 authors experimented with investigating the effects of incorporating reduced graphene oxide (rGO) nanoflakes into the CH₃NH₃PbI₃ absorber a, which is one of the star rising components of a PSC. It is critical to improving the perovskite films' quality, namely their crystallinity and shape, to manufacture effective PSC. It is widely known that uniformity, smoothness, grain size, and layer thickness are the most critical deciding variables in the production of composite materials Kim et al., (2015). In particular, the rapid interaction between the lead precursor and the methylammonium salt during the crystallization of perovskite from the blended precursor solution is responsible for the tiny grain size that leads to poor film optoelectronic quality of perovskite. As a result, efficient management of the nucleation process is critical to enhancing the film's physical characteristics (Balis et al., 2018). Indeed, thick perovskite layers with homogeneous and big grains result in the most outstanding amount of light-harvesting, with single perovskite nanocrystals acting as perfect absorbers when combined with other perovskite layers.

Researchers demonstrate that when rGO is added to the perovskite solution MAPbI₃, it helps increase grain size while creating a more homogeneous and smooth film with enhanced crystallinity, increasing the PCE of the corresponding photovoltaic PSC. More importantly, after 50 days of storage in a moderately humid, dark environment, their first PCE was higher than expected.

The difference in grain size possessed by CH₃NH₃PbI₃ layers, with and without rGO, may be seen in the figure 3.33 below, produced on pure TiO₂. The inclusion of rGO inside the compact layer seems to enhance light harvesting, which may be attributed to better perovskite crystallization (Zhao et al., 2018). Furthermore, a slight rise in absorption is seen in g- CH₃NH₃PbI₃ grown on g-TiO₂, indicating an even more outstanding quality for the perovskite films in terms of enhanced crystallinity bigger MAPbI₃ polycrystals leading to a higher quantity of photo-generated electrons and holes. The addition of rGO causes a net increase in the size of the CH₃NH₃PbI₃ grains, from 1024nm from figure 3.33 (b) to 1086nm from figure 3.33 (d). In addition, the perovskite grain size was enhanced in the latter instance, reaching a mean value of 1146nm referred figure 2 (e). Apart from giant crystals, these grains create a smooth and thick film with fewer grain boundaries, linked with reduced surface trap density.

The existence of rGO in the PSC results from this advancement. PSC provides enhanced optical and conductivity, better electron transport rate, and charge mobility, promotes the development of large perovskite crystals with improved crystallinity and serves as a passivator of perovskite trap states. Furthermore, the presence of rGO in the CH₃NH₃PbI₃ layer enhances the size of the perovskite grains and promotes the formation of smooth and homogeneous films. Consequently, the electrical and optical characteristics of the PSC's photovoltaic performance were enhanced, demonstrating the critical function of graphene materials in PSC performance in terms of efficiency and stability.

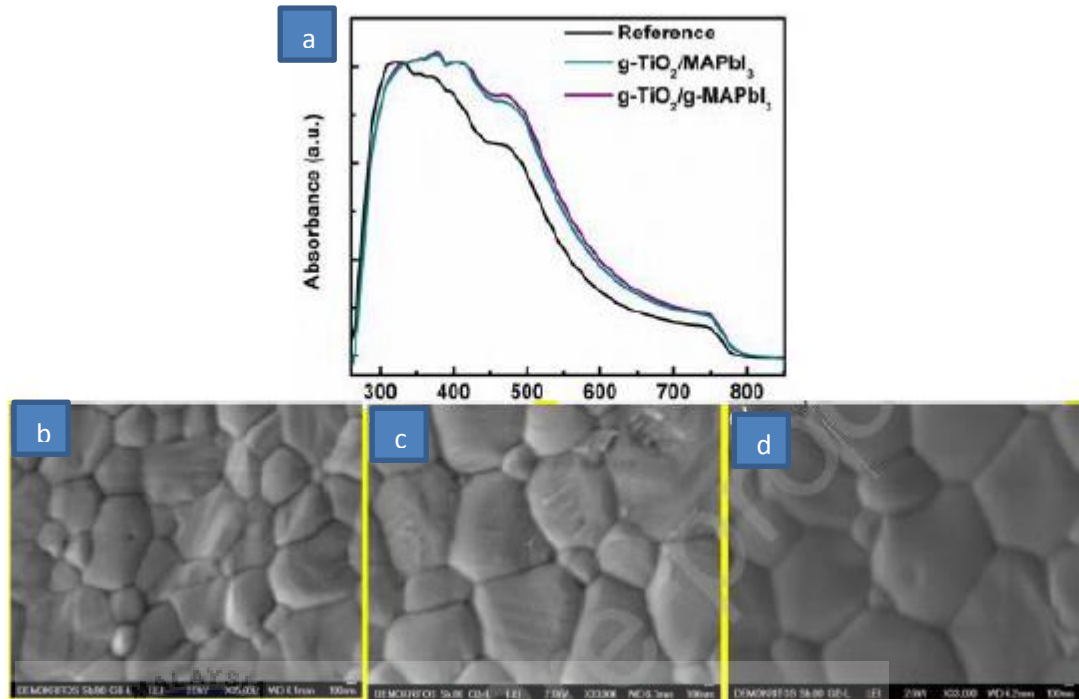


Figure 3.34 UV-Vis and SEM result of difference grain size (Balis et al., 2018)

2. Influence of Sulfonated Graphene group in the optical properties

Based on an experiment from Hue et al., (2017), the authors investigated the use of sulfonated graphene oxide as a cementitious grain-boundary passivation for flexible perovskite solar cells with improved environmental stability and mechanical resilience. The authors use sulfonated graphene oxide (s-GO) to create cementitious grain boundaries (GBs) by reacting with the $[\text{PbI}_6]^{4-}$ present at GBs. The resulting s-GO- $[\text{PbI}_6]^{4-}$ complex is capable of efficiently passivating empty iodine faults, and devices containing s-GO show exceptional waterproofness and flexibility owing to the tough and insoluble GBs. The authors get a champion PCE of 20.56 % in a device treated with s-GO as a result of this experiment. In this study, the optical characteristics of the S-GO by evaluating the UV-Vis Spectroscopy results from the performed experiment.

As a result, authors optimize a 0.05 mg/mL s-GO concentration in the perovskite precursor. Before adding additives to the perovskite precursor, the s-GO dispersion is ultrasonically vibrated to guarantee its dispersibility and detailed size of s-GO. The addition of s-GO results in a significant increase in grain size compared to the control sample, which contains small grains. The increased grain size is due to the sulfonic group of s-GO with the

lead atom of perovskite, which effectively optimizes perovskite precursor nucleation. Compared to the control sample, the appearance of highly distinct Bragg spots and diffraction rings in the perovskite film containing s-GO suggests that the film has a higher degree of crystallinity and orientation (Ren et al., 2020). The increased diffraction intensity further confirms the perovskite films with s-greater GO's crystallinity and bigger grain size (Ye et al., 2017). Meanwhile, this finding is consistent with the increased absorption in the UV-vis spectral region in range of 400nm to 800nm as shown in figure 3.35.

As a consequence of the findings, the authors conclude that the grain size increases by undergoing the sulfonation process, resulting in increased absorbance. As a result, we may conclude that the sulfonation process ultimately contributes to enhancing optical characteristics without impairing grain size growth.

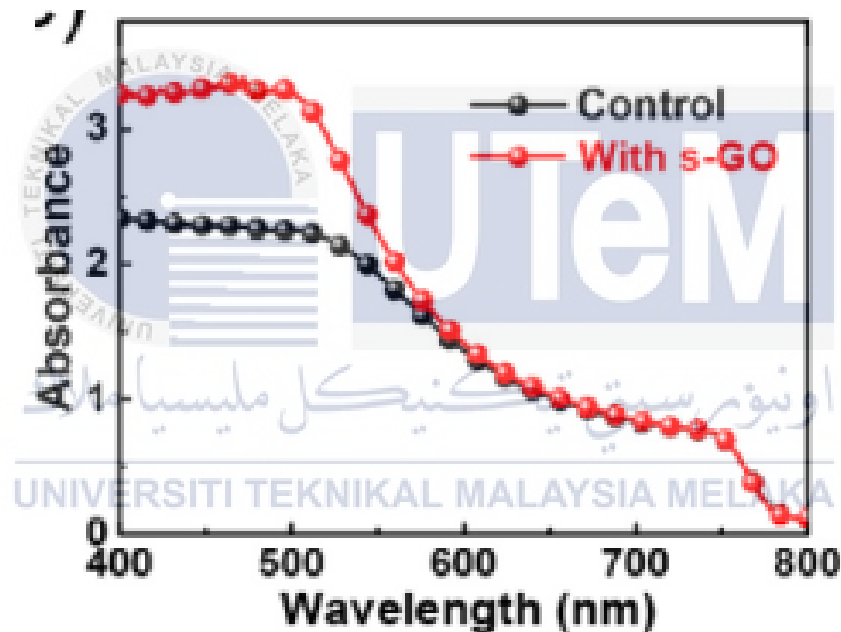


Figure 3.35 UV-Vis spectra between sGO and GO (Hu, X et al., 2021)

3. Influence of grain size in the optical properties

Using an experiment from Mamun 2019, it proven that increased particle size improves optical characteristics in the PSC. In particular, the author has created $\text{CH}_3\text{NH}_3\text{PbI}_3$ films with three distinct grain sizes ranging from 1–2 μm to 10–20 μm and $>50 \mu\text{m}$, as shown in figure 3.36 below. According to the experiment results, the scientists discovered that perovskite films with bigger grains ($>50 \mu\text{m}$) had the greatest emission peak at 755 nm. In addition, the authors found that the intensity of perovskite films with a larger grain size was three to six times stronger than that of perovskite films with smaller grain size, a significant advantage that resulted in improved optical quality solar cells due to this outstanding benefit.

For the uninitiated, the energy conversion efficiencies of the perovskite solar cells with smaller grains were 2.59 % and 9.19 %, respectively; however, a significant rise in efficiency to 13.72 % was seen for the perovskite solar cell with bigger grains. As previously stated, the increase in grain size is strongly linked to an increase in light absorption in the wavelength range of 400 nm to 600 nm, according to the authors. It is noteworthy that the absorption edge of the more notable grain perovskite film was well defined between 700 and 800 nm, while the absorption edge of the smaller grain perovskite solar cells was not clearly defined but progressively reduced. Finally, compared to smaller grain PSCs, more prominent grain PSCs outperform them in almost all aspects of the performance spectrum.

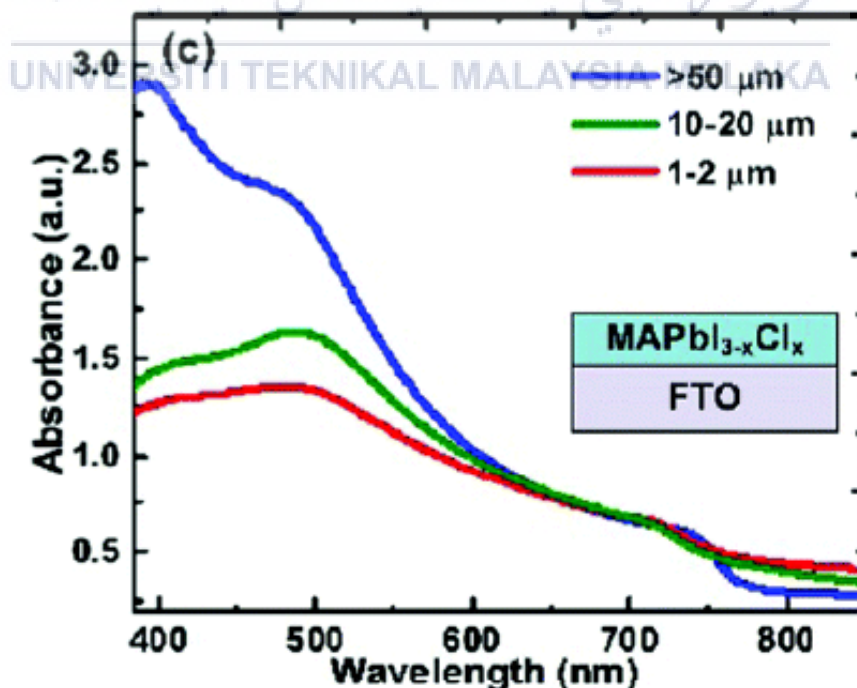


Figure 3.36 Absorbance (UV-Vis) with different grain size (Mamun 2019)

3.8 Summary of Chapter 3

In this new era technology, the third generation of solar cells which is halide perovskite solar cells being the star rising that possess many excellent properties to become the most suitable candidate for better and stable solar cells for successful commercialization of the PSCs. In order to enhance the reliability of the PSCs, this report added functionalized rGO to the structure of the device and highlighted the importance of the approach applied to charging transport media, as well as approach aimed at improving the efficiency of the device. In short, the integration of functionalized rGO will be evaluated to expose the potential factor for an outstanding performance against the efficiency of PSC power conversion as we intend to provide an outline to boost the performance of solar cells, which may be useful particularly for versatile system applications for highly effective photovoltaic systems.

3.9 Expected Result

In this study, rGO undergoes functionalization before being added to the perovskite solution to promote the tunable work function to the rGO. To help perovskite create a homogeneous membrane and be oriented evenly, the functionalized rGO is anticipated to surround the functionalized cation in perovskite. This technique should enhance perovskite grain size and reduce grain borders, improving perovskite morphology. With enhanced perovskite morphology, charge transport should be efficient, reducing carrier recombination and improving cell efficiency. Moreover, the functionalized rGO interfacial layer was proposed to protect the perovskite layer from ambient humidity or moisture exposure. The rGO bandgap should be adjusted to the perovskite layer's LUMO energy level during functionalization to maximize electron collecting efficiency. The functionalized rGO interface layer is anticipated to replace metal oxides as an electron transport layer in flexible device applications. Because rGO is a two-dimensional material, the functionalized rGO interfacial layer should not interfere with the optical properties of the perovskite layer. We found that the interface structure of anode/functionalized rGO/perovskite + functionalized rGO/hole transport layer (HTL)/cathode has superior morphological and photochemical characteristics and is appropriate for use in flexible PV devices.

CHAPTER 4

RESULTS AND DISCUSSION

This chapter aims to explain and discuss all of the experimental and postulated results gathered from various tests and analyses. The previous research statement states and supports all of the discussion and hypotheses based on the experimental results. There are three main sections in this chapter. The first is the morphological characteristics of the perovskite material after adding sulfonated reduced graphene oxide (s-rGO) as determined by Scanning Electron Microscopy (SEM) findings from a laboratory experiment. Second, a critical evaluation of the optical characteristics of perovskite materials under the impact of graphene-related material characterization using ultraviolet-visible (UV-Vis) spectrophotometry owing to UV-Vis machine failure. Lastly, the difference of rGO and sulfonated reduced graphene oxide (s-rGO) I_D/I_G ratio, determine the structural properties of bonding between perovskite materials with S-rGO, determined by Raman Spectroscopy from carried out a laboratory experiment.

4.1 Structural properties

An ideal characterization instrument should be quick and non-destructive, provide high resolution, provide structural and electronic information, and be usable at laboratory and mass-production scales. Raman spectroscopy (Raman et al., 1928) meets all of these criteria. Raman spectroscopy has become one of the most common methods for characterizing disordered and amorphous carbons, fullerenes, nanotubes, diamonds, and carbon chains (Ferrari et al., 2004). Raman methods are beneficial for graphene (Ferrari et al., 2007) because the lack of a bandgap renders all wavelengths of incoming light resonant,

and therefore the Raman spectrum includes information on both atomic structures. Raman spectroscopy, on the other hand, works for all graphene samples (Ferrari et al., 2007). Furthermore, it can detect undesired by-products, structural degradation, functional groups, and chemical changes introduced during the production, processing, or deployment of graphene (Bonaccorso et al., 2012). It is well known that the intensity ratio (I_D/I_G) is usually used to determine the level of defects. This statement also supported by Palma and colleagues in 2016, Suragtkhuu et al., (2020) and Guo et al., (2017), where the authors stated that the I_D/I_G ratio of a graphene composite's Raman spectrum gives information on the degree of flaws.

To summarize, according to the all results of the previous research gathered by an expert on the sulfonation and reduction processes of graphene oxide, both studies indicate that the D peak has increased. According to the phase diagram, the oxygen groups in the basal plane of the second phase have reduced after sulfonation, and there are more isolated carbon atom domains in the sulfonation graphene oxide powder than the graphene oxide in the first phase. The reduction process produces chemicals such as hydrazine radicals and assaults the oxygen functional groups before the reduction process is finished, resulting in damage to the graphitized structure and a slight rise in the I_D/I_G ratio while this is occurring.

4.2 Morphological properties based on experimental findings.

It was utilized in this section to examine the features and properties of the perovskite material that was created by adding sulfonated reduced graphene oxide (s-rGO). A total of three samples were investigated in this experiment which denotes by samples A, B, and C. Starting with A 0 % S-rGO (which is 100 percent % MAPbI₃), the samples go through various composition ratios to include B 20 % of S-rGO and C 40 % of S-rGO. When the electrons in the beam come into contact with the sample, they generate signals that may be used to identify the grain size of the sample. From the grain size obtain the result than discussed.

Figure 4.1 to 4.8 show images of a Perovskite thin film with functionalized reduced graphene oxide with a unique composition, generated by electrospinning at 20kV and magnifications of 10 000 and 20000, respectively, with functionalized reduced graphene oxide. As the grain size is investigated in the following picture, the morphological grain size varies with composition S-rGO. When S-rGO is added to sample B, the grain size of pure Perovskite rises by a factor of three. As we can see from the imageJ, sample A has particle sizes ranging from 220 nanometers to 550 nanometers, with a mean particle size of 384 nanometers. The particle size distribution in nanometers shows that sample A has particle sizes ranging from 300 nanometers to 1000 nanometers, with a mean particle size of 638 nanometers. When comparing the findings obtained to those obtained with Pure MAPbI₃, the particle size has risen almost 50%. When comparing sample A with sample B, it is noticed that the pinholes are more extensive in size. The particle size distribution cannot be estimated using the imageJ in sample C because the particles have gathered together into a ball. It seems that the particle did not disperse uniformly and preferred to cluster together, as seen by the SEM picture. The agglomeration of sample C revealed that integrating s-rGO up to 40% content may hinder the formation of a better morphology in the perovskite thin film.

4.2.1 SEM Morphological Experimental Results

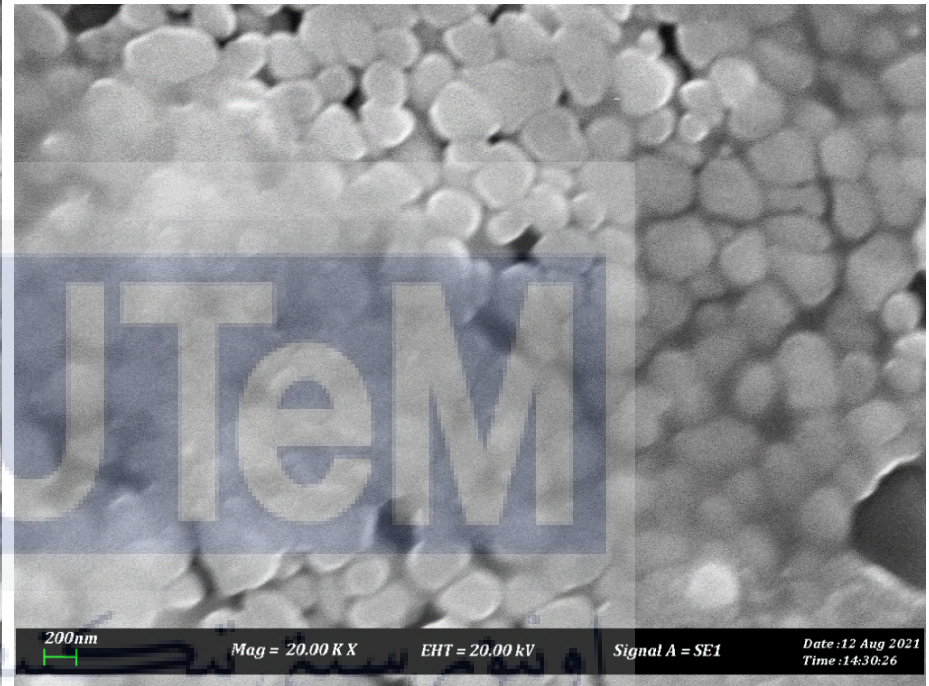
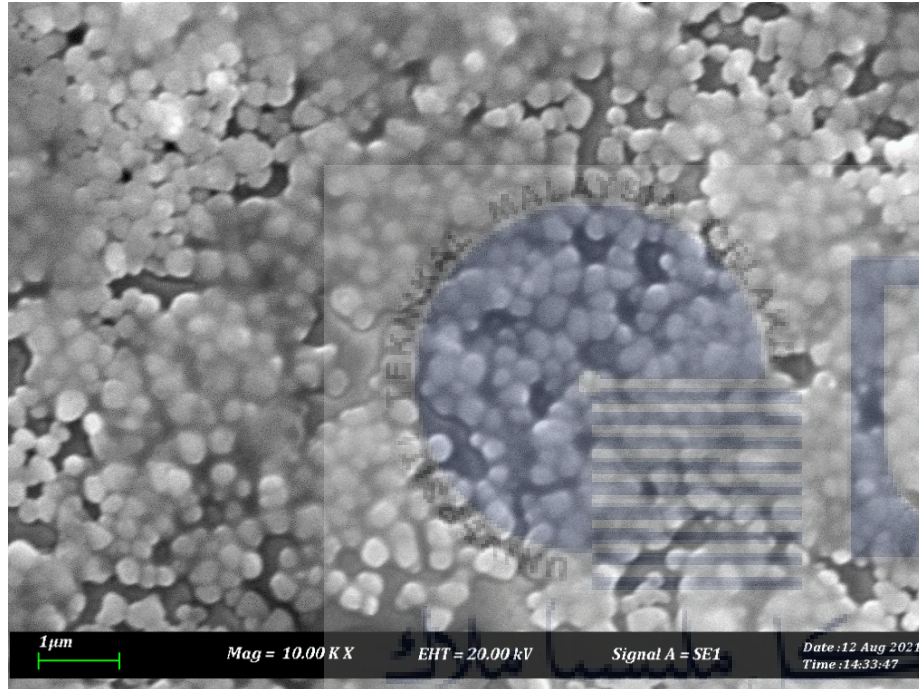


Figure 4.1 Sample A (0% S-rGO) grain size at 10.00K mag, 1µm.

Figure 4.2 Sample A (0% S-rGO) grain size at 20.00K, 200nm

UNIVERSITI TEKNIKAL MALAYSIA MELAKA

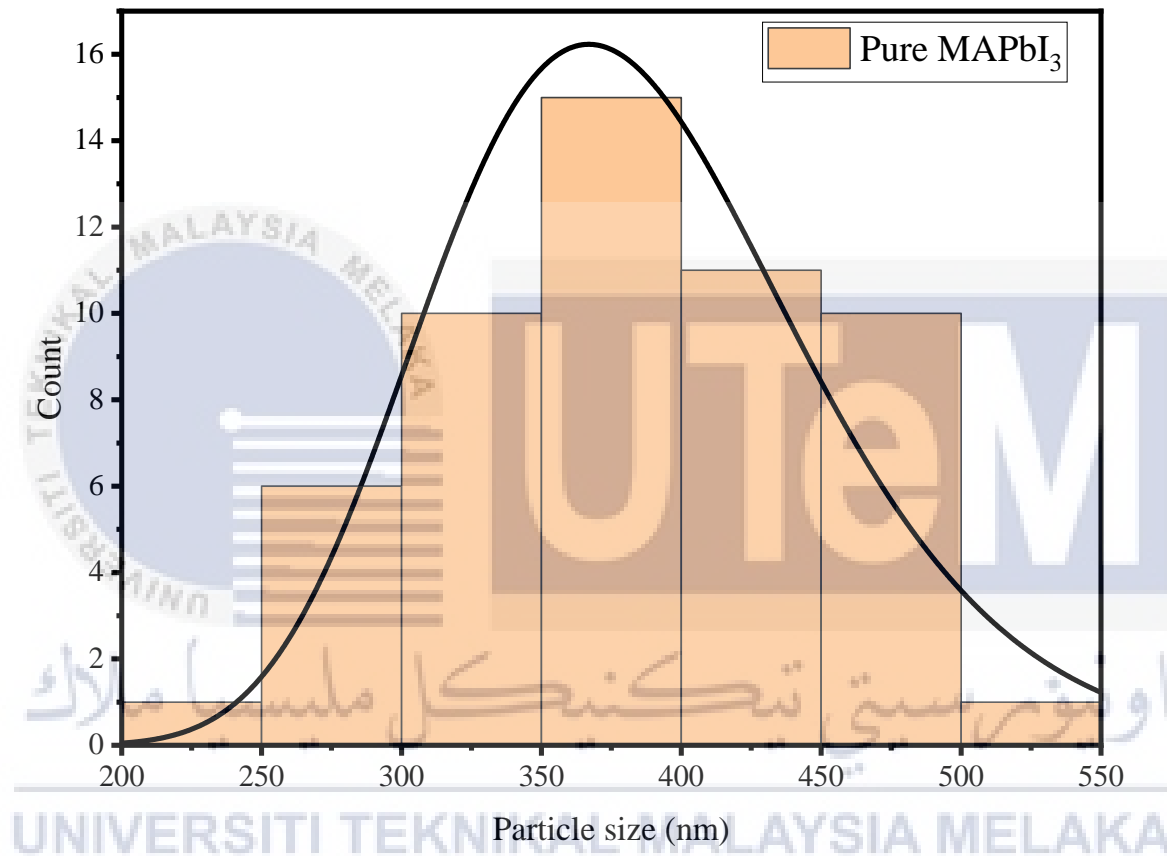


Figure 4.3 Particle distribution of Sample A (0% S-rGO) grain size (nm) with average 384nm

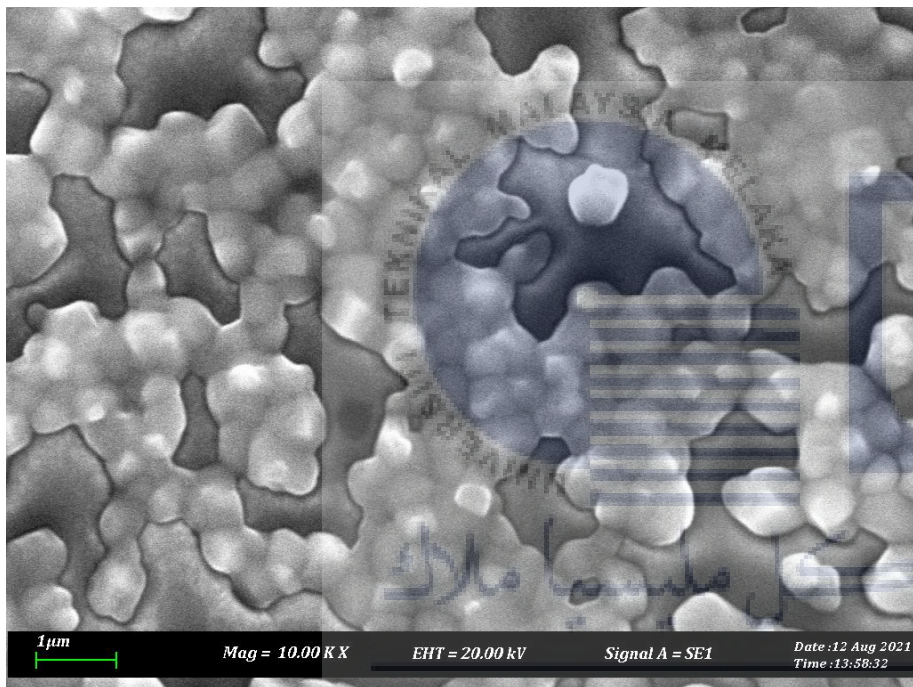


Figure 4.4 Sample B (20% S-rGO) grain size at 10.00K mag, 1µm

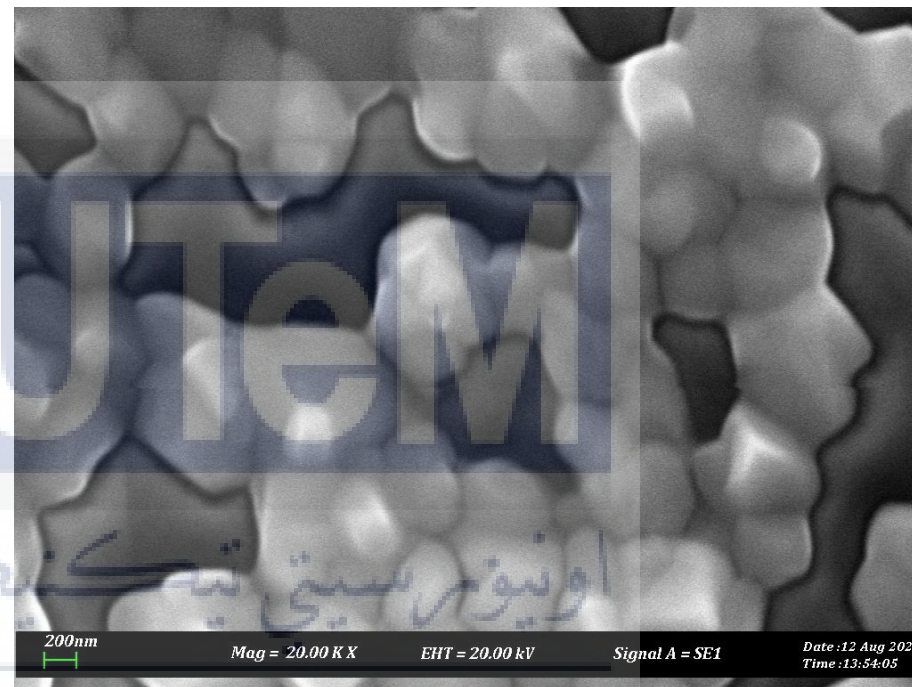


Figure 4.5 Sample B (20% S-rGO) grain size at 20.00K mag, 200nm

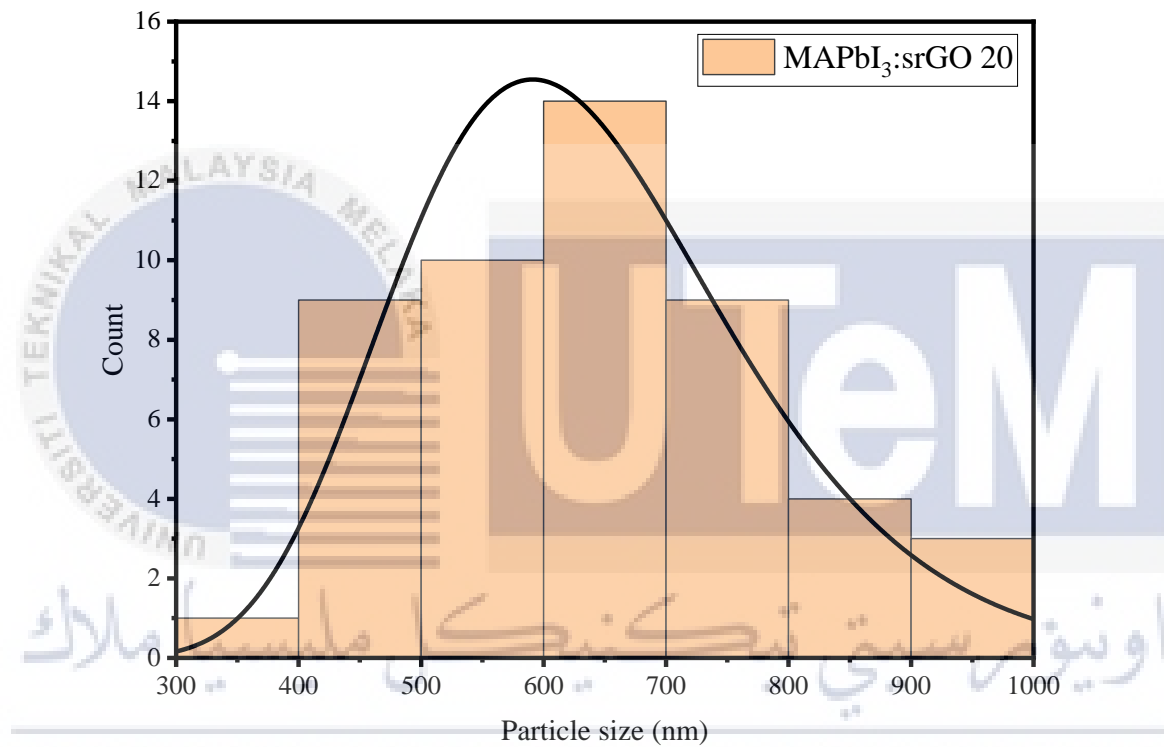


Figure 4.6 Particle distribution of Sample B (20% S-rGO) grain size (nm) with average 638nm

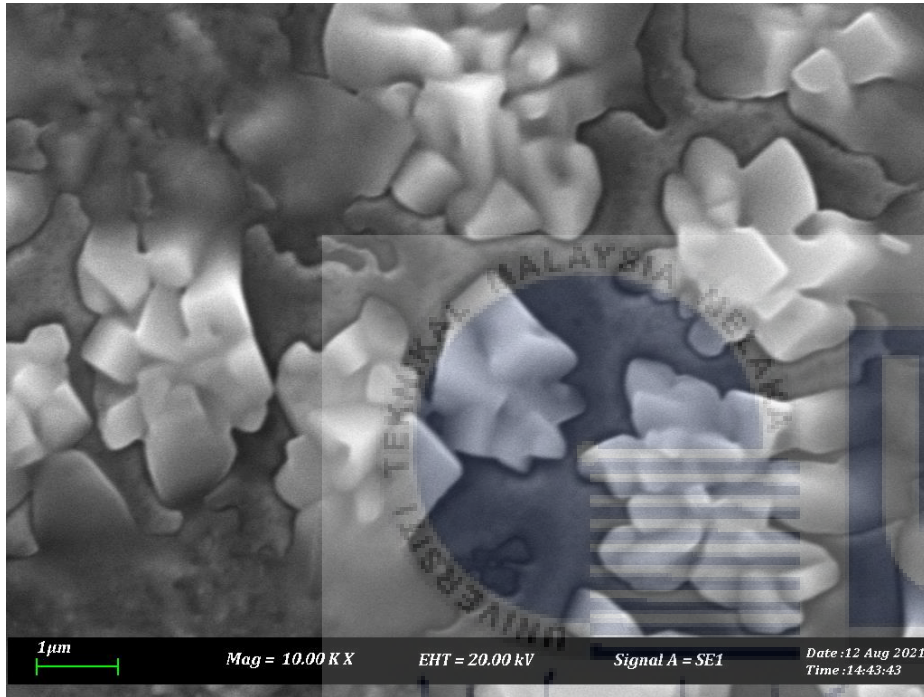


Figure 4.7 Sample C (40% S-rGO) grain size at 10.00K mag, 1 μ m



Figure 4.8 Sample C (40% S-rGO) grain size at 20.00K mag, 200nm

Aside from increasing the size of perovskite grains, the incorporation of rGO into the $\text{CH}_3\text{NH}_3\text{PbI}_3$ layer allows for the creation of smooth and homogenous films to be formed (Balis et al., 2019) rGO that has been functionalized enhances the hydrophobicity of rGO while also increasing the structural stability of PCS (Z.Yin et al., 2014)—from above SEM results, proven that S-rGO helps in the increase the Perovskite grain size. As a result, sample B, containing 20 % S-rGO in perovskite formation, shows increment grain size compared to sample A. Also, sample B shows a more negligible agglomeration effect compared to sample C. The presence of sulfonic group (SO_3H) in the rGO after the sulfonated process increases the perovskite grain size. For further work, we should examine a lower ratio below 20% S-rGO to get a more well disperse perovskite thin film without the presence of pinholes.

4.2.2 Sulfonated reduced graphene oxide (S-rGO) influences grain size

The next stage was to look into the impact of sulfonated reduced graphene oxide (S-rGO) on grain size. Negatively charged sulfonic acid ($-\text{SO}_3\text{H}$) groups are linked to the S-rGO. MA^+ in the solution will interact with $-\text{SO}_3^-$ when S-rGO scatter in the precursor solution ($-\text{SO}_3^-$ exchanges I^- from MAI). As a consequence, a cluster of MAI molecules will form around the s-rGO. The presence of MAI definitely would increase the perovskite grain size (Zhou et al., 2014). The morphologies of the resultant $\text{CH}_3\text{NH}_3\text{PbI}_3$ perovskite films were analyzed by conventional SEM characterization. The perovskite film produced from the precursor without S-rGO has a poor crystalline shape, as illustrated in figure 4.1 and 4.2 sample A with tiny perovskite crystal grain size and pinholes between two grains.

Meanwhile, sample B show that the perovskite film produced from the precursor with the addition of S-rGO has a better crystalline shape, with larger crystal grains and fewer pinholes between two grains. Presence shows how the S-rGO influences the enlargement of the grain size and decreases the grain boundary of a perovskite film. The present research shows that s-rGO may be suitable grain growing and carrier carrying materials for efficient PSCs (Zhang et al., 2016). It also shows that carbon materials with high conductivity and the necessary charge have a significant potential to improve the power conversion efficiency of PSCs. Expert-led research discovered that devices using 0.05 mg ml of s-CNTs in the perovskite precursor solution achieve excellent performance (Hu et al., 2020).

4.2.3 Reduced graphene oxide (rGO) influences grain size

Additional benefits of using reduced graphene oxide in the production of perovskite thin films are also discussed here. The rGO structure is chemically functional to enhance the optical and electrical characteristics. This reduction makes rGO a semi-metal with a working function of 4.9 eV, hole conductivity of 0.05 to 4 S cm⁻¹, and hole mobility of 2–200 cm²V⁻¹S⁻¹, which is higher than GO. Application of rGO typically involves the chemical functioning of organic or inorganic materials Gong et al., 2016. Interfacing with such functionalized rGO has garnered interest for a wide variety of applications since it helps to improve the performance of electronic devices. In addition, thin-film containing rGO was better when Perovskite thin film exposed the circumstances of oxygen and water. In addition, the high thermal conductivity of rGO, which aids the heat drainage across the cell, resulted in thermal stress stability. In an important study reported by Han and colleagues in 2017, aging of PSCs was decreased under high humidity circumstances (>75%) and temperature (85°C) with modest losses of PCE (from 16,3% to 15,7%), while at air temperatures of 35°C and 40% humidity, PSCs had neglected to show their stability when treated. Finally, rGO owning high thermal and electric conductivity and its solution-process ability, impermeability, and hydrophobicity, are suitable with perovskite thin-film production for an outstanding and enhanced solar cell.

UNIVERSITI TEKNIKAL MALAYSIA MELAKA

4.2.4 Pre heating process overcome humidity effect on Perovskite grain size

The following discussion will focus on the impact of humidity on the size of Perovskite grains. The material's sensitivity to moisture, humidity and grain size might be influenced and result in the degradation of Perovskite solar cells. At ambient temperature, both the synthesis and manufacturing processes take place. Due to the weather's impact, the room's relative humidity (RH) reached 80% during the fabrication process. According to Hong et al. (2016), despite advances in PSCs, several issues remain, including long-term stability and fabrication environment. Thus, it is shown that the temperature and humidity of the air may affect final quality. By identifying the variables that limit the development of PbI₂ films and thus contribute to the deterioration of the Perovskite thin film it is expected

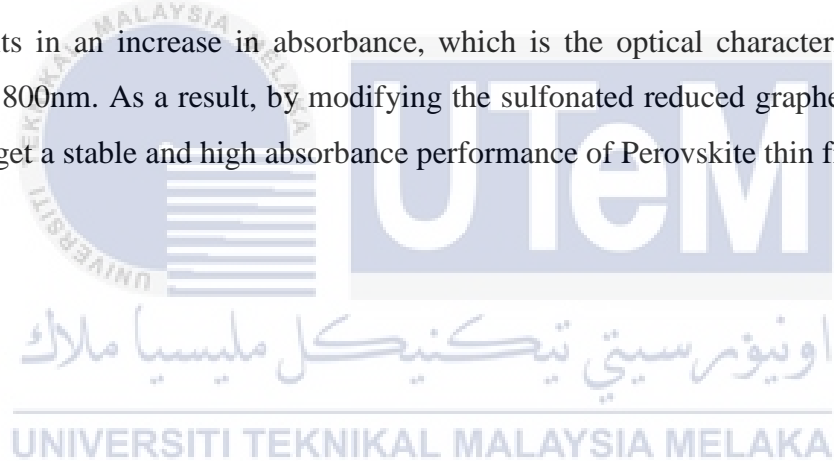
that both moisture and oxygen effects can be mitigated by concurrently heating the substrate and PbI_2 solution during deposition to oppose their in-diffusion.

Before starting the fabrication process, the substrate and PbI_2 were preheated to 80 °C. When oxygen is present, the precursor solution wetting on the substrates, impairing the formation of high-quality perovskite films. When the PbI_2 solution is placed on a heated substrate, the water and oxygen molecules that have been absorbed on the substrate surface are loosed. Cheng and colleagues (2017) affirm that when operating in ambient air with a relative humidity of 70%, a straightforward preheating method is utilized to produce high-quality perovskite films. PbI_2 and perovskite films generated at an 80 °C of preheating temperature aid in optimizing the homogeneity and grain size of PbI_2 films on coated substrates in the presence of ambient air. Preheating is intended to mitigate the adverse effects of moisture and oxygen on the development of PbI_2 films. Cheng et al., 2017 demonstrated that preheating the PbI_2 solution and substrates in air improves the perovskite layer's uniformity and particle size. Additionally, preheating is an effective method for enhancing the wetting behavior of PbI_2 and the substrate surface in the air since preheating reduces the contact angle from 36.54 ° to 19.16°. In brief, the preheating process eliminates the moisture and oxygen absorbed by the substrate and aids in the improvement of Perovskite particle size during room temperature production.

4.3 Optical properties

The perovskite solar cell (PSC) must have a high light absorption coefficient (10^5 cm^{-1}) in order to absorb more light in the film, a longer carrier lifetime in order to increase the diffusion length of the carrier and reduce compound loss, and a good transport balance between the load in the perovskite and the collecting electrode in order to maintain its excellent efficiency and stability (Miller et al, 2014).

To recapitulate, based to the findings of earlier study performed by an expert on the impact of grain size on S-GO and GO, rGO and GO combined. From the results of the study, it is clear that the sulfonation, reduction, and grain size processes all play critical roles in tailoring and enlarging the grain size, resulting in an increase in the absorbance of Perovskite thin film. The authors of all the research establish a connection between all of the factors, which results in an increase in absorbance, which is the optical characteristics between 400nm and 800nm. As a result, by modifying the sulfonated reduced graphene oxide, it is possible to get a stable and high absorbance performance of Perovskite thin film.



CHAPTER 5

CONCLUSION

5.1 Conclusion

Objective 1: To prepare the sulfonated functionalized of reduced graphene oxide (S-rGO) in perovskite thin film.

To summarise goal 1, this project aims to produce sulfonated functionalized reduced graphene oxide (S-rGO) thin films in perovskite. Experiments were conducted on the top-down synthesis of rGO from graphite flakes until reduced graphene oxide was produced in the lab at room temperature using a modified Hummer's technique. The synthesis procedure is then continued to make the S-rGO using sulfanilic acid in the sulfonation process. The Raman characterization was intended to confirm the success of the sulfonation process at this stage between S-rGO and rGO of the Perovskite thin film. From the previous study by experts, it is essential to conduct a thorough investigation to establish the structural characteristics of materials to avoid defects in the final product later. Gue et al., 2017 and Suragtkhuu et al., 2020 were used to estimate Raman's I_D/I_G ratios, demonstrating the closed ratio range that should be attained throughout our characterization. The D and G bands for rGO and S-rGO should be between 1350cm^{-1} and 1580cm^{-1} . However, I expect that S-rGO will have a lower I_D/I_G ratio than rGO. I anticipated a rise in the number of oxygen groups in the basal plane, resulting in a low number of isolated sp^3 carbon domains and a low degree of distortion after the sulfonation process on the rGO. Following that, the synthesis process continues with preparing MAI + IPA and PbI_2 + DMF + DMSO solutions for the two-step MAPbI_3 deposition. The whole synthesis procedure was carried out at room temperature.

Objective 2: To optimize the morphology of MAPbI₃ perovskite film with the different ratio of S-rGO integrate in perovskite solution.

To summarize goal 2, this project aims to analyze the morphology of MAPbI₃ perovskite film with the different ratios of S-rGO integrate into perovskite solution. Fabrication of perovskite thin films was carried out at room temperature and relative humidity of 80%. I prepared three different ratios to start from:

- Sample A contained 0% S-rGO (0.05g of MAPbI₃),
- Sample B contained 20% of S-rGO (0.01g of S-rGO : 0.04g of MAPbI₃), and
- Sample C contained 40% of S-rGO (0.02g of S-rGO : 0.03g of MAPbI₃)

After completing the fabrication process, SEM was utilized to evaluate the morphological features of the Perovskite grain size based on a varied ratio of S-rGO doped in MAPbI₃ after the Perovskite thin film was manufactured. Sample B, which includes 20% S-rGO in perovskite synthesis, has a larger particle size than sample A, as shown by imageJ. Sample B has a particle size distribution ranging from 300 nm to 1000 nm. Meanwhile, the particle size average is 638 nm. The particle size distribution for sample A was determined to be in the range of 200 nm to 550 nm. The average particle size is 384 nm. We can see from the findings that the particle size has risen when compared to Pure MAPbI₃. However, more extensive pinholes were observed in comparison to sample A.

The particle size distribution for sample C cannot be estimated using the imageJ software. According to the SEM picture of sample C, the particle did not distribute uniformly and clustered together. According to the SEM picture of sample C, clustered grain size demonstrated that incorporating s-rGO up to 40% inhibits the better morphology of the perovskite thin film. The presence of a sulfonic group (SO₃H) in the rGO following the sulfonation process increases the size of the perovskite grain. In order to get a well-dispersed perovskite thin-film free of pinholes, a small ratio of s-rGO below 20% should be investigated in the future study.

Objective 3: To investigate the effect in optical properties via CRITICAL REVIEW of perovskite material with different surface morphology.

To summarise goal 3, this project aims to study the effect of grain size on S-GO and GO and rGO and GO combined in the optical properties. This objective was performed by a critical review method. The study's findings indicate that the sulfonation, reduction, and grain size processes contribute significantly to tailoring and expanding the grain size, which increases the absorbance of Perovskite thin film. The researchers create a link between all of the variables, which leads to an increase in absorbance, which is the optical properties between 400nm and 800nm. Consequently, I believe that by altering the sulfonated reduced graphene oxide, it is feasible to get a Perovskite thin film with a stable and high absorbance performance.

5.2 Recommendation for Future Work

- For the best morphology reduced ratio of S-rGO doped in MAPbI₃ by 5%, 10%, and 15% in future study due to the agglomeration up to 40% of S-rGO.
- To study the cause of pinholes in the sample B (20% of S-rGO)
- Optical and structural characteristics of S-rGO were determined experimentally.

5.3 Sustainable Design and Development

Within this short period of time, perovskite solar cells have established a prominent place in the photovoltaic family. It has developed into one of the most promising photovoltaic technologies for the future. Capable of meeting our energy requirements more cheaply and efficiently if we could develop cheaper and mass production of Perovskite Solar Cells. Since solar cells are renewable energy, by applying solar cells for the future, we could save our earth. Solar energy is an ecologically friendly form of energy since it generates almost no pollution. Waste and pollution are unavoidable throughout the manufacture, shipping, and installation of solar cells. Solar cells are a hot topic in green energy and are generally seen as a feasible method for climate change mitigation. As a consequence, this is an innovative market that is always being studied and improved to ensure rapid implementation.

5.4 Complexity

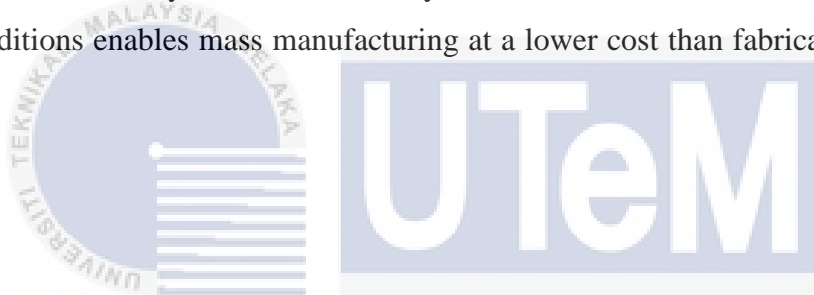
The complexity of this study is when I encounter the presence of pinholes in Sample B (20% of S-rGO). The existence of a pinhole is caused by an incomplete conversion of the lead iodide into the Perovskite Methylammonium Iodide during the manufacturing process. Pinholes are one of the morphological flaws that may develop in a Perovskite thin film. Thus this is not a positive indication for the thin film's performance. Even though I had taken precautions to prevent pinholes, such as using an anti-solvent that served as a sealant, the pinholes continued to appear. Anti-solvent (Chlorobenzene) aids in the sealing of the Perovskite structure layer in order to achieve a highly crystalline, smooth, and pinholes-free Perovskite thin film. After the fabrication process is complete, the Perovskite thin film is annealed at a annealed at 120°C for 20 minutes in order to reduce the amount of moisture in the thin film. On the other hand, there are still pinholes to be found. In the future, a thorough investigation will be required to determine the causes of the issue and prevent it from occurring again.

In addition as a future engineer, PSM has taught me to push myself and work efficiently under pressure to complete my project successfully, especially in the current conditions, when most of the plan is impossible to execute owing to Covid-19. I still have to

do my project and be accountable for it. Somehow I manage to finish my project within the specified time frame. Turnout, I like working under stress because I think it prepares me for subsequent job environments.

5.5 Long Life Learning

Hopefully, S-rGO MAPbI₃ Perovskite Thin Film will be the first step toward resolving the MAPbI₃ issue, and once we can manufacture complete S-rGO incorporated MAPbI₃ Perovskite Solar Cells, we will be able to improve and add value to Perovskite Solar Cells significantly. Additionally, the successful synthesis of Perovskite thin films under air ambient conditions enables mass manufacturing at a lower cost than fabrication in a glove box.



5.6 Achievement



Publish the paper to Nanotechnology Malaysia Annual Symposium

Title: Utilizing sulfonated reduced graphene oxide as a dopant to enhance perovskite morphology.

Authors: N.E. Safie¹, N.S.S.S. Omar¹, N.A.A. Razak¹, M.A. Azam^{1*}

¹Fakulti Kejuruteraan Pembuatan,

Universiti Teknikal Malaysia Melaka,

76100 Durian Tunggal, Melaka, MALAYSIA.

*Corresponding email: asyadi@utem.edu.my

REFERENCES

- Abdolhosseinzadeh, S., Asgharzadeh, H., & Seop Kim, H. (2015). Fast and fully-scalable synthesis of reduced graphene oxide. *Scientific Reports*, 5(1).
- Agresti, A., Pescetelli, S., Taheri, B., Del Rio Castillo, A. E., Cinà, L., Bonaccorso, F., & Di Carlo, A. (2016). Graphene-Perovskite Solar Cells Exceed 18 % Efficiency: A Stability Study. *ChemSusChem*, 9(18), 2609–2619.
- Akhtar, K., Khan, S. A., Khan, S. B., & Asiri, A. M. (2018). Chapter 4 Scanning Electron Microscopy: Principle and Applications in Nanomaterials Characterization. *Handbook of Materials Characterization*, 113-145.
- Ali, H. M. (2020). In tube convection heat transfer enhancement: SiO₂ aqua based nanofluids. *Journal of Molecular Liquids*, 308, 113031.
<https://doi.org/10.1016/j.molliq.2020.113031>
- Anaraki, E. H., Kermanpur, A., Steier, L., Domanski, K., Matsui, T., Tress, W. Correa-Baena, J.-P. (2016). Highly efficient and stable planar perovskite solar cells by solution-processed tin oxide. *Energy & Environmental Science*, 9(10), 3128–3134.
- Azpiroz, J. M., Mosconi, E., Bisquert, J., & De Angelis, F. (2015). Defect migration in methylammonium lead iodide and its role in perovskite solar cell operation. *Energy & Environmental Science*, 8(7), 2118–2127.

- Balis, N., Zaky, A. A., Perganti, D., Kaltzoglou, A., Sygellou, L., Katsaros, F., Stergiopoulos, T., Kontos, A. G., & Falaras, P. (2018). Dye Sensitization of Titania Compact Layer for Efficient and Stable Perovskite Solar Cells. *ACS Applied Energy Materials*, 1(11), 6161–6171. <https://doi.org/10.1021/acsaem.8b01221>
- Balis, N., Zaky, A. A., Athanasekou, C., Silva, A. M. T., Sakellis, E., Vasilopoulou, M., Falaras, P. (2020). Investigating the role of reduced graphene oxide as a universal additive in planar perovskite solar cells. *Journal of Photochemistry and Photobiology A: Chemistry*, 386, 112141.
- Bianco, A., Cheng, H. M., Enoki, T., Gogotsi, Y., Hurt, R. H., Koratkar, N., Kyotani, T., Monthieux, M., Park, C. R., Tascon, J. M., & Zhang, J. (2013). All in the graphene family – A recommended nomenclature for two-dimensional carbon materials. *Carbon*, 65, 1–6. <https://doi.org/10.1016/j.carbon.2013.08.038>
- Brittman, S., Adhyaksa, G. W. P., & Garnett, E. C. (2015). The expanding world of hybrid perovskites: materials properties and emerging applications. *MRS Communications*, 5(1), 7–26. <https://doi.org/10.1557/mrc.2015.6>
- Carl Englert, B. (2007). Nanomaterials and the environment: uses, methods and measurement. *Journal of Environmental Monitoring*, 9(11), 1154. <https://doi.org/10.1039/b705988d>

Chen, H., & Yang, S. (2017). Stabilizing and scaling up carbon-based perovskite solar cells. *Journal of Materials Research*, 32(16), 3011–3020.

Cheng, Y., Xu, X., Xie, Y., Li, H. W., Qing, J., Ma, C., Lee, C. S., So, F., & Tsang, S. W. (2017). 18% High-Efficiency Air-Processed Perovskite Solar Cells Made in a Humid Atmosphere of 70% RH. *Solar RRL*, 1(9), 1700097.
<https://doi.org/10.1002/solr.201700097>

Correa-Baena, J.-P., Anaya, M., Lozano, G., Tress, W., Domanski, K., Saliba, M., Hagfeldt, A. (2016). Unbroken Perovskite: Interplay of Morphology, Electro-optical Properties, and Ionic Movement. *Advanced Materials*, 28(25), 5031–5037.

Emami, S., Andrade, L., & Mendes, A. (2018). Recent Progress in Long-term Stability of Perovskite Solar Cells. *U.Porto Journal of Engineering*, 1(2), 52–62.

Ferrari, A. C., & Basko, D. M. (2013). Raman spectroscopy as a versatile tool for studying the properties of graphene. *Nature Nanotechnology*, 8(4), 235–246.

<https://doi.org/10.1038/nnano.2013.46>

Ferrari, A. C., Meyer, J. C., Scardaci, V., Casiraghi, C., Lazzeri, M., Mauri, F., Piscanec, S., Jiang, D., Novoselov, K. S., Roth, S., & Geim, A. K. (2006). Raman Spectrum of Graphene and Graphene Layers. *Physical Review Letters*, 97(18).

<https://doi.org/10.1103/physrevlett.97.187401>

Ferrari, A. C., & Robertson, J. (2000). Interpretation of Raman spectra of disordered and amorphous carbon. *Physical Review B*, 61(20), 14095–14107.

<https://doi.org/10.1103/physrevb.61.14095>

Feria, D. N., Chang, C.-Y., Mahesh, K. P. O., Hsu, C.-L., & Chao, Y.-C. (2020). Perovskite solar cells based on a perovskite film with improved film coverage. *Synthetic Metals*, 260, 116283.

Gielen, D., Boshell, F., Saygin, D., Bazilian, M. D., Wagner, N., & Gorini, R. (2019). The role of renewable energy in the global energy transformation. *Energy Strategy Reviews*, 24, 38–50.

Gong, X., Liu, G., Li, Y., Yu, D. Y. W., & Teoh, W. Y. (2016). Functionalized-Graphene Composites: Fabrication and Applications in Sustainable Energy and Environment. *Chemistry of Materials*, 28(22), 8082–8118.

<https://doi.org/10.1021/acs.chemmater.6b01447>

Guo, H., Huang, X., Pu, B., Yang, J., Chen, H., Zhou, Y., Yang, J., Li, Y., Wang, Z., & Niu, X. (2017). Efficiency enhancement in inverted planar perovskite solar cells by synergetic effect of sulfated graphene oxide (sGO) and PEDOT:PSS as hole transporting layer. *RSC Adv.*, 7(79), 50410–50419.

<https://doi.org/10.1039/c7ra10113a>

Habisreutinger, S. N., McMeekin, D. P., Snaith, H. J., & Nicholas, R. J. (2016). Research Update: Strategies for improving the stability of perovskite solar cells. *APL Materials*, 4(9), 091503.

Habte, A. T., & Ayele, D. W. (2019). Synthesis and Characterization of Reduced Graphene Oxide (rGO) Started from Graphene Oxide (GO) Using the Tour Method with Different Parameters. *Advances in Materials Science and Engineering*, 2019, 1–9.

Hadadian, M., Smått, J.-H., & Correa-Baena, J.-P. (2020). The role of carbon-based materials in enhancing the stability of perovskite solar cells. *Energy & Environmental Science*, 13(5), 1377–1407.

Han, G. S., Yoo, J. S., Yu, F., Duff, M. L., Kang, B. K., & Lee, J. K. (2017). Highly stable perovskite solar cells in humid and hot environment. *Journal of Materials Chemistry A*, 5(28), 14733–14740. <https://doi.org/10.1039/c7ta03881j>

Hirata, M., Gotou, T., Horiuchi, S., Fujiwara, M., & Ohba, M. (2004). Thin-film particles of graphite oxide 1: *Carbon*, 42(14), 2929–2937.

<https://doi.org/10.1016/j.carbon.2004.07.003>

Hu, X., Meng, X., Yang, X., Huang, Z., Xing, Z., Li, P., Tan, L., Su, M., Li, F., Chen, Y., & Song, Y. (2021). Cementitious grain-boundary passivation for flexible perovskite solar cells with superior environmental stability and mechanical robustness. *Science Bulletin*, 66(6), 527–535. <https://doi.org/10.1016/j.scib.2020.10.023>

- Hummers, W. S., & Offeman, R. E. (1958). Preparation of Graphitic Oxide. *Journal of the American Chemical Society*, 80(6), 1339. <https://doi.org/10.1021/ja01539a017>
- Hussain, I., Tran, H. P., Jaksik, J., Moore, J., Islam, N., & Uddin, M. J. (2018). Functional materials, device architecture, and flexibility of perovskite solar cell. *Emergent Materials*, 1(3–4), 133–154.
- Im, J.-H., Lee, C.-R., Lee, J.-W., Park, S.-W., & Park, N.-G. (2011). 6.5% efficient perovskite quantum-dot-sensitized solar cell. *Nanoscale*, 3(10), 4088.
- Jamal, M. S., Bashar, M. S., Hasan, A. K. M., Almutairi, Z. A., Alharbi, H. F., Alharthi, N. H., Akhtaruzzaman, M. (2018). Fabrication techniques and morphological analysis of perovskite absorber layer for high-efficiency perovskite solar cell: A review. *Renewable and Sustainable Energy Reviews*, 98, 469–488.
- Johansson, M. B., Xie, L., Kim, B. J., Thyr, J., Kandra, T., Johansson, E. M. J., Boschloo, G. (2020). Highly crystalline MAPbI₃ perovskite grain formation by irreversible poor-solvent diffusion aggregation, for efficient solar cell fabrication. *Nano Energy*, 78, 105346.
- Kafle, B. P. (2019). Application of Reduced Graphene Oxide (rGO) for Stability of Perovskite Solar Cells. *Carbon Nanostructures*, 203–229.
https://doi.org/10.1007/978-3-030-30207-8_8

- Kim, H. D., Ohkita, H., Benten, H., & Ito, S. (2015). Photovoltaic Performance of Perovskite Solar Cells with Different Grain Sizes. *Advanced Materials*, 28(5), 917–922. <https://doi.org/10.1002/adma.201504144>
- Kim, M. J., Jeong, Y., Sohn, S., Lee, S. Y., Kim, Y. J., Lee, K., Kahng, Y. H., & Jang, J. H. (2013). Fast and low-temperature reduction of graphene oxide films using ammonia plasma. *AIP Advances*, 3(1), 012117. <https://doi.org/10.1063/1.4789545>
- Kim, S., Jeong, I., Park, C., Kang, G., Han, I. K., Kim, W., & Park, M. (2019). Morphology control of perovskite in green antisolvent system for MAPbI₃-based solar cells with over 20% efficiency. *Solar Energy Materials and Solar Cells*, 203, 110197.
- Kim, S., Lee, H. S., Kim, J. M., Seo, S. W., Kim, J. H., Jang, C. W., & Choi, S.-H. (2018). Effect of layer number on flexible perovskite solar cells employing multiple layers of graphene as transparent conductive electrodes. *Journal of Alloys and Compounds*, 744, 404–411.
- Koefoed, L., Pedersen, S. U., & Daasbjerg, K. (2017). Bipolar electrochemistry—A wireless approach for electrode reactions. *Current Opinion in Electrochemistry*, 2(1), 13–17.
- Kojima, A., Teshima, K., Shirai, Y., & Miyasaka, T. (2009). Organometal Halide Perovskites as Visible-Light Sensitizers for Photovoltaic Cells. *Journal of the American Chemical Society*, 131(17), 6050–6051.

Kumar, R., Mehta, B. R., Bhatnagar, M., S, R., Mahapatra, S., Salkalachen, S., & Jhavar, P. (2014). Graphene as a transparent conducting and surface field layer in planar Si solar cells. *Nanoscale Research Letters*, 9(1), 349. <https://doi.org/10.1186/1556-276x-9-349>

Leijtens, T., Bush, K., Cheacharoen, R., Beal, R., Bowring, A., & McGehee, M. D. (2017). Towards enabling stable lead halide perovskite solar cells; interplay between structural, environmental, and thermal stability. *Journal of Materials Chemistry A*, 5(23), 11483–11500.

Li, H., Tao, L., Huang, F., Sun, Q., Zhao, X., Han, J., Wang, M. (2017). Enhancing Efficiency of Perovskite Solar Cells via Surface Passivation with Graphene Oxide Interlayer. *ACS Applied Materials & Interfaces*, 9(44), 38967–38976.

Liu, Y., Akin, S., Pan, L., Uchida, R., Arora, N., Milić, J. V., Grätzel, M. (2019). Ultrahydrophobic 3D/2D fluoroarene bilayer-based water-resistant perovskite solar cells with efficiencies exceeding 22%. *Science Advances*, 5(6), eaaw2543.

Mamun, Abdullah A.. "Effect of Grain Size and Interface Engineering on the Photovoltaic Performance and Stability of Perovskite Solar Cells" (2019). Doctor of Philosophy (PhD), Dissertation, Electrical & Computer Engineering, Old Dominion University, DOI: 10.25777/6hp4-s975

Meyer, Amidon, G., P., & Mudie, D. (2016). Chapter 10. Particle, Powder, and Compact Characterization. *Developing Solid Oral Dosage Forms*, 271-294.

Miller, J. L. (2014). Unusual defect physics underlies perovskite solar cells' exceptional performance. *Physics Today*, 67(5), 13–15.

Milić, J. V., Arora, N., Dar, M. I., Zakeeruddin, S. M., & Grätzel, M. (2018). Reduced Graphene Oxide as a Stabilizing Agent in Perovskite Solar Cells. *Advanced Materials Interfaces*, 5(22), 1800416. <https://doi.org/10.1002/admi.201800416>

Morales-Acosta, D., Flores-Oyervides, J. D., Rodríguez-González, J. A., Sánchez-Padilla, N. M., Benavides, R., Fernández-Tavizón, S., & Mercado-Silva, J. A. (2019). Comparative methods for reduction and sulfonation of graphene oxide for fuel cell electrode applications. *International Journal of Hydrogen Energy*, 44(24), 12356–12364.

Palma, A. L., Cinà, L., Pescetelli, S., Agresti, A., Raggio, M., Paolesse, R., Bonaccorso, F., & di Carlo, A. (2016). Reduced graphene oxide as efficient and stable hole transporting material in mesoscopic perovskite solar cells. *Nano Energy*, 22, 349–360. <https://doi.org/10.1016/j.nanoen.2016.02.027>

Park, N.-G. (2015). Perovskite solar cells: an emerging photovoltaic technology. *Materials Today*, 18(2), 65–72.

Pirhadi, V., & Razavi, A. (2018). Integrability of Transitive Jacobi Manifolds. *Iranian Journal of Science and Technology, Transactions A: Science*, 43(4), 1657–1664. <https://doi.org/10.1007/s40995-018-0609-6>

Pistor, P., Ruiz, A., Cabot, A., & Izquierdo-Roca, V. (2016). Advanced Raman Spectroscopy of Methylammonium Lead Iodide: Development of a Non-destructive Characterisation Methodology. *Scientific Reports*, 6(1).

Qiu, X., Dong, T., Ueda, M., Zhang, X., & Wang, L. (2017). Sulfonated reduced graphene oxide as a conductive layer in sulfonated poly(ether ether ketone) nanocomposite membranes. *Journal of Membrane Science*, 524, 663–672.

<https://doi.org/10.1016/j.memsci.2016.11.064>

Ren, H., Yu, S., Chao, L., Xia, Y., Sun, Y., Zuo, S., Li, F., Niu, T., Yang, Y., Ju, H., Li, B., Du, H., Gao, X., Zhang, J., Wang, J., Zhang, L., Chen, Y., & Huang, W. (2020). Efficient and stable Ruddlesden–Popper perovskite solar cell with tailored interlayer molecular interaction. *Nature Photonics*, 14(3), 154–163.

<https://doi.org/10.1038/s41566-019-0572-6>

Rocha, F. S., Gomes, A. J., Lunardi, C. N., Kaliaguine, S., & Patience, G. S. (2018). Experimental methods in chemical engineering: Ultraviolet visible spectroscopy-UV-Vis. *The Canadian Journal of Chemical Engineering*, 96(12), 2512–2517.

<https://doi.org/10.1002/cjce.23344>

Oliva, F., Kretschmar, S., Colombara, D., Tombolato, S., Ruiz, C. M., Redinger, A., Saucedo, E., Broussillou, C., de Monsabert, T. G., Unold, T., Dale, P. J., Izquierdo-Roca, V., & Pérez-Rodríguez, A. (2016). Optical methodology for process

monitoring of chalcopyrite photovoltaic technologies: Application to low cost Cu(In,Ga)(S,Se)₂ electrodeposition based processes. *Solar Energy Materials and Solar Cells*, 158, 168–183. <https://doi.org/10.1016/j.solmat.2015.12.036>

Safie, N. E., Azam, M. A., Aziz, M. F. A., & Ismail, M. (2020). Recent progress of graphene-based materials for efficient charge transfer and device performance stability in perovskite solar cells. *International Journal of Energy Research*.

Saliba, M., Matsui, T., Seo, J.-Y., Domanski, K., Correa-Baena, J.-P., Nazeeruddin, M. K., Grätzel, M. (2016). Cesium-containing triple cation perovskite solar cells: improved stability, reproducibility and high efficiency. *Energy & Environmental Science*, 9(6), 1989–1997.

Santos, L. R., Dos Santos, E. A., Pinheiro, R. M., & Ferreira, E. J. L. (2017). Carbon-Based Materials: Recent Advances, Challenges, and Perspectives. *Energy & Environmental Science*, 12(2), 103.

Scanning Electron Microscopes - EVOCD. (2017, April 12). Integrated Computational Material Engineering.

https://icme.hpc.msstate.edu/mediawiki/index.php/Scanning_Electron_Microscopes.html

Sha, W. E. I., Ren, X., Chen, L., & Choy, W. C. H. (2015). The efficiency limit of CH₃NH₃PbI₃ perovskite solar cells. *Applied Physics Letters*, 106(22), 221104.

Shi, Z., & Jayatissa, A. (2018). Perovskites-Based Solar Cells: A Review of Recent Progress, Materials and Processing Methods. *Materials*, 11(5), 729.

Singh, A. K. (2016). Chapter 4 - Experimental Methodologies for the Characterization of Nanoparticles. *Engineered Nanoparticles*, 2, 125-170.

Sögüt, E. G., Karataş, Y., Gülcan, M., & Kılıç, N. A. (2020). Enhancement of adsorption capacity of reduced graphene oxide by sulfonic acid functionalization: Malachite green and Zn (II) uptake. *Materials Chemistry and Physics*, 256, 123662.

<https://doi.org/10.1016/j.matchemphys.2020.123662>

Stankovich, S., Dikin, D. A., Piner, R. D., Kohlhaas, K. A., Kleinhammes, A., Jia, Y., Wu, Y., Nguyen, S. T., & Ruoff, R. S. (2007). Synthesis of graphene-based nanosheets via chemical reduction of exfoliated graphite oxide. *Carbon*, 45(7), 1558–1565.

<https://doi.org/10.1016/j.carbon.2007.02.034>

Stranks, S. D., Burlakov, V. M., Leijtens, T., Ball, J. M., Goriely, A., & Snaith, H. J. (2014). Recombination Kinetics in Organic-Inorganic Perovskites: Excitons, Free Charge, and Subgap States. *Physical Review Applied*, 2(3).

Suragtkhuu, S., Tserendavag, O., Vandandoo, U., Bati, A. S. R., Bat-Erdene, M., Shapter, J. G. Davaasambu, S. (2020). Efficiency and stability enhancement of perovskite solar cells using reduced graphene oxide derived from earth-abundant natural graphite. *RSC Advances*, 10(15), 9133–9139.

Vasilopoulou, M., Fakharuddin, A., Coutsolelos, A. G., Falaras, P., Argitis, P., Yusoff, A. R. M., & Nazeeruddin, M. K. (2020). Molecular materials as interfacial layers and additives in perovskite solar cells. *Chemical Society Reviews*, 49(13), 4496–4526.

Wali, Q., Iftikhar, F. J., Khan, M. E., Ullah, A., Iqbal, Y., & Jose, R. (2020). Advances in stability of perovskite solar cells. *Organic Electronics*, 78, 105590.

Wang, R., Mujahid, M., Duan, Y., Wang, Z., Xue, J., & Yang, Y. (2019). A Review of Perovskites Solar Cell Stability. *Advanced Functional Materials*, 29(47), 1808843.

<https://doi.org/10.1002/adfm.201808843>

UNIVERSITI TEKNIKAL MALAYSIA MELAKA

Wang, Z., Shi, Z., Li, T., Chen, Y., & Huang, W. (2016). Stability of Perovskite Solar Cells: A Prospective on the Substitution of the A Cation and X Anion. *Angewandte Chemie International Edition*, 56(5), 1190–1212.

Xiao, Z., Dong, Q., Bi, C., Shao, Y., Yuan, Y., & Huang, J. (2014). Solvent Annealing of Perovskite-Induced Crystal Growth for Photovoltaic-Device Efficiency Enhancement. *Advanced Materials*, 26(37), 6503–6509.

<https://doi.org/10.1002/adma.201401685>

- Xu, L., & Cheng, L. (2013). Graphite Oxide under High Pressure: A Raman Spectroscopic Study. *Journal of Nanomaterials*, 2013, 1–5. <https://doi.org/10.1155/2013/731875>
- Yang, Z., Zhang, S., Li, L., & Chen, W. (2017). Research progress on large-area perovskite thin films and solar modules. *Journal of Materiomics*, 3(4), 231–244.
- Yang, Z., Pan, J., Liang, Y., Li, Q., & Xu, D. (2018). Ambient Air Condition for Room-Temperature Deposition of MAPbI₃ Films in Highly Efficient Solar Cells. *Small*, 14(45), 1802240. <https://doi.org/10.1002/sml.201802240>
- Ye, S., Rao, H., Zhao, Z., Zhang, L., Bao, H., Sun, W., Li, Y., Gu, F., Wang, J., Liu, Z., Bian, Z., & Huang, C. (2017). A Breakthrough Efficiency of 19.9% Obtained in Inverted Perovskite Solar Cells by Using an Efficient Trap State Passivator Cu(thiourea)I. *Journal of the American Chemical Society*, 139(22), 7504–7512. <https://doi.org/10.1021/jacs.7b01439>
- Yin, W.-J., Shi, T., & Yan, Y. (2014). Unusual defect physics in CH₃NH₃PbI₃ perovskite solar cell absorber. *Applied Physics Letters*, 104(6), 063903.
- Yohk co.ltd. (2020, October 15). *Basic of Raman scattering | Nanophoton*. Nanophoton |. <https://www.nanophoton.net/lecture-room/raman-spectroscopy/lesson-1-1>

- Yousif, Q. A., & Agbolaghi, S. (2019). A Comparison Between Functions of Carbon Nanotube and Reduced Graphene Oxide and Respective Ameliorated Derivatives in Perovskite Solar Cells. *Macromolecular Research*, 28(5), 425–432.
- Zhang, F., Cong, J., Li, Y., Bergstrand, J., Liu, H., Cai, B. Sun, L. (2018). A facile route to grain morphology controllable perovskite thin films towards highly efficient perovskite solar cells. *Nano Energy*, 53, 405–414.
- Zheng, L., Zhang, D., Ma, Y., Lu, Z., Chen, Z., Wang, S., Xiao, L., & Gong, Q. (2015). Morphology control of the perovskite films for efficient solar cells. *Dalton Transactions*, 44(23), 10582–10593. <https://doi.org/10.1039/c4dt03869j>
- Zhang, S., Xie, M., Li, F., Yan, Z., Li, Y., Kan, E. Zeng, H. (2015). Semiconducting Group 15 Monolayers: A Broad Range of Band Gaps and High Carrier Mobilities. *Angewandte Chemie*, 128(5), 1698–1701.
- Zhang, Y., Tan, L., Fu, Q., Chen, L., Ji, T., Hu, X., & Chen, Y. (2016). Enhancing the grain size of organic halide perovskites by sulfonate-carbon nanotube incorporation in high performance perovskite solar cells. *Chemical Communications*, 52(33), 5674–5677. <https://doi.org/10.1039/c6cc00268d>
- Zhou, H., Chen, Q., Li, G., Luo, S., Song, T. B., Duan, H. S., Hong, Z., You, J., Liu, Y., & Yang, Y. (2014). Interface engineering of highly efficient perovskite solar cells. *Science*, 345(6196), 542–546. <https://doi.org/10.1126/science.1254050>

Zhou, D., Zhou, T., Tian, Y., Zhu, X., & Tu, Y. (2018). Perovskite-Based Solar Cells: Materials, Methods, and Future Perspectives. *Journal of Nanomaterials*, 2018, 1–15.

Zhao, X., Tao, L., Li, H., Huang, W., Sun, P., Liu, J., Liu, S., Sun, Q., Cui, Z., Sun, L., Shen, Y., Yang, Y., & Wang, M. (2018). Efficient Planar Perovskite Solar Cells with Improved Fill Factor via Interface Engineering with Graphene. *Nano Letters*, 18(4), 2442–2449. <https://doi.org/10.1021/acs.nanolett.8b00025>



APPENDIX A: GANTT CHART PSM 1 SEMESTER 1 2020/2021

NO	TASK	WEEK													
		1	2	3	4	5	6	7	8	9	10	11	12	13	14
		Chapter 1				/	Chapter 2				/	Chapter 3			
1	Undersanding morphological and optical properties of perovskite														
2	Understanding rGO synthesis method and properties														
3	Understanding functionalized rGO method and properties														
4	Understanding expected result/effect on the morphological properties														
5	Understanding expected result/effect on optical properties														
6	Writing of chapter 1, 2, 3														
	Planning														
	Actual														

UNIVERSITI TEKNIKAL MALAYSIA MELAKA

APPENDIX B: WORK PLANNING FOR FOLLOWING PSM 2

PROJECT ACTIVITIES	MONTHS				
	JAN	FEB	MAC	APR	MEI
Synthesis of rGO from graphite powder (top-down method)					
Synthesis of functionalized rGO via sulfonating process using sulphuric acid					
Preparation of functionalized rGO doped perovskite solution					
Fabricate functionalized rGO doped perovskite thin film					
Sample testing and evaluation (morphological and optical analysis)					
Writing report					

APPENDIX C: GANTT CHART PSM 2 SEMESTER 2 2020/2021

